STUDYING ZINC HOMEOSTASIS IN *ESCHERICHIA COLI* USING CARBONIC ANHYDRASE-BASED RATIOMETRIC SENSORS

by

Da Wang

A dissertation submitted in partial fulfillment
of the requirements for the degree of
Doctor of Philosophy
(Chemical Biology)
in the University of Michigan
2012

Doctoral Committee:

Professor Carol A. Fierke, Chair
Professor Raoul Kopelman
Professor James E. Penner-Hahn
Professor Joel A. Swanson

DEDICATION

To my parents.

ACKNOWLEDGEMENTS

There are many people I would like to thank through my graduate school. First, I would like to thank my advisor Dr. Carol Fierke for giving me great guidance and support through my graduate schooling. She has always been encouraging, understanding, helpful and supportive in both science and my personal life. I have learnt so much from her that will benefit me lifelong wherever I go. I would like to thank my committee, Prof. James Penner-Hahn, Prof. Raoul Kopelman, and Prof. Joel Swanson. I have benefited greatly from the helpful advice and insightful comments about my work over the past years. I truly appreciate the help.

I would also like to thank my collaborators Dr. Richard Thompson and Dr. Bryan McCranor at the University of Maryland School Of Medicine. Dr. Thompson has been very instrumental in solving many of the practical issues of sensor development, and Dr. McCranor kindly provided assistance in sensor development for mammalian cell imaging. I appreciate their input that helped move the project forward.

I would like to thank all my labmates for creating such a great and wonderful lab culture. It has been a delightful experience working with you. I would like to thank Dr. Tamiika Hurst for her hard work that laid the groundwork for the sensor development, and mentoring me when I first started working on this project. I greatly appreciate Andrea Stoddard's generous help throughout the years and her contribution to the CA team. I would like to thank Dr. Sam Gattis for mentoring me through my first project in

the lab. I had many inspiring discussions about my work with Dr. Terry Watt, Dr. Nathan Zahler, Dr. John Hsieh and Dr. Lubomir Dostal, and I would like to thank them for sharing their wisdom. I appreciate Corissa Lamphear, Noah Wolfson, and Carol Ann Pitcairn's initiatives and efforts for organizing all the lab activities. I had many fun memories working with Caleb Joseph, Xiaomu Guan, Wan Lim, Elaina Zverina, Xin Liu, Byung Chul Kim, Mike Howe, Yu Chen and Elia Wright. Thank you all for being such wonderful colleagues and friends. I also enjoyed working with the rotating students: Chenxi Shen, Si Yang, Kristin Ko, and Olijahwon Hosteen.

I could not possibly express enough of my gratitude to my family, who has always been the strongest support for me. Even though we have been globes away during my graduate study, their love and support have always provided strength for me to overcome obstacles and move forward. Live long and prosper.

TABLE OF CONTENTS

LIST OF FIGURES

LIST OF TABLES

LIST OF ABBREVIATIONS

AAS	atomic absorption spectroscopy
AD	activation domain
AF594	AlexaFluor594
BT	bleedthrough
CA	carbonic anhydrase
CDF	cation diffusion facilitator
CFP	cyan fluorescent protein
CHEF	chelation-enhanced fluorescence
DBD	DNA binding domain
DMSO	dimethyl sulfoxide
DNSA	dansylamide
DPA	di-2-picolyamine
DPS	dapoxyl sulfonamide
ECFP	enhanced cyan fluorescent protein
EDTA	ethylenediaminetetraacetic acid
EGTA	ethylene glycol-bis(2-aminoethylether)-N,N,N′,N′-tetraacetic acid
EYFP	enhanced yellow fluorescent protein
FCCP	carbonyl cyanide-*p*-trifluoromethoxyphenylhydrazone
FRET	Förster resonance energy transfer
GFP	green fluorescent protein
GSH	glutathione
HEPES	4-(2-hydroxyethyl)-1-piperazineethanesulfonic acid
HPLC	high-performance liquid chromatography
HTM	heavy transition metals

ICP-MS	inductively coupled plasma mass spectrometry
ICT	intramolecular charge transfer
I_{FP}	fluorescence intensity of red fluorescence protein channel
I_{FRET}	fluorescence intensity of FRET channel
$I_{FRET,adj}$	DPS background-adjusted fluorescence intensity of FRET channel
IPTG	isopropyl β-D-1-thiogalactopyranoside
LC-MS	liquid chromatography–mass spectrometry
LPS	lipopolysaccharide
MES	2-(N-morpholino)ethanesulfonic acid
MFS	major facilitator superfamily
MOPS	4-morpholinepropanesulfonic acid
MT	metallothionein
MTF-1	metal response element-binding transcription factor-1
NTA	nitrilotriacetic acid
PET	photoinduced electron transfer
RFP	red fluorescent protein
RND	resistance-nodulation-cell division (transporters)
RT-PCR	reverse transcriptase polymerase chain reaction
SDS-PAGE	sodium dodecyl sulfate polyacrylamide gel electrophoresis
TAME	tosyl-L-argininyl-methyl ester
TCEP	tris(2-carboxyethyl)phosphine hydrochloride
TFA	trifluoroacetic acid
TMD	transmembrane domains
TPEN	N,N,N’,N’-tetrakis(2-pyridylmethyl)ethylenediamine
TSQ	*p*-toluenesulfonamide quinoline
WT	wild type
XRF	x-ray fluorescence
YFP	yellow fluorescent protein
ZIP	Zrt- and Irt-like proteins
ZnT	zinc transporter

ABSTRACT

STUDYING ZINC HOMEOSTASIS IN *ESCHERICHIA COLI* USING CARBONIC ANHYDRASE-BASED RATIOMETRIC SENSORS

by

Da Wang

Chair: Carol A. Fierke

Zinc is an essential element for numerous cellular processes. In this work, we developed a series of highly selective, sensitive and quantitative zinc sensors based on carbonic anhydrase (CA). An aryl sulfonamide ligand of CA exhibits a large fluorescence signal coupled to zinc binding, forming a Förster resonance energy transfer (FRET) pair with a red fluorescent protein fused to CA. These sensors respond to alterations in physiological free zinc concentrations, and are applied to *Escherichia coli* to quantify the readily exchangeable zinc concentration. In minimal media, *E. coli* BL21(DE3) cells expressing the CA sensors exhibit a median intracellular readily exchangeable zinc concentration of 20 pM.

To understand the functions of ZitB and ZntA, important transporters in zinc detoxification in *E. coli*, we applied the sensor H94N CA_TagRFP to monitor the intracellular free zinc changes in wild type, Δ*zitB* and Δ*zntA* strains upon sudden exposure to toxic levels of zinc ("zinc shock"). The intracellular free zinc increases

transiently from picomolar to nanomolar levels. The corresponding zinc-dependent changes in the *zntA* mRNA level indicate that ZntR-mediated transcription of *zntA* exhibits an apparent $K_{1/2}$ for zinc activation in the nanomolar range *in vivo*. In the Δ*zitB* strain the free zinc concentration rises more rapidly after zinc shock compared to wild-type cells, while a prolonged accumulation of free zinc is observed in the Δ*zntA* strain. Based on these results, we propose that ZitB functions as a constitutive, first-line defense against toxic zinc influx, while ZntA is up-regulated to efficiently lower the free zinc concentration.

The zinc detoxification functions of three transporters and a periplasmic protein regulated by the BaeS/R two-component system were explored. The effects of single gene knockouts in the BaeS/R regulon on changes in cell growth rate, free zinc, total zinc and total copper after zinc shock were investigated to evaluate their functions. Two exporters, MdtABC and MdtD, and the periplasmic protein, Spy, are involved in zinc detoxification based on the growth defects and increases in free and total zinc/copper that were observed in the single knockout strains. These proteins potentially complement the ATP-driven zinc export mediated by ZntA in *E. coli*.

CHAPTER I

INTRODUCTION

1.1 ZINC IN BIOLOGY

1.1.1 Cellular Functions of Zinc

Zinc is an essential element in the cell, playing important catalytic, structural, and regulatory roles[1-3]. It is the second most abundant transition metal in the cell, next to iron[2]. Bioinformatic studies revealed that 3 ~ 10% of all proteins in the human genome contain potential zinc binding sites[4]. Zinc is an essential cofactor in more than 300 proteins from all six classes of enzymes[2]. Given its importance, zinc homeostasis is regulated through an extensive network of transporters, ligands and transcription factors in the cell[5-8]. Although zinc is an essential nutrient, excess zinc is cytotoxic, at least partly due to inhibition of key enzymes and competition with essential copper ions[9]. The disturbance of intracellular zinc homeostasis is associated with various human health problems[10-13].

Unlike other essential transition metals in the cells such as iron and copper, zinc is redox inert and can form stable complexes with macromolecules with variable coordination geometry, which makes it a good candidate to assume a diverse set of functions in biology[14]. As a d^{10} metal, zinc is not susceptible to ligand field stabilization

effects[1]; therefore, zinc can adopt various coordination numbers ranging from 4 to 8, with 4 – 6 commonly observed in protein binding sites[15]. The most prevalent coordination number in proteins is 4 with a tetrahedral or distorted tetrahedral geometry.

A catalytic zinc ion normally binds to an active site interacting with three amino acid ligands, His being the most frequent, followed by Glu, Asp and Cys[1, 2]. A solvent molecule (most commonly water) generally acts as the fourth ligand, and could be ionized or displaced during catalysis. There are three catalytic mechanisms involving zinc known to date[1]. In the nucleophilic mechanism (e.g. carbonic anhydrase), zinc lowers the pK_a of the solvent molecule to produce a zinc-bound hydroxide which subsequently acts as a nucleophile on the substrate[16]. In the general base-catalyzed mechanism (e.g. carboxypeptidase A), zinc decreases the basicity of the metal bound water with the assistance of a general base (typically Glu or Asp)[17]. The third mechanism (e.g. alkaline phosphatase) involves displacement of water from the fourth coordination position by a substrate prior to catalysis which activates the substrate for the subsequent catalytic reaction[18].

The structural role of zinc is best exemplified by "zinc fingers", small protein structural motifs stabilized by one or more coordinated zinc ions. The canonical C_2H_2 zinc finger motif was first found in the *Xenopus* transcription factor IIIA[19]. Later a diverse set of structures were found in a broad range of proteins involved in various cellular processes. These zinc fingers have been classified based on ligand geometry[20], ligand type[21], and the structural properties near the zinc binding sites[22]. Structurally, C_2H_2-like finger, treble clef finger and the zinc ribbon comprise the majority of the zinc finger motifs[22]. Zinc fingers typically function as binding modules that interact with

nucleic acids, proteins and small molecules[23]. Through these interactions, zinc fingers are involved in many fundamental cellular processes, especially those in cell cycle control and programmed cell death[22, 23]. Therefore, engineering zinc fingers to regulate gene expression has been extensively investigated as a potential strategy for targeted therapy[24].

Fluctuation in free zinc concentration in cells has been proposed to be a potential mediator of various physiological and pathological processes[13]. The observation of selective storage and release of zinc from pre-synaptic vesicles was the first discovery that implies a regulatory role for zinc in the brain[25]. In the immune system, a temporary decrease in intracellular free zinc triggered by lipopolysaccharide (LPS) influences the function of dendritic cells[26]. Furthermore, temporary free zinc peaks ("zinc sparks") were detected in mammalian eggs upon fertilization are critical for regulating meiotic progression[27, 28]. Zinc sparks, similar to the Ca^{2+} waves, were also observed during cardiac excitation-contraction cycles in isolated cardiomyocytes[29]. These discoveries led to the proposal that zinc may act as a signaling molecule similar to calcium in certain cellular processes; however, unlike in Ca^{2+} signaling where calmodulin is a primary target, zinc may bind to and affect a wide range of molecular targets.

1.1.2 Zinc and Human Health

Given the important roles of zinc, disturbance of its homeostasis can cause various health problems in the human body. Daily zinc requirements vary with age and growth stage; normal adults require 10 ~ 15 mg/day on average. Zinc deficiency causes growth retardation, defects in reproductive organs, dysfunction of the immune system

and cognitive problems[2, 30]. Zinc deprivation renders airway epithelial cells susceptible to apoptosis induced by oxidants, as well as antigen-induced airway inflammation[31, 32]. Accumulating evidence indicates that abnormalities in zinc concentration and/or distribution might play pathological roles in Alzheimer's disease, diabetes, asthma and prostate cancer[11]. Studies have shown that dietary zinc supplementation protects mice against chemically induced diabetes, and the zinc concentration in serum is significantly lower in patients with Type I diabetes[33, 34]. Zinc is abundant in the pancreas where a significant fraction is packed into secretary vesicles with insulin in the beta cells[35]. The exact function of the released zinc accompanying insulin is unclear, though there are studies indicating it moderates the secretion of glucagon by alpha cells, as well as displaying insulinominetic effects by inhibiting the enzyme tyrosine phosphatase 1B, a key regulator of insulin receptor[36, 37]. Large amount of zinc are present in the brain, mostly concentrated in the glutamate synaptic vesicles of pre-synaptic nerve terminals. Zinc is released along with glutamate during neurotransmission and then taken up by the post-synaptic cells; the concentrations in the synaptic cleft may reach as high as 300 μM. The excess zinc, unless promptly removed, could be toxic to the adjacent neurons and cause damages[25]. Zinc may be involved in Alzheimer's disease at multiple levels. Two secretases in amyloid precursor protein (APP) processing require zinc to function[38]. Zinc, copper and iron can dramatically increase amyloid-beta (Aβ) aggregation and precipitation[39]. Chelation of zinc and copper has shown to reduce the formation of Aβ plaque and improve the cognitive ability in animal studies[40].

1.2 CELLULAR ZINC HOMEOSTASIS

1.2.1 Intracellular Zinc Concentrations

Since zinc plays various important roles in the cell, zinc homeostasis is highly regulated through influx/efflux pumps, ligand buffering and compartmentalization in eukaryotic cells. Although zinc is considered a trace element in the living organisms, the intracellular concentration of total zinc is actually fairly high. Measured by atomic absorption spectroscopy (AAS) or inductively couple plasma mass spectroscopy (ICP-MS), the total zinc content in cells from a variety of species and cell types is 0.1 - 0.5 mM[6]. O'Halloran *et al.* first proposed the concept of "zinc quota", which is defined the total zinc content of a cell required for its optimum growth[41]. The zinc quota for *Escherichia coli*, yeast and many mammalian cells were estimated at 10^5, 10^7 and 10^8 atoms of zinc per cell[6]. Adjusted for the cell volume, these total zinc concentrations all fall within the 0.1 – 0.5 mM range. Some specialized mammalian cells, such as pancreatic beta cells, store high concentration of zinc in the vesicles and do not conform to this general rule.

The intracellular free zinc concentration, on the other hand, is very low since the majority of the zinc is bound to the large amount of zinc ligands in the cells, including proteins, nucleic acids and small molecules (Eq.1.1, K_{Zn} reflects the apparent ensemble zinc binding affinity in the cell).

$$K_{Zn} = \frac{[Zn^{2+}]_{free}[L_1 + L_2 + L_3 + ...]}{[Zn \cdot L_1 + Zn \cdot L_2 + Zn \cdot L_3 + ...]} \qquad \text{Eq. 1.1}$$

Free zinc (or so called "labile zinc", "readily exchangeable zinc"), is defined as the portion of zinc that is coordinated to weak or rapidly exchangeable ligands such as water or chloride. The free zinc concentration, sometimes denoted as "pZn (= - log[Zn^{2+}])", is

estimated to be low because of the relatively high concentrations and affinities of cellular zinc ligands. In *E. coli*, the free zinc level was proposed to be in the fM range based on the femtomolar affinity of zinc-responsive transcription factors [41]. Measurement of free zinc concentrations in cells has been challenging, with published values ranging from pM to nM levels in eukaryotic cells [42-46]. Additionally, the concentration and distribution of intracellular free zinc may change in response to various physiological and pathological conditions [5, 47]. Quantitative analysis of intracellular readily exchangeable zinc concentration under relevant conditions will facilitate the understanding of zinc homeostasis and the potential role of zinc in regulating a variety of cellular processes.

1.2.2 Zinc Homeostasis in Eukaryotic Cells

Regulation of intracellular zinc homeostasis in eukaryotic cells is carried out through an extensive network of transporters, cellular ligands, and transcription factors[5, 6]. In a zinc deficient environment, the cells up-regulate high affinity zinc importers and mobilize the stored zinc to maintain the functions of essential proteins. Under high zinc stress, the cells deploy effective efflux and sequestration of free zinc to specialized zinc binding proteins or certain organelles to maintain the free zinc concentration at a non-toxic level. In eukaryotes, a universal transcription factor regulates the expression of several zinc transporters and protein ligands to achieve a global balance within the cell[48, 49]. The proposed cellular network for zinc homeostasis regulation in yeast and mammalian cells are illustrated in Fig. 1.1 and Fig. 1.2.

1.2.2.1 Eukaryotic Zinc Transporters

Two major families of zinc transporters are found in eukaryotic cells, the ZIP (Zrt- and Irt-like protein) and CDF (cation diffusion facilitator) proteins. Mammalian members of CDF transporters are also named ZnT (zinc transporter). The key function of ZIP family transporter is to increase the cytosolic zinc concentration, either through import from the extracellular space or release from cellular organelles; while the key function of CDF family is to reduce the cytosolic zinc concentration through export to extracellular space or sequestration into organelles[6].

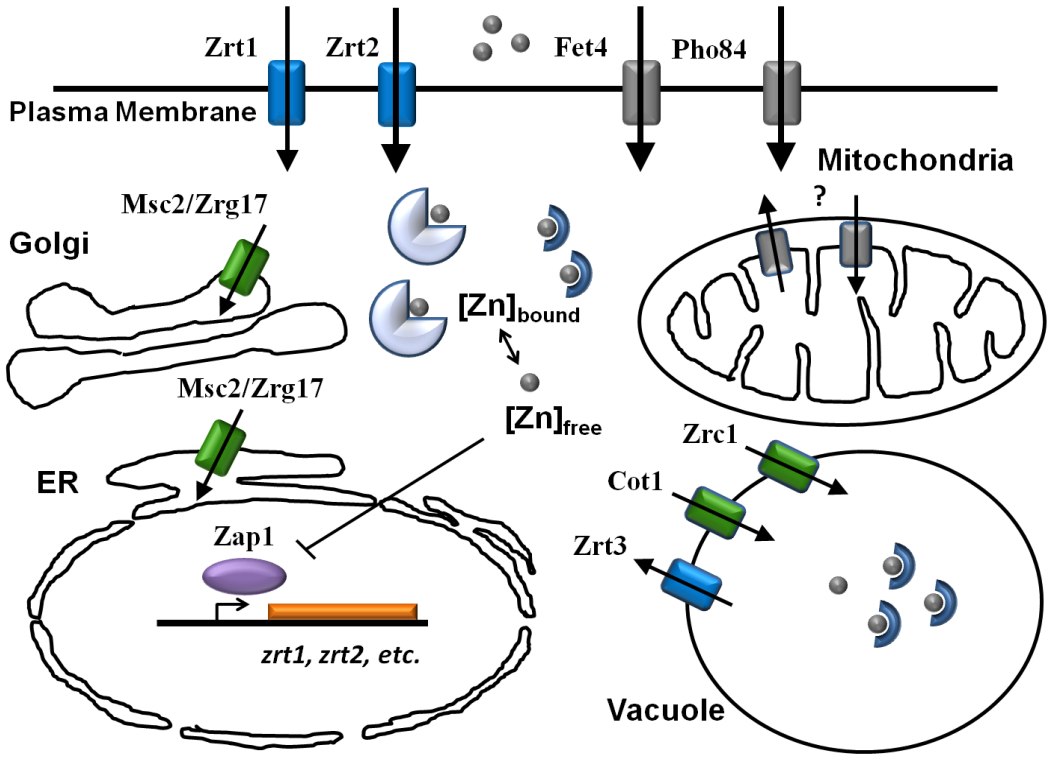

Figure 1.1. Zinc homeostasis in *S. cerevisiae*. Under high zinc stress, the major detoxification mechanism in yeast is zinc sequestration into the vacuole catalyzed by Cot1 and Zrc1. Under zinc deficient conditions, the zinc-dependent transcription factor, Zap1, up-regulates the expression of the plasma membrane transporters Zrt1/2 and Fet4 as well as the vacuole transporter Zrt3 to promote zinc intake and mobilization from the vacuole to maintain the cytosolic zinc level. ZIP and CDF transporters are colored in blue and green, respectively.

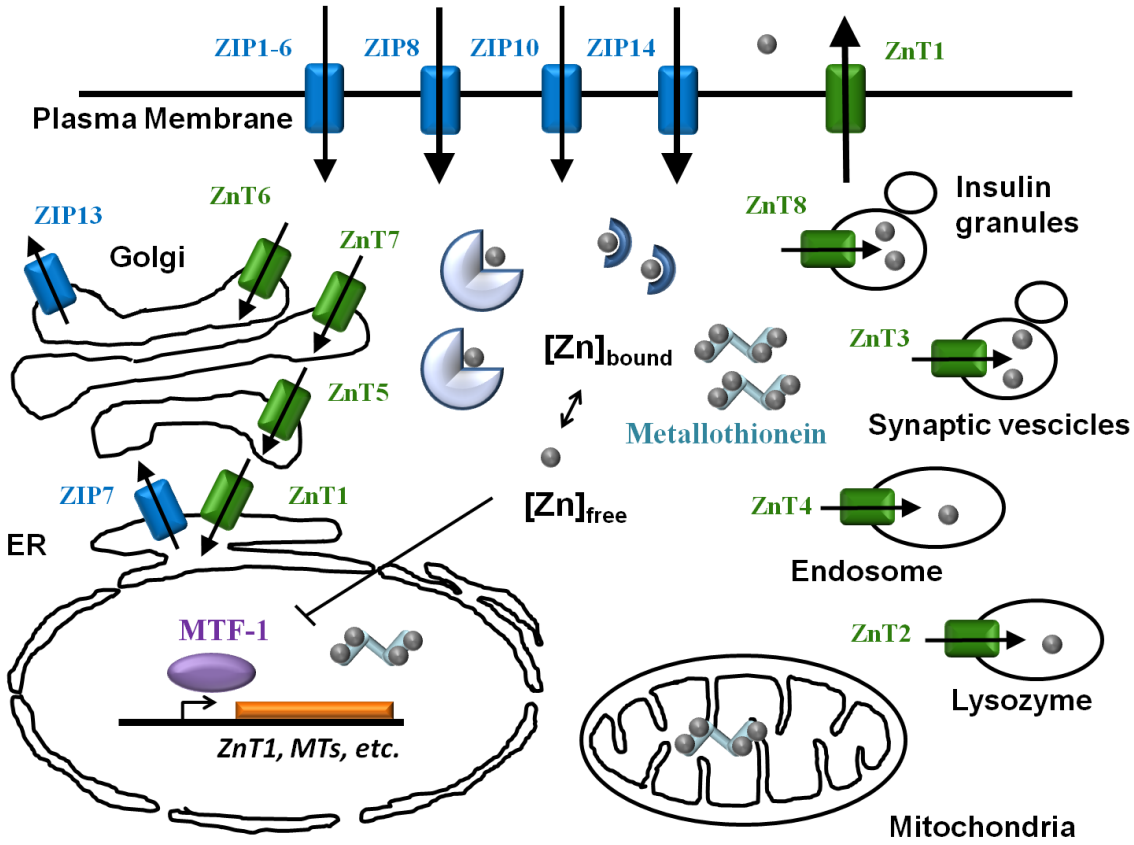

Figure 1.2. Zinc homeostasis in mammalian cells. MTF-1 is the zinc-dependent transcription factor that is the major regulator of zinc homeostasis in mammalian cells. MTF-1 up-regulates the expression of the membrane zinc exporter ZnT1 and metallothionein to enhance zinc efflux and sequestration by intracellular ligands under high zinc stress. ZIP transporters increase the cytosolic zinc concentration by importing zinc from the outside or releasing zinc from the organelles into the cytosol. ZnT transporters decrease the cytosolic zinc concentration by zinc efflux to the outside or sequestration into organelles. ZIP (blue) and ZnT (green) transporters carry various tissue-specific functions. Some ZnT type transporters shuttle zinc into specialized secretory vesicles, including insulin granules and synaptic vesicles.

ZIP Family Zinc Transporters

Structurally, ZIP proteins have eight predicted transmembrane domains (TMDs) with extracellular N- and C- terminal extensions. A conserved histidine-rich region

occurs on the intracellular loop between TMD 3 and 4 with unclear function (with the exception of Zip14, which has an extracellular His-rich loop). TMD 4 and 5 are predicted to form a cavity for the passage of metals due to the sequence conservation and amphipathic nature of these domains[50]. The mechanism of transport by ZIP family members is believed to be a facilitated process driven by the concentration gradient of HCO_3^- and is not ATP dependent[51].

In yeast, Zrt1 and Zrt2 are ZIP family transporters located on the plasma membrane[6]. Zrt1 is a high affinity zinc importer with an apparent zinc affinity of ~ 10 nM[52]. Zrt1 is up-regulated through the zinc-responsive transcription factor Zap1 under zinc limiting conditions and is required for growth under these conditions. Zrt2 has a lower apparent zinc affinity of ~ 100 nM[53]. Zrt2 is induced by Zap1 under mild zinc limiting conditions but suppressed under severe zinc deficiency[54]. This delicate transcriptional control ensures that the cells are able to adjust to changes to environmental zinc quickly. A third ZIP family member, Zrt3, is located on the membrane of the vacuole to release zinc from storage in the vacuole under zinc deficient conditions[55]. Zrt3 is also up-regulated under low zinc conditions by Zap1.

In humans, 14 members of the ZIP family have been identified, ZIP1 – 14[50]. These zinc importers are expressed to various degrees in different tissues and carry out distinct functions. ZIP1 is expressed in a wide variety of tissues and cells, and localized to different areas of the cell in a cell-type-specific manner[56]. Down-regulation of ZIP2 and ZIP3 as well as lower zinc contents were observed in prostate cancer patients[57]. ZIP4 is abundantly expressed in small intestines, stomach, colon and kidney, carrying out important functions for zinc absorption and reabsorption. Mutation in this gene causes

acrodermatitis enteropathica (AE), a rare, autosomal recessively inherited disease of intestinal zinc malabsorption[58]. Expression of ZIP4 appears to be regulated by both transcriptional and post-transcriptional mechanisms in response to zinc availability[56]. ZIP6 is expressed more in tissues sensitive to steroid hormones such as the placenta, mammary gland, and prostate. Recent studies also find that ZIP6 is associated with the development of estrogen-receptor-positive cancers, and is also important to the innate immune response of dendritic cells[26, 59]. ZIP8 and ZIP14 are the main transporters for Cd^{2+} upon cadmium exposure[60]. ZIP10 is expressed in the kidney, and is the only Zip genes that is regulated by the metal response element (MRE)-binding transcription factor-1 (MTF-1)[61]. ZIP13 is located on the Golgi apparatus. Defects in ZIP13 are associated with spondy-locheiro dysplastic form of Ehlers-Danlos syndrome (SCD-EDS), a rare genetic disease that features dysfunction of lysyl hydroxylase (LH1)[62]. The ZIP13-/- knockout is proposed to cause elevated intracellular Zn^{2+} which competes with the Fe^{2+} cofactor required for proper function of LH1.

CDF Family Zinc Transporters

The CDF family can be divided into three subfamilies. Subfamily I is found primarily in prokaryotic cells, while subfamilies II and III are in both prokaryotes and eukaryotes[63]. Most CDF proteins have six transmembrane domains (TMDs) and cytoplasmic N- and C-terminal extensions, with the exception of Msc2 and ZnT5 which have several TMDs in addition to the 6 canonical motifs[64, 65]. CDFs also feature a long histidine-rich loop between TMDs IV and V, which is predicted to be a metal binding site

important for function. Many CDF transporters appear to function as Zn/H^+ or Zn/K^+ antiporters, utilizing the gradient of H^+ or K^+ to drive zinc transport[66].

CDF zinc transporters are important in maintaining cytosolic zinc concentrations and ensuring proper distribution of zinc through various cellular organelles. There are no plasma membrane zinc efflux systems in yeast, an unusual instance among eukaryotes. Instead, yeast detoxifies excess zinc through storage in the vacuole and endoplasmic reticulum[6]. Upon exposure to high environmental zinc, excess zinc is shuttled into the vacuole of *S. cerevisiae* through two Zn^{2+}/H^+ antiporters, Zrc1 and Cot1[67]. Zinc binds to anions in the vacuole, primarily phosphate, and is released by the transporter Zrt3 to replenish the cytosolic pool under zinc deficiency conditions. The heteromeric CDF transporters Msc2/Zrg17 transport the cytosolic zinc into ER for utilization by newly synthesized metalloproteins in yeast[68].

Ten members of the ZnT family (a nomenclature for mammalian CDF zinc transporters), have been found so far in humans, performing various functions in inter- and intra-cellular trafficking of zinc in a tissue-specific manner[50]. ZnT1 is ubiquitously expressed, with elevated levels found in tissues associated with zinc acquisition, reabsorption and transfer, such as basolateral membranes of small intestines, tubules of kidney and villous yolk sac membrane. The ZnT1-/- knockout in mice is embryonic lethal, suggesting a critical role in early embryonic development[69]. The expression of ZnT1 responds to the dietary zinc supply, and is up-regulated by MTF-1 under zinc deficiency[70]. Many ZnT family members are involved in specialized secretion of zinc in various tissues. ZnT4 is required for the transfer of zinc to milk, and its mutation causes a “lethal milk” phenotype that the offspring die from severe zinc deficiency in mice[71].

ZnT3 is localized to certain synaptic vesicles that accumulate high levels of zinc together with neurotransmitters such as glutamate[72]. ZnT8 in pancreatic β-cells enriches zinc for packaging with insulin in the secretary vesicles[73].

1.2.2.2 Metallothioneins

Metallothioneins are small cysteine-rich proteins that play important roles in metal detoxification and protection against oxidative stress[74]. Four isoforms of metallothioneins are found in humans[75], MT-1 and MT-2 are ubiquitous but elevated in the liver and kidneys. MT-3 and MT-4 are primarily found in the central nervous system and certain epithelial tissues, respectively. MT-1 and MT-2 are up-regulated by the metal response element (MRE)-binding transcription factor-1 (MTF-1) under various stimuli including metal ions, glucocorticoids, cytokines and oxidative stress[76, 77]. Mammalian metallothioneins have two domains: a β-domain with 9 Cys, which sequesters 3 Cd^{2+}/Zn^{2+} or 6 Cu^{+} ions as thiolates, and an α-domain with 11 Cys sequestering 4 Cd^{2+}/Zn^{2+} or 6 Cu^{+} ions[78]. Metallothionein can bind to Zn^{2+} with varying affinities from $K_D \sim 20$ nM to $K_D \sim 2$ pM, and functions as an important zinc buffer in the cell that sequesters excess zinc ions and releases them under starvation conditions[43]. MT-null mice showed growth deficiency under both low and high zinc conditions[78].

1.2.2.3 Transcription Factors of Zinc Regulation

Zap1 in Yeast

Zap1 is the central regulatory transcription factor of zinc homeostasis system under zinc deficiency. Zap1 binds to the zinc-responsive element (ZRE) sequence in the promoter region of its target genes, and acts as a transcriptional activator in most of the cases[79]. Structurally, Zap1 has a C-terminal DNA-binding domain (DBD) consisting of five C_2H_2 zinc finger motifs. Two activation domains, AD1 and AD2, activate transcription in response to low zinc levels in the nucleus[80]. Zinc binding to AD1 and AD2 inhibits their ability to activate transcription. Zinc binding to AD2 is labile involving a constant cycle of zinc binding and release, allowing for rapid sampling of the cell's zinc status[81]. More than 80 genes were identified as direct targets of Zap1 activation in yeast, and several genes are repressed in a Zap1-dependent manner[49]. To maintain cytosolic zinc concentration under zinc deficiency, Zap1 up-regulates membrane zinc transporters to promote zinc intake catalyzed by Zrt1, Zrt2 and Fet4, as well as mobilization from the vacuole by Zrt3. Zap1 also mediates other adaptive responses including isozyme switching, oxidative stress responses and phospholipid synthesis, etc.

MTF-1 in Mammalian Cells

Metal responsive element-binding transcription factor-1(MTF-1) plays critical role in defense against heavy metals and oxidative stress in mammals. It has an N-terminal DNA-binding domain consisting of 6 regulatory C_2H_2 zinc fingers, and a C-terminal transcription activation domain. The zinc fingers of MTF-1 appear to have affinities in the picomolar to low nanomolar (10^{-10} – 10^{-9} M) range[82, 83]. While the majority of MTF-1 resides in the cytosol, exposure to high zinc induces rapid

translocation of MTF-1 from the cytosol to the nucleus where it binds to the metal responsive element (MRE) sequence in the promoter regions of the target gene and activates transcription[84]. The identified direct targets of MTF-1 include the zinc exporter ZnT1, metal-inducible metallothioneins, and glutamate-cysteine ligase heavy chain (γGCS_{hc}), an oxidative stress-related protein[85]. Many other genes are also appear to be regulated by MTF-1, though not in a metal dependent manner.

1.2.3 Zinc Homeostasis in Prokaryotes

Bacteria often need to be able to adapt to dramatic changes in environmental zinc concentrations. Therefore, an effective regulatory mechanism is necessary for surviving in low zinc conditions or protecting the cells from the toxic effects of excess zinc. Zinc homeostasis in prokaryotes is primarily achieved by the influx and efflux systems that are regulated separately by their own transcription factors[7]. Bacteria generally lack metallothionein-like proteins to function as a specialized intracellular zinc buffering agent, with the exception of cyanobacteria and mycobacteria[86]. In some gram-negative bacteria, such as *E. coli*, certain periplasmic proteins that participate in defense against envelope stress, such as ZraP and Spy, are also up-regulated in response to zinc, potentially alleviating protein denaturation under high zinc conditions[87-89]. Below we demonstrate zinc regulation in prokaryotes using *E. coli* as an example (Fig. 1.3).

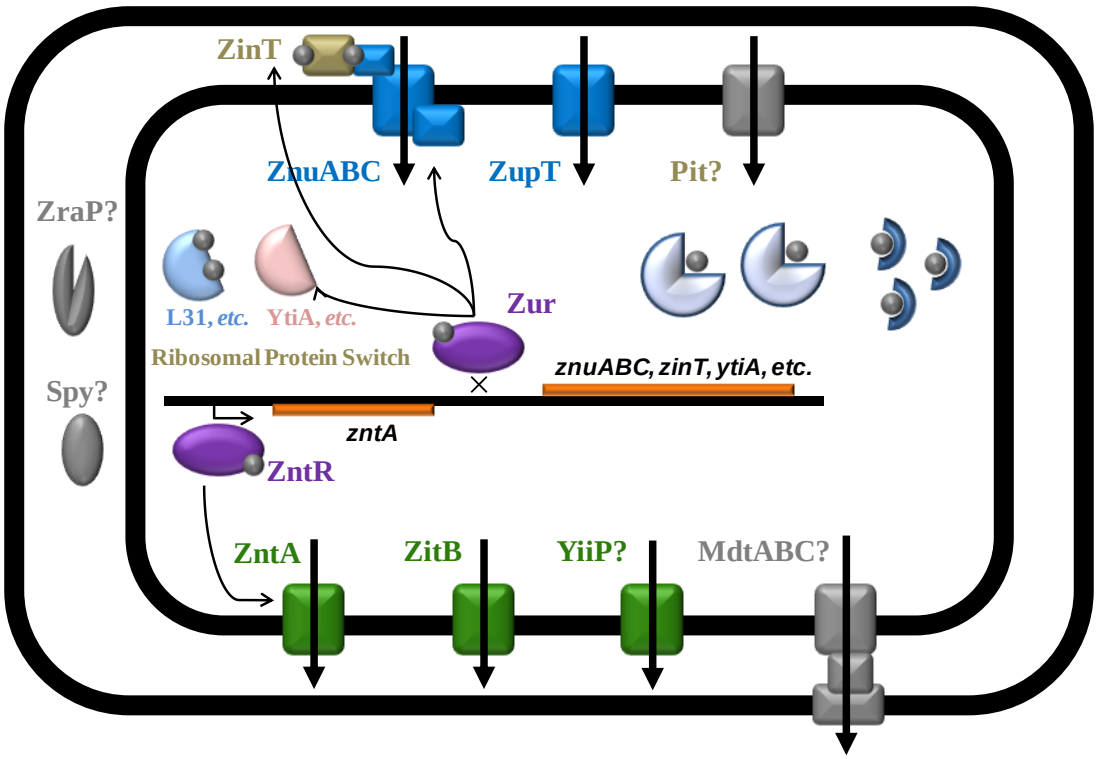

Figure 1.3. Zinc homeostasis in *E. coli*. Zinc homeostasis is primarily controlled by membrane transporters. ZntR activates the expression of ATP dependent zinc exporter ZntA under high zinc stress. Zinc deficiency is sensed by Zur, which de-represses the expression of the high affinity exporter ZnuABC. Ribosomal protein switch under zinc deficient conditions are also controlled by Zur, releasing zinc for use by other key cysosolic metalloproteins.

1.2.3.1 Zinc Transporters and Regulators

Binding-protein-dependent ABC (ATP-binding cassette) transporters are responsible for zinc uptake under low zinc concentration. In *E. coli*, the high affinity zinc uptake system ZnuABC (zinc uptake) is an ABC transporter that was first found up-regulated in cells grown on plates containing high EGTA[90]. ZnuA is a periplasmic metal binding protein that binds zinc specifically. ZnuB is the transmembrane ion channel, and

ZnuC is the cytoplasmic ATPase that drives the conformational change necessary for metal transport through ATP hydrolysis[90]. Later a fourth component of this transporter system, ZinT, was discovered. This protein cooperates with ZnuA in zinc recruiting by forming a binary complex and it is important for metal scavenging during severe zinc shortage[91, 92]. ZnuABC has an apparent K_D for zinc transport of ~ 9 nM. Over expression of ZnuABC renders the cells hypersensitive to zinc toxicity, while deletion of ZnuABC inhibits cell growth under zinc depleted conditions[90]. ZnuABC and ZinT are also important for the virulence of some pathogens, as inactivation of the these genes reduces the ability of bacteria to adhere to epithelial cells as well as its virulence[93].

ZnuABC and ZinT are both regulated by the Fur family transcription factor Zur (zinc uptake regulation)[94]. Zur forms a homodimer that can bind two zinc ions per dimer. Zur acts as a repressor that binds to DNA in the presence of Zn^{2+}, and dissociates from DNA in the presence of chelators, therefore enabling the transcription of the target genes[90, 95]. Previous experiments have shown that *in vitro* Zur-mediated mRNA transcription was inhibited by femtomolar zinc[41]. In addition to ZnuABC and ZinT, Zur also controls the replacement of zinc-binding ribosomal proteins with non-zinc-binding paralogues under zinc deficiency in *B. subtilis*[96]. Therefore, Zur could be recognized as a regulator for adaption to zinc depletion.

ZupT is a ZIP family member transporter that mediates zinc uptake in *E. coli*. Over-expression of ZupT enhances zinc uptake and renders cells hypersensitive to zinc toxicity[97]. Growth of *E. coli* with the double knockout of *znuABC* and *zupT* was inhibited by EDTA at a much lower concentration than the single knockout mutants or wild type[97]. ZupT transports a broad spectrum of divalent ions, including Fe^{2+}, Co^{2+}, and

Mn^{2+} [98]. ZupT is constitutively expressed at a low level and it is not subject to metal regulation. Other metal transporters could also be involved in zinc transport at zinc replete and non-toxic concentrations. For example, co-transport of metals with phosphate via the inorganic phosphate transporter Pit was observed[99].

Three types of zinc export systems have been identified in bacteria: resistance-nodulation-cell division (RND)-type multi-drug efflux transporters, P-type ATPases, and cation diffusion facilitators (CDF)[7]. P_{1B}-type ATPases are commonly found in most organisms for catalysis of heavy metal transport, including the copper exporters CopA/B in *E. coli* and cadmium/zinc exporters CadA in *B. subtilis*[100]. P_{1B}-type ATPases contain 6 – 8 transmembrane domains, a large cytosolic ATP binding loop, and a cytosolic metal binding domain. The cytosolic metal binding domain recruits metal ions frequently complexed with chaperones or chelators and transfers the uncomplexed ions to the transmembrane ion channel[101]. RND-type (resistance-nodulation-cell division) multi-drug resistant transporters are only found in a few gram-negative bacteria. They generally form a trans-envelope channel that allows very efficient export of substrates across the membrane envelope of the cell to the outside[102]. A member of this family, CzcABC, was found to be the major defense for the highly zinc resistant bacteria *R. metallidurans*[103].

E. coli ZntA (zinc transporter A) is a P_{1B}-type ATPase responsible for detoxification of Zn^{2+} and Cd^{2+}. This protein has eight transmembrane domains with a conserved metal binding CPC motif on TMD VI, a second metal binding site on the cytosolic N-terminus, and an ATPase catalytic loop between TMD VI and VII[104]. Deletion of ZntA dramatically increases the cells sensitivity to zinc and cadmium, while

over-expression of ZntA confers enhanced resistance[105]. ATP-driven zinc transport of ZntA exhibits an apparent K_m of 9 μM, significantly higher than the estimated free zinc concentration in cells[104]. Indeed, *in vitro* studies suggesting that thiolate-bound Cd^{2+} or Zn^{2+} are the best substrates for ZntA[106].

As the most important exporter for zinc detoxification in *E. coli*, ZntA is regulated by ZntR, a MerR-like transcription factor that is activated by zinc[107]. ZntR forms a dimer that binds 1 to 2 zinc ions per monomer, depending on the reducing potential[107]. The apo-ZntR dimer binds to the promoter of the *zntA* gene and weakly represses transcription; zinc-bound ZntR is a transcriptional activator that induces DNA unwinding to enhance RNA polymerase binding to the -35 and -10 positions of the promoter to initiate transcription[107]. In addition, formation of the Zn-ZntR-DNA complex also reduces degradation of ZntR catalyzed by *E. coli* proteases[108]. *In vitro* measurements indicate that ZntR has an apparent femtomolar affinity for both zinc binding and zinc-dependent activation of transcription in TPEN-chelated zinc buffers[41, 109].

Another zinc exporter, ZitB, belongs to the CDF family. Over-expression of ZitB enhances the cells' zinc resistance[110]. Although deletion of *zitB* alone does not have an effect on cells' survival under high zinc, double deletion of *zitB* and *zntA* does render the cells slightly more sensitive to zinc stress compared to the single deletion of *zntA*[110]. ZitB is an antiporter catalyzing the exchanges of Zn^{2+} or Cd^{2+} for H^+. The exchange stoichiometry of metal ion for proton is likely to be 1:1[111]. Stopped-flow measurements of tansmembrane fluxes of metal ions revealed that ZitB-mediated zinc transport has a K_m of ~105 μM[111]. β-galactosidase activity in a *zitB-lacZ* transcriptional fusion strain was

significantly higher after 3 h of incubation with 50 – 100 μM zinc, though no specific regulator for ZitB expression has been found[110].

Yiip, a homolog of ZitB, is another CDF protein and Me^{2+}/H^{+} antiporter. However, the role of Yiip in zinc regulation *in vivo* is less well-defined. Though transcription of *yiip* is induced by zinc and *in vitro* thermodynamic studies demonstrated a nanomolar K_m for zinc transport, no involvement of Yiip in zinc homeostasis could be detected in the cell[112, 113]. Yiip appears to function as an iron exporter *in vivo* as reduced accumulation of ^{35}Fe was observed when Yiip was expressed *in trans* and double deletion of *yiip* and *fur* enhances cells' sensitivity to iron compared to deletion of *fur* alone[114].

A RND-type transporter, MdtABC-TolC complex, is involved in metal resistance in *Salmonella* as deletion of these genes inhibits cell growth in medium containing high zinc and copper[115]. MdtB and MdtC form a heterodimeric channel across the inner membrane, and are connected to TolC on the outer membrane through the membrane fusion protein MdtA[116]. Expression of these proteins is regulated by BaeS/R, a two-component transcription regulatory system that responds to copper and zinc[117]. The role of MdtABC-TolC in metal homeostasis in *E. coli* is yet to be established.

1.2.3.2 Intracellular and Periplasmic Ligands

Among bacteria, metallothein-like metal binding proteins that modulate intracellular zinc homeostasis have only been identified in cyanobacteria and mycobacteria[86]. In addition to the tight-binding zinc metalloproteins, small molecules and nucleic acids have been proposed to be involved in modulation of cytosolic zinc concentration as well as the zinc transport systems. The role of glutathione (GSH), an

abundant thiol-containing molecule and low affinity zinc ligand, in zinc homeostasis was studied in *E. coli*[118]. While the loss of the ability to synthesize GSH influenced metal tolerance in wild-type cells only slightly, deletion of the GSH biosynthetic pathway in *zntA* deletion cells led to a strong decrease in resistance to Zn and Cd toxicity. Ribosomal proteins are also proposed as potential zinc storage sites. Three non-zinc-binding ribosomal protein paralogs (YtiA, RpmGC and YhzA) are part of the Zur regulon in *B. subtilis*[91]. Under zinc starvation conditions, these non-Zn-containing ribosomal proteins can replace the Zn-containing proteins (L31, L33, L34), therefore mobilizing the ribosomal zinc for usage by other key metalloproteins. Since ribosomes are highly abundant in the cell, this replacement could contribute to a significant portion of the intracellular zinc pool.

In gram-negative cells, some periplasmic proteins are involved in defending the cells against zinc stress. Two periplasmic proteins are up-regulated under high zinc stress[7]. ZraP (zinc resistance-associated protein) is a 12-kDa periplasmic protein with two His-rich motifs that bind zinc specifically (affinity measured *in vitro* $Zn^{2+} > Co^{2+} > Cd^{2+}$). The expression of ZraP is up-regulated through a two-component system ZraS/R upon zinc exposure, confering zinc resistance[119]. ZraP is also a zinc-dependent molecular chaperone that is involved in the envelope stress response, protecting proteins from denaturation caused by various stresses[88]. Spy, another small periplasmic protein belonging to the same family as ZraP, is also induced under high zinc as well as other envelope stress conditions[87, 120].

1.3 ZINC QUANTIFICATION AND SENSOR DEVELOPMENT

1.3.1 Methods for Quantifying Total Zinc

Total zinc content in biological samples can be detected fairly accurately at the current state of technologies. Analysis could be performed at nanogram level of zinc with precision of 1 ~ 2%[2]. Since zinc contains a filled d orbital ($3d^{10}4s^{0}$), it cannot be directly detected by optical absorption, emission, electron paramagnetic resonance, or related techniques. Atomic absorption spectroscopy (AAS), inductively coupled plasma mass spectroscopy (ICP-MS), and x-ray fluorescence (XRF) are the three most commonly used analytical techniques for total zinc quantification in biological samples[121-124]. However, none of these methods are suitable for imaging zinc in live samples.

Flame AAS is a widely accepted method that requires a low cost instrument and is easy to use. However, AAS is not suitable for measuring multiple elements simultaneously. Therefore, flame AAS is suitable for running through a large number of samples for a limited number of elements. On the other hand, ICP-MS requires a more sophisticated instrument with high maintenance costs and specialized operation, but it has exceptional multi-element measurement capacity and good detection limits.

Spatial information about metal ions is completely lost during sample preparations for AAS and ICP-MS. X-ray fluorescence (XRF) is a nondestructive method for the elemental analysis of solids and liquids, and has been employed to image metal distribution in dehydrated biological samples[124]. In this method, the sample is irradiated by an intense x-ray beam that causes the emission of fluorescence x-rays from inner shell electrons of metal ions. The wavelength of the emitted x-rays tells the identity

of the element and the intensity determines the concentration. XRF can detect more than 10 elements simultaneously. Combining x-ray fluorescence and traditional light microscopy (brightfield or fluorescence), one can determine the metal distribution and total concentration in the cell sample[125], although XRF does not allow live cell imaging.

1.3.2 Methods for Detecting and Quantifying Free Zinc

Research in zinc biology has highlighted the importance of changes in the intracellular free zinc in regulating various cellular processes. To understand the role of zinc in the cell, it is necessary to establish correlations between changes in zinc concentration and other cellular events. Therefore, zinc sensors that meet the following criteria for live cell imaging are in great need:

(i) Selective binding of zinc over other metals abundant in the cell. Intracellular free Ca^{2+}, Mg^{2+} and Fe^{2+} are estimated at 0.05 – 1 μM[126-128], 0.5 – 1 mM[129], and 0.1 – 10 μM[130-132] respectively, orders of magnitudes higher than the estimated free zinc concentration at the pM to low nM range. High selectivity for zinc binding is necessary in the presence of these metals.

(ii) Appropriate affinity and a wide dynamic range to measure dramatic changes in free zinc. While intracellular free zinc in normal resting cells is estimated in the pM range, free zinc can increase dramatically to μM and possibly mM levels in some cases. For example, intracellular zinc release under oxidative stress has been reported at the μM level, and pre-synaptic zinc release is estimated at the sub-mM level[25, 133]. A sensor with

a K_D comparable to the estimated range of free zinc concentration in the sample is optimal for these measurements.

(iii) Fast kinetics to ensure rapid response and reversibility. Many biological processes occur within seconds, or even milliseconds. It is critical to use a sensor that has very fast on- and off-rate constants to accurately report the changes of the zinc, especially to study zinc signaling.

(iv) Sensitivity and significant signal changes. To minimize the background and increase the signal-to-noise ratio, sensors that exhibit large changes in signal upon zinc binding are highly desirable.

(v) Solubility and permeability. The sensor should be delivered to the cells with minimal invasion, and remain in place during the course of study. Many small molecule sensors are delivered in a cell-permeable ester form across the membrane into the cells, and then retained in the cytosol thereafter in an acid form after the cellular esterase breaks the bond. Genetically encoded sensors have the natural advantage of being expressed in the cell.

(vi) Ratiometric measurements. To advance the understanding of zinc homeostasis, more accurate quantification of the zinc concentrations is required, especially in determining potential molecular targets of free zinc ions based on the affinity of the proteins. Therefore, sensors that utilize ratiometric parameters to control for the variations in loading concentration, cell thickness, and optical artifacts are of great value.

(vii) pH stability. Although the pH of cytosol is generally considered neutral within the range of 7.2 – 7.4, it does fluctuate under various physiological conditions[134]. In addition, pH can vary significantly in various organelles, ranging from ~ 4.5 in lysosomes to ~ 8 in mitochondria.

(viii) Phototoxicity and photostability. High energy short wavelength UV light is detrimental to the cells, and is associated with higher background noises by inducing cellular autofluorescence. A fluorescent sensor with a longer wavelength spectrum is more favorable.

Over the past two decades, we have seen substantial progress in the development of zinc sensors. The majority of the efforts have been focused on chemical fluorescent zinc sensors, though very exciting development in protein-based sensors has occurred in recent years[135]. Examples of small molecule zinc sensors and protein-based sensors are reviewed in the following sections.

1.3.2.1 Small Molecule Zinc Sensors

Chemical fluorescent zinc indicators typically consist of a zinc-chelating unit, such as iminodiacetate (IDA) or di-2-picolyamine (DPA), and a fluorescent reporting moiety that undergoes changes in quantum yield, emission wavelength, and/or fluorescence life time upon zinc binding. One of the mechanisms typically accounts for the zinc-binding induced fluorescence changes, photoinduced electron transfer (PET) or intramolecular charge transfer (ICT) (reviewed by Silva *et al.*[136]). For a PET sensor, the zinc chelating moiety normally contains a relatively high-energy non-bonding electron pair (e.g. nitrogen atom), which can quench the excited fluorophore by transferring an

electron. Zinc binding can switch on the fluorophore by blocking this quenching via coordinating and reducing the energy of the electron pair. A spacer module, normally less than a three-carbon linker for maximum PET efficiency, is needed to hold the chelator and fluorophore together at a proper distance for PET to occur. Most PET-type chemical zinc sensors utilize an increase in fluorescence intensity for detection of zinc, and are therefore not ratiometric. The ICT mechanism is generally used to generate ratiometric sensors. When a π-electron conjugation system is formed between the fluorophore and the directly connected chelator, the intermolecular charge transfer from the electron donor to the receptor is enhanced upon excitation by light. When the chelator is the electron rich donor, interaction with a cation reduces the charge transfer and result in a red shift of the emission spectrum. On the other hand, if the chelator is the electron receptor, zinc binding further strengthens the push-pull effects and results in a blue shift of the emission spectrum. A change in the ratio of emission from two wavelengths is therefore correlated with zinc binding to the sensor. Many types of small molecule zinc sensors have been developed based on these mechanisms (Fig. 1.4).

Quinoline-based sensors were the very first to be used in biological samples. Quinoline and its derivatives, especially 8-hydroxyquinoline and 8-aminoquinoline, are fluorogenic chelators for transition metals. TSQ (*p*-toluenesulfonamide quinoline) was first sensor that had sufficient selectivity for zinc for application in biological samples[137]. It was first used to stain the high zinc section in the hippocampus, leading to the discovery of the role of zinc in neurobiology. However, TSQ suffers from many drawbacks, including UV excitation, modest quantum yield, pH sensitivity, and importantly, poor water solubility[138]. TSQ also has an ambiguous zinc binding

stoichiometry, complicating its application in the cell. Zinquin, a second generation TSQ derivative, has a significantly enhanced fluorescence signal and improved pH profile, though it also suffers from other limitations similar to those of TSQ[139], including formation of ternary complexes with zinc and other biological molecules[140]. AQZ, a water-soluble carboxamidoquinoline derivative, exhibits an 8-fold increase in quantum yield and a 75 nm red-shift in emission spectrum thereby allowing ratiometric measurements. This sensor has been tested in yeast for zinc detection despite sensitivity to pH changes[141]. 6-MeOBQDMEN, a bisquinoline derivative, displays a relatively stable 40-fold increase in fluorescence intensity across pH range 4 - 8. It was tested for zinc sensing in cells but had limited water solubility[142].

The Zinpyr family sensors, developed by Lippard *et al*., are PET-based zinc indicators utilizing di-2-picolyamine (DPA) or its derivatives as the chelating moiety and fluorescein as the reporter[143-145]. Di-2-picolyamine (DPA) and its derivatives are popular choices as the chelating moieties. DPA is a metal binding fragment of TPEN, a high affinity transition metal chelator with high selectivity for Zn^{2+} over alkali and alkaline-earth metal ions. DPA is coupled with fluorescein, a fluorophore that has high extinction coefficient, high quantum yield and good water solubility. The first eight ZP sensors have sub-nanomolar affinities for zinc. Sensors ZP1-3 are cell permeable but exhibit high fluorescent background in the absence of zinc. To minimize the background from protonation of the tertiary nitrogen atom, substitution of halogen has been made on fluorescein. However, these substitutions resulted in low quantum yield[146]. Later a carboxylic acid was added to the 5 or 6 position of the fluorescein of ZP1 (Fig. 1.4), lowering the pK_a of the sensor and reducing the background. Improved ZP1 and ZP8

were used to image high level of zinc in hippocampal neurons[147, 148]. ZP1 has also been labeled with the substrate for the human DNA repair enzyme alkylguaninetransferase (SNAP-Tag) for localization in Golgi apparatus and mitochondria in Hela cells expressing AGT in specific locations[149].

Zin-naphthopyr 1 (ZNP-1) is a ratiometric sensor based on a seminaphtho-fluorescein platform that switches between taumeric forms of fluorescein and naphthofluorescein[150]. ZNP-1 is a single excitation-duo emission sensor with two emission peaks at 624 nm and 528 nm. Zinc binding can induce an 18-fold increase in the emission at 624 nm with little effects on fluorescence at 528 nm, which can be used for ratiometric measurements. However, it can be competitively quenched by other transition metals such as Fe^{2+}, which could potentially explain its lack of fluorescent signal in resting cells even with a 0.5 nM affinity[150].

To improve the zinc binding kinetics, DPA-derivatives such as *N*,*N*-di-(2-picolyl) ethylenediamine (DPEN) were used as the chelating moiety in the ZnAF sensors[151]. ZnAF-1 has a zinc affinity of 0.78 nM with fast zinc binding and improved metal selectivity. To make the sensors ratiometric, ZnAF-R1 and ZnAF-R2 (Fig. 1.4) were developed using benzofuran derivatives as fluorophores instead of fluorescein[152]. These sensors utilize the internal change transfer mechanism to generate a cation-induced blue shift in absorbance. The fluorescence emission ratio when excited at 340 nm and 380 nm was used for quantifying zinc. ZnAF-R2 sensors were tested for detection of free zinc changes in macrophage cells[152].

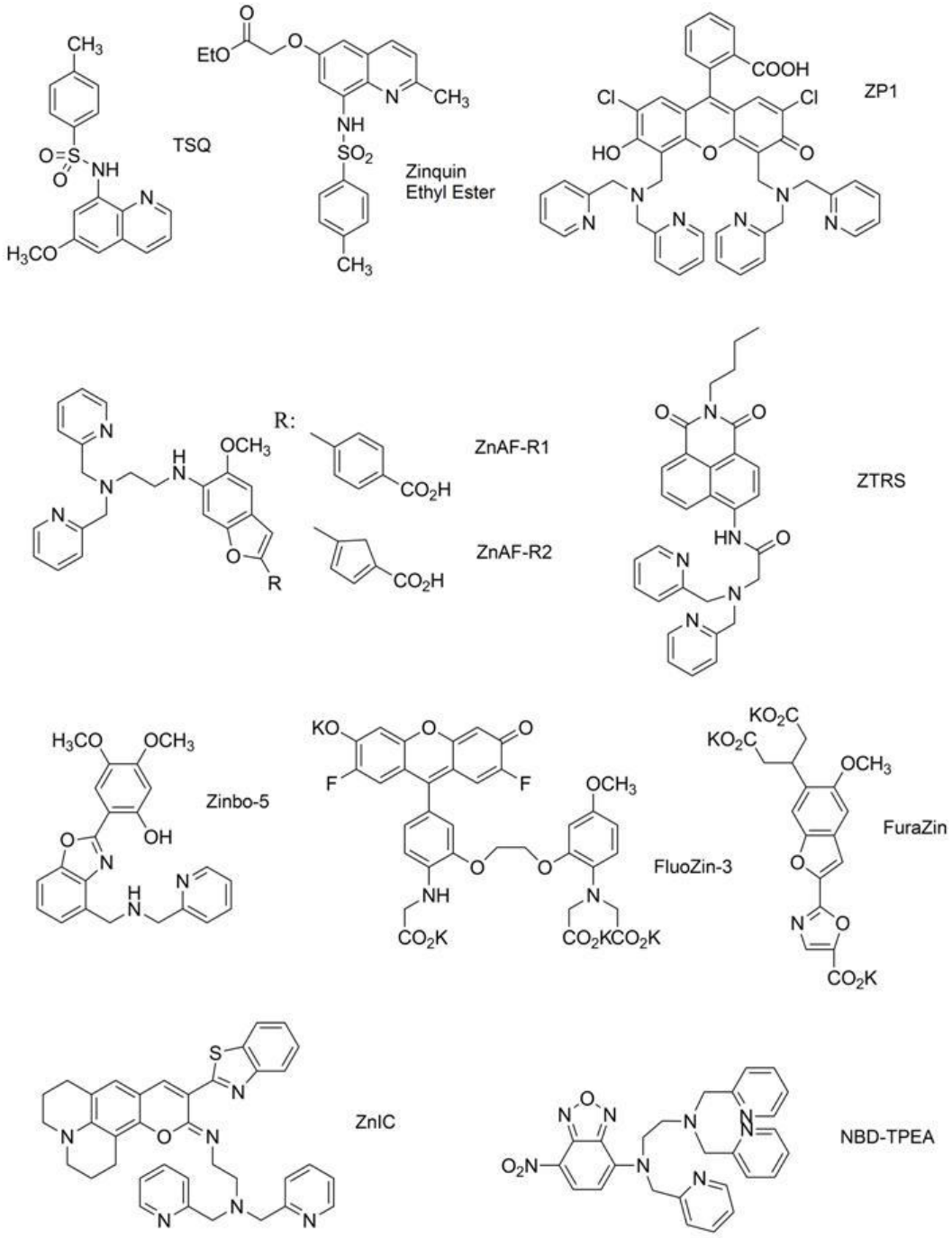

Figure 1.4. Examples of small molecule zinc sensors[153].

Lack of selectivity against heavy transition metals (HTMs) is a common drawback of DPA-based zinc sensors. Recently, Xu *et al.* reported a sensor with amide/di-2-picolyamine as the zinc binding scaffold coupled with a naphthalimide fluorophore, termed ZTRS, which possesses good selectivity against other heavy metals[154]. Zinc binds to ZTRS in an imidic acid tautomeric form, while other HTMs bind to the sensor in an amide tautomeric form. ZTRS has an apparent affinity for zinc of ~ 5 nM, exhibiting a 22-fold increase in fluorescence as well as a red-shift in emission from 483 nm to 514 nm upon zinc binding. ZTRS has been applied in mammalian cells and zebrafish embryos for living imaging of zinc. Though ZTRS cannot detect zinc in resting cells, it does show strong fluorescence in the zebrafish embryos and changing patterns as the embryo grows[154].

An emission ratiometric zinc sensor, Zinbo-5, was developed with benzoxazole as the fluorescent reporter and an aminomethyl pyridine moiety as the zinc binding component[155]. It exhibits a red-shift in emission from 407 nm to 443 nm as well as enhancement in fluorescence intensity with increasing zinc concentration. Zinbo-5 has a zinc affinity of 2.2 nM, and shows minimal fluorescence when used in mouse fibroblast cells without additional zinc[155].

Another class of widely used chemical zinc sensors marketed by Invitrogen was developed by modifying the existing BAPTA-based calcium sensors[156]. Fluorescent chemosensors nominally designed for Ca^{2+} or Mg^{2+} detection could theoretically be used for measuring zinc as these sensors normally have higher affinity for zinc than for Ca^{2+} or Mg^{2+}[157, 158]. To enhance the selectivity towards zinc and reduce the interference from cellular Ca^{2+}/Mg^{2+}, one or more of the original chelating moiety was removed to abolish

the calcium binding capacity. Most of the sensors have zinc affinities in the micromolar range (2 ~ 40 μM), suitable only for application in detecting high zinc content in the neurons. FluoZin-3 is the only sensor in this family that has nanomolar affinity (K_D ~ 15 nM), and has been widely used for detection of large increases in intracellular free zinc[159-165]. FuraZin and IndoZin are two ratiometric indicators with K_D ~ 3 μM. FuraZin exhibits a fluorescence excitation wavelength shift from 378 to 330 nm with increasing zinc binding, while IndoZin shows a blue shift in emission from 480 nm to 395 nm[156]. However, when tested in cultured neurons for zinc measurements, FuraZin-1, FluoZin-2 and Newport Green showed little difference in apparent sensitivity to zinc due to high sensor concentration, even though these dyes exhibited various zinc affinities *in vitro* from 20 nM to 3 μM[166].

NBD-TPEA is another ratiometric zinc sensor with micromolar affinity reported recently[167]. It can be excited with visible light at 469 nm, which is important for application *in vivo* since it reduces the UV light-induced damage to the cells. It was adapted from a reported Cu^{2+} sensor, 4-bis(pyridine-2-ylmethyl)amino-7-nitro-2,1,3-benzoxadiazole (NBD-BPA). To enhance zinc binding, an additional BPA moiety was introduced to replace one of the pyridine of NBD-BPA to coordinate with Zn^{2+} in a synergic manner with the retained (pyridine-2-yl)methylamine (PMA) motif. NBD-TPEA exhibits an emission shift from 550 to 534 nm together with a decrease in fluorescence intensity upon zinc binding. When applied to cells, it tends to accumulate in lysosome and Golgi. It has been used to visualize zinc in zebrafish embryos[167].

Iminocoumarin-based ratiometric fluorescent zinc sensors have been developed recently[168]. ZnIC was constructed with iminocoumarin as the fluorophore and

(ethylamino)-dipicolylamine as the zinc chelator. It exhibits a red shift in emission from 543 nm to 558 nm, and has an apparent zinc affinity of 1.4 pM *in vitro*. The sensor has good selectivity and the fluorescence ratio is almost pH insensitive, which makes it a good candidate for application in the cell. It was used for imaging zinc in HEK293 cells and staining the zinc rich region of a rat hippocampal slice[167].

1.3.2.2 Protein/Peptide-based Zinc Sensors

While significant progress has been made in the development of small molecule zinc sensors, few of them are able to quantify the free zinc in normal resting cells due to the limit in affinity, lack of ratiometric response, and/or other issues. Recent years there have been exciting developments in protein-based zinc sensors. Most protein-based sensors are designed with a cation-binding domain and a pair of fluorophores, such as fluorescent proteins, capable of undergoing fluorescence resonance energy transfer (FRET) (Fig. 1.5). Zinc binding can induce a conformational change that alters the orientation and distance of the fluorescent proteins, causing a change in the FRET efficiency. This change in FRET is by definition ratiometric, therefore can be used for quantifying zinc concentration with proper calibrations. These sensors can be readily expressed in the cell without the difficulty of sensor loading. Furthermore, they can be tagged with organelle-specific sequences and targeted to subcellular compartments for accurately tracking zinc in the cell. These unique advantages have been demonstrated in the following work.

The zinc finger domain has picomolar to nanomolar affinity and superior selectivity for zinc, making it a very good candidate as the chelating moiety for zinc

sensors. Berg *et al.* developed a FRET-based sensor (CP-L-F) using a synthetic zinc finger domain. In this synthetic sensor, the zinc finger domain was conjugated to a pair of FRET fluorophores, fluorescein (F) and lissamine (L). Zinc binding causes the domain to fold and bring the fluorophores close together, generating a 2-fold increase in FRET emission. The apparent dissociation constant for Zn(CP-L-F) was estimated to be 1 pM at pH 7.1, indicating that the fluorophores did not affect the zinc binding affinity of the domain[169]. In ZNS1, a sensor developed by Imperiali *et al.*, a fluorophore was incorporated near the zinc binding pocket. Without zinc, the fluorophore is exposed to the polar environment of the solution and the fluorescence is quenched; upon zinc binding, the pocket is enclosed and the fluorophore is shielded from the polar environment, resulting in an almost 7-fold increase in emission[170]. A third set of sensors was designed based on chelation-enhanced fluorescence (CHEF). A novel fluorescent zinc binding amino acid containing 8-hydroxy-5-(N,N-dimethylsulfonamido)-2-methylquinoline (Sox), and another traditional amino acid zinc ligand, such as Cys, were linked together by a beta turn peptide. Zinc binding to Sox and the other ligand induces a fluorescence enhancement[171]. Though these synthetic sensors appear promising, they cannot be readily delivered into the cells for imaging.

To overcome this, Palmer *et. al.* developed genetically encoded sensors that can be expressed in the cells by flanking the zinc finger motif with a FRET pair, yellow fluorescent protein (YFP) and cyan fluorescent protein (CFP)[46] (Fig. 1.5(a)). The group developed methods for *in situ* calibration of the sensors in mammalian cells and also targeted the sensors to mitochondria. These sensors exhibit moderate changes in FRET

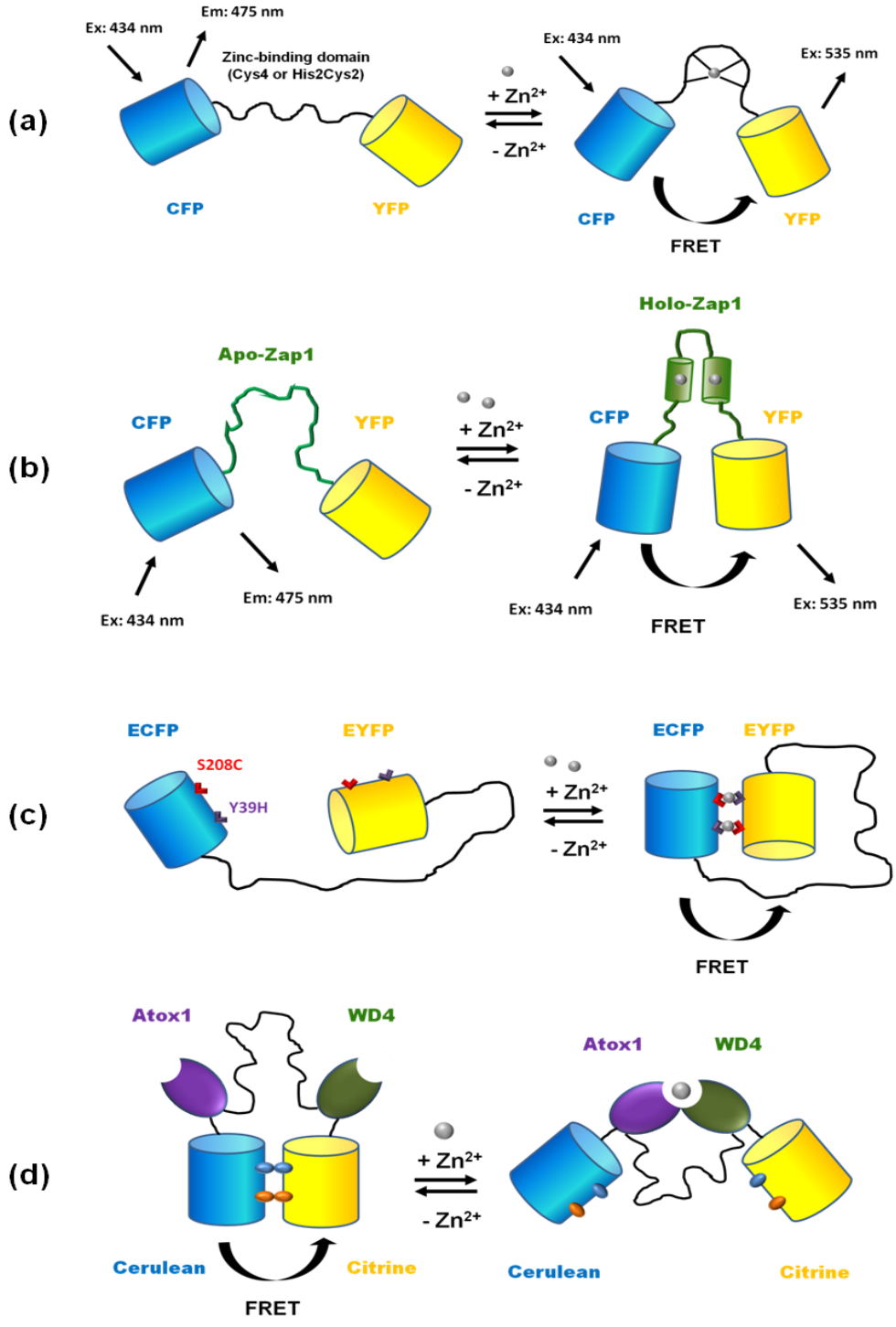

Figure 1.5. Examples of FRET-based protein sensors[45, 46, 172, 173].

ratio in the cell. Zif1, the sensor with 2 cysteines and 2 histidines as the zinc ligands, has an apparent zinc affinity of 1.5 μM, and the one with 4 histines has an affinity of 200 μM. The decrease in zinc affinity implies that the zinc binding structure is perturbed when conjugated with larger fluorescent proteins. These sensors were not sensitive enough to detect free zinc in resting cells.

Eide *et al*. cleverly engineered the zinc transcription factor Zap1 into a fluorescent indicator to report its own zinc binding status[81]. The zinc fingers pairs of Zap1 were flanked by enhanced yellow fluorescent protein (EYFP) and enhanced cyan fluorescent protein (ECFP), allowing detection of zinc-induced conformation changes by FRET (Fig. 1.5(b)). By using these reporters, the authors were able to study the kinetics of zinc binding to the Zap1 in response to changes in environmental zinc. Palmer *et al*. further optimized this construct into a genetically encoded sensor that can be applied to mammalian cells[172]. In the new sensor ZapCY1, CFP was truncated, EYEP was replaced with the more pH stable fluorescent protein citrine, and the linker was altered to optimize the FRET response. ZapCY1 has an apparent K_D of 2.5 pM and exhibits excellent metal selectivity against Cu^{2+} and Fe^{2+}. Using a combination of ZapCY1 and ER-targeted Zif1, the authors provide evidence that excess zinc is sequestered into ER and Golgi, and Ca^{2+} signaling interactively influences Zn^{2+} homeostasis.

Merkx *et al*. developed a series of chelating fluorescent protein chimeras to enhance the FRET efficiency between the fluorescence signals upon zinc binding (Fig. 1.5(c))[173]. Two complementary zinc coordinating residues, Y39H and S208C, were introduced on the surfaces of the enhanced cyan and yellow fluorescent proteins connected by a flexible peptide linker. Zinc binds to the complementary sites and brings

the YFP and CYP very close together, resulting in a 4-fold increase in FRET ratio. These sensors, called ZinCh, have apparent zinc affinities in the sub-micromolar range, too low to measure resting zinc levels.

Another novel strategy developed by the Merkx group utilizes a modified pair of copper chaperones as the zinc binding scaffold. The first sensor CALWY consists of two metal binding domains, Atox1 (a copper chaperone) and WD4 (domain 4 of ATP7B, a copper transporter)[174]. Variants of this sensor have high zinc affinities in the pM to nM range at pH 7.5[175]. However, Cu^{+} competitively binds to the sensor and the changes in FRET between ECFP and EYFP were too small to be useful for *in vivo* measurements. The authors improved CALWY by replacing the fluorescent proteins with brighter Cerulean and Citrine, and introducing mutations (S208F and V224L) on the surface of both domains to promote heterodimer formation between the fluorescent proteins[45]. Therefore, a conformation change induced by zinc binding to Atox and WD4 breaks the FRET pair apart, resulting in a 2.4-fold decrease in fluorescence in the presence of zinc (Fig. 1.5(d)). Mutations in the zinc binding domain and variations in linker length produced a series of protein-based zinc sensors with affinity from 2 pM to 2.9 nM and improved selectivity of Zn^{2+} over Cu^{+}. These sensors were applied in INS-1 cells and Hela cells to measure intracellular free zinc, concluding with an estimate of ~ 400 pM[45].

The development of these sensors provides researchers with great tools to study zinc fluctuation and distribution in the low concentration range in normal resting cells. However, all of these high affinity sensors have multiple (2 - 4) cysteines as the zinc chelating ligands, which are susceptible to oxidation. Therefore they are not suitable for studying zinc changes under oxidative stresses. Carbonic anhydrase based zinc sensors

have three histidines as the zinc ligands, and are less sensitive to oxidation. Our group has developed a series of carbonic anhydrase-based zinc sensors for application in eukaryotes and prokaryotes, detailed in the next section.

1.4 CARBONIC ANHYDRASE-BASED ZINC SENSORS

1.4.1 Zinc Binding Properties of Carbonic Anhydrase

Carbonic anhydrase was first discovered in red blood cells catalyzing the reversible hydration of CO_2 to HCO_3^- [176]. As one of the first metalloenzyme discovered, its metal binding characteristics have been extensively studied. The crystal structure of α-carbonic anhydrase demonstrated that a catalytic zinc ion is located in the active site, coordinated in tetrahedral geometry by three histidine residues (His94, His96 and His119) and a solvent molecule (H_2O)[177] (Fig. 1.6). These direct ligands form hydrogen bonds to the indirect ligands Glu92, Asn244 and Glu117, respectively, and a metal-bound hydroxide forms a hydrogen bond to Thr199 at neutral pH. This delicate hydrogen bond network is conserved in all catalytically active α-carbonic anhydrase, and modulates the zinc binding affinity and kinetics[178].

Mutagenesis studies have revealed the contribution of each ligand residue to zinc binding, and produced a series of mutants with varying binding zinc affinity and kinetics. Replacement of any of the three direct His ligands resulted in a 3 ~ 4 orders of magnitude reduction in the zinc binding affinity[179-181]. Wild type CA binds zinc with an affinity of 0.8 pM at neutral pH, while the H94Q, H94N, and H94A mutants have reported zinc affinities of 8 nM, 40 nM and 270 nM[180, 182]. These mutants are therefore suitable as scaffolds to detect higher zinc concentrations.

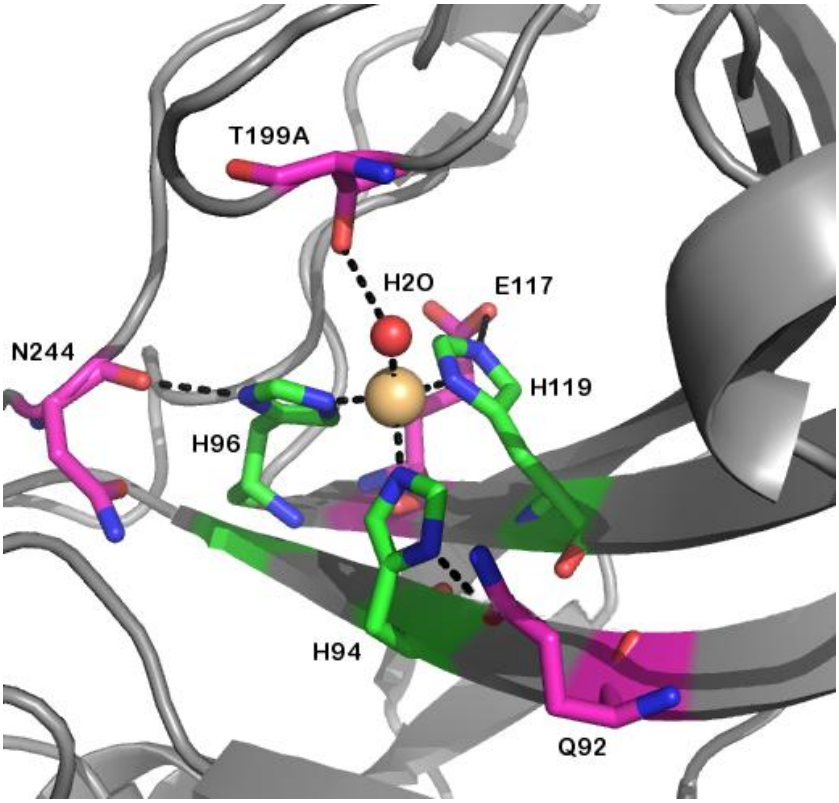

Figure 1.6. Structure of the zinc binding site in carbonic anhydrase. (PDB ID: 2CBA).

Changes in the second shell ligands have more subtle effects on zinc binding. Q92A, E111A and T199A mutants have reported apparent zinc affinities of 18 pM, 40 pM and 60 pM[183]. More importantly, changes in these ligands enhance the zinc binding kinetics significantly without sacrificing the affinity. In wild type CA, zinc equilibration is limited by both the high zinc affinity and the slow dissociation rate[184]. It is proposed that zinc binds to CA in a two-step mechanism where the zinc ion first binds to His94 and His96 near the active site surface, followed by slow addition of the third His ligand H119

and dissociation of water ligands. Breaking the hydrogen bond between His119 and E117 increases the flexibility of the H119, resulting in a 5,000 increase in the dissociation rate[183]. Fast binding equilibrium is very important for creating a sensor that can react to real time changes in free zinc concentration.

Equilibration of CAII with zinc can also be facilitated by the addition of certain chelators, including dipicolinic acid, but not others, including EDTA[185, 186]. Catalysis of metal exchange by dipicolinic acid is proposed to occur by the formation of a holo-CAII and dipicolinic acid ternary complex. This type of chelator-catalyzed zinc exchange could mimic intracellular mechanisms that are proposed to enhance zinc equilibration[41, 44]. Carbonic anhydrase binds zinc with high selectivity. It has little affinity for other competing metals in the cell; the dissociation constant for Ca^{2+} and Mg^{2+} is larger than 10 mM, and the affinity for Fe^{2+} is estimated to be significantly higher than 100 μM[187-189]. Like small molecule ligands, the transition metal affinity of wild type CAII follows the Irving-Williams series ($Mn^{2+}<Co^{2+}<Ni^{2+}<Cu^{2+}>Zn^{2+}$), except that the zinc affinity has increased significantly compared to the rest of the transition metals. Copper is the only biologically relevant metal that binds CA tighter than zinc with an ~ 0.1 pM affinity[190]. However, the readily exchangeable Cu^{2+} concentration is estimated at ~1×10^{-18} M[191], orders of magnitude below the detection limit. Furthermore, except for H119Q CAII, the metal selectivity of all the mutants described above also follow the inherent metal ion affinity trend suggested by Irving-Williams series, largely in line with wild type CA. In summary, the high selectivity and tunable metal affinity makes carbonic anhydrase a good scaffold for developing zinc sensors.

1.4.2 Development of Carbonic Anhydrase-based Zinc Sensors

Metal binding to CA needs to be transduced into a detectable signal for sensing. This was made feasible with the discovery of changes in fluorescence emission of the aryl sulfonamide inhibitor of CA, dansylamide (DNSA), upon selective binding to holo-CA (zinc-bound CA)[192]. DNSA has very weak affinity for apo-CA, and is virtually non-fluorescent when it is not bound to CA. When bound to holo-CA, DNSA exhibits enhanced lifetime, a dramatic increase in quantum yield, and a large blue-shift in emission[193]. Based on these properties, a myriad of carbonic anhydrase-derived sensors have been developed and tested using intensity, wavelength ratiometric, fluorescence lifetime, or fluorescence anisotropy detection[194-197]. More aryl sulfonamide inhibitors, such as ABD-N, ABD-M, and dapoxyl sulfonamide (DPS), were developed and optimized for various imaging methods.

As the fluorescence intensity of the free aryl sulfonamides is very low, they are not suitable for wavelength ratiometric measurements. DNSA and ABD-N were applied to quantify zinc only in circumstances when the zinc concentration (1 – 100 nM) is much lower than the concentration of apo-CAII and sulfonamide (1 – 20 μM) in a stoichiometric manner[197, 198]. The fluorophores are not suitable for measuring free zinc in the cell when zinc is buffered and the total zinc concentration is much higher. Alternative detection methods, such as fluorescence lifetime and polarization, have been used to quantify zinc at lower concentrations[194, 196, 199-201]. Though very accurate with an expanded dynamic range, the instruments and expertise required for measuring fluorescence lifetime and polarization are not readily available in most of the labs.

To make a wavelength ratiometric sensor, a second fluorophore was attached to CA as a FRET acceptor to the active site dapoxyl sulfonamide[44, 202] (Fig. 1.7). Dapoxyl sulfonamide (DPS) binds selectively to holo-CA with an affinity of ~ 0.1 μM[203]. Free DPS is virtually non-fluorescent when excited at 350 nm. Upon binding to holo-CA, it exhibits a 90-fold increase in fluorescence intensity and a large blue-shift from a peak at 605 nm to 530 nm[203]. This enhancement in intensity and blue shift significantly increases the FRET signal between DPS and the attached red fluorophore, AlexaFluor594 (AF594), representing the zinc-bound portion of the CA sensor. Another channel with excitation at 530 nm reports the total amount of the CA sensor. Therefore, the fluorescence intensity ratio at two excitation wavelengths, 350 nm and 530 nm, represents the zinc bound fraction of the CA sensor, which can be correlated to the free zinc concentration when calibrated under equilibrium conditions. This fluorescence zinc sensor has an apparent K_D of ~130 pM as measured in Zn-NTA chelated buffers at pH 7.0[44]. This ratiometric zinc sensor was delivered to mammalian cell lines PC-12 and CHO through a TAT-tag fused to the N-terminus of CA. Intracellular free zinc was measured at 5 ~ 10 pM in resting cells[44].

PEBBLE (Probe Encapsulated By Biologically Localised Embedding) nanosensors with CA and DPS encapsulated in nontoxic matrix are also under development (Si Di, *et al.* unpublished). In general, PEBBLEs have the advantages of protecting sensors from sequestration and interference by unwanted interactions in the cell[204]. In addition, a second fluorophore can be encapsulated to function as an internal reference to create ratiometric measurements. PEBBLE sensors can be delivered into the cells using several methods, including endocytosis, microinjection, liposome and cell-

penetrating peptides[204]. PEBBLEs with several small molecule zinc indicators have been developed and applied in mammalian cells[204].

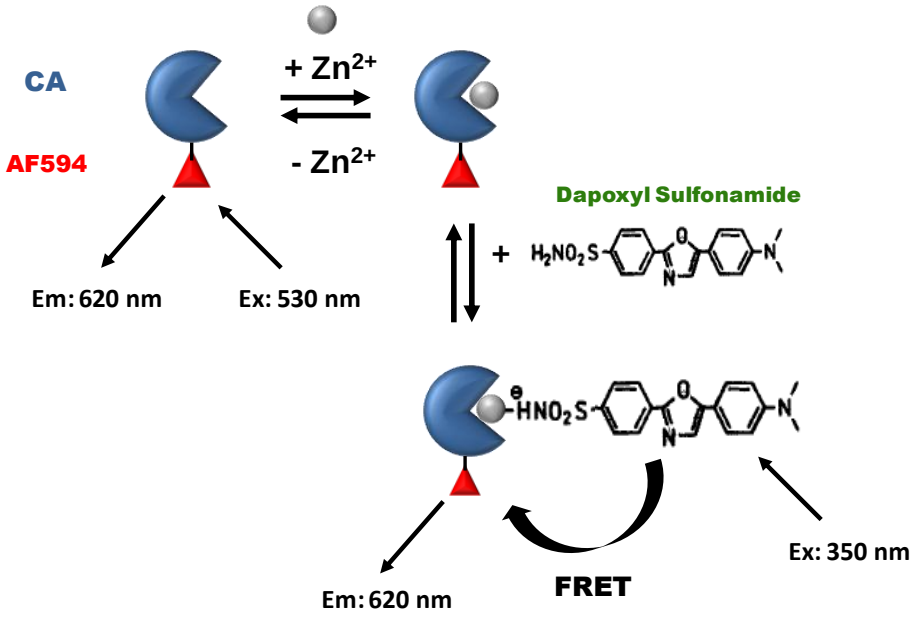

Figure 1.7. Schematic illustration of a CA-based ratiometric zinc sensor.

There are several drawbacks of these methods that a genetically encoded sensor can address. First, TAT-mediated delivery is limited to certain mammalian cell lines and is associated with vesicular localization of the sensor, while expression of the biosensors can be readily achieved in various model organisms, such *E. coli* and *S. cerevisiae*. Second, genetically encoded sensors can be targeted to subcellular organelles to monitor zinc levels in various cellular locations. Finally, production of genetically encoded sensors is cost-effective once established, and both the retention time and the sensor level can be readily manipulated. Therefore, in this work, we focused on the development of

genetically encoded CA-based ratiometric biosensors for quantification of the intracellular free zinc. We have created a series of sensors that can measure free zinc in the picomolar to nanomolar range, and applied these sensors in the prokaryotic model organism *E. coli* for quantification of intracellular free zinc. In the work described in Chapter III, we monitored the intracellular zinc fluctuations upon sudden exposure to external zinc ("zinc shock"). Based on the different patterns of free zinc changes, we proposed different functions for the zinc exporters ZntA and ZitB in zinc detoxification. By correlating the intracellular free zinc concentration and the mRNA level of ZntA, we concluded that ZntR-mediated *zntA* transcription is under kinetic control of zinc availability, and responds to nanomolar free zinc levels. In Chapter IV, we demonstrated that the BaeS/R regulon, a two-component regulatory system responding to envelope stresses, is involved in defense against toxic levels of external zinc. These findings can further our understanding of zinc homeostasis regulation in bacteria, and facilitate the discovery of novel antibiotics based on disruption of metal homeostasis.

CHAPTER II

DEVELOPMENT OF GENETICALLY ENCODED ZINC SENSORS AND INTRACELLULAR FREE ZINC MEASURMENTS IN *E.COLI*

2.1 INTRODUCTION

Zinc plays important catalytic, structural and regulatory roles in the cell as an essential element[2]; however, excess zinc can be toxic to the cell, potentially due to inhibition of key enzymes, competition with other metal cation binding sites, and deprivation of essential copper[205, 206]. Therefore, cells need to achieve a delicate balance between ensuring sufficient concentration of zinc to fulfill the essential biological functions while limiting the concentration to prevent toxic effects. One fundamental parameter in zinc biology, the intracellular free zinc concentration, has been measured in mammalian cells using various zinc sensors[44, 45, 172]; however, the intracellular free zinc concentrations in other organisms such as bacteria and yeast remain unknown. Although it was proposed that the intracellular free zinc concentration in *E. coli* is in the femtomolar range based on *in vitro* measurements of the apparent K_m of DNA binding and transcription initiation of zinc responsive transcription factors[41], *in vivo* experimental data remains absent. This is in part due to lack of highly sensitive quantitative zinc sensors applicable to measurements in bacteria. Some commonly used small molecule fluorescent zinc sensors (FluoZin-3 and Zinquin) failed to generate signals in *E. coli* in

our trials (data not shown), potentially due to sensor loading issues or low affinities. Tools for accurate quantification of intracellular free zinc concentration are needed for understanding zinc homeostasis and regulation in bacteria.

In the work described in this chapter, we developed genetically encoded CA-based ratiometric zinc sensors and applied them to measure intracellular free zinc concentrations in *E. coli* BL21(DE3). We constructed a series of genetically encoded ratiometric sensors based on carbonic anhydrase (CA) by substituting the chemically conjugated fluorophore used in our previous sensors with a red fluorescent protein (RFP) as the FRET acceptor (Fig. 2.1)[44]. We tested various RFPs and chose TagRFP as the acceptor based on its brightness and fast maturation. To expand the dynamic range, we also created a series of sensors with various affinities through mutations at the CA active site and alterations of linker length between CA and RFP. Application of these genetically encoded sensors in the fast growing organism *E. coli* is complicated by the long maturation time of the fluorescent protein compared to the short doubling time of the bacteria. To solve this problem, we developed an expression-dilution method that allows the expression and maturation of the sensor in the cell before measuring zinc concentrations in log phase. To control for various artifacts and accurately measure intracellular free zinc in *E. coli*, we developed the methods for *in situ* calibration of these CA_RFP sensors. Based on the *in situ* calibration and sensor occupancies in the cell, we measured the intracellular free zinc in *E. coli* BL21 (DE3) grown in minimal medium at 10 ~ 40 pM using three CA_RFP sensors. This is the first experimental quantification of free zinc concentration in bacteria. An analysis among an *E. coli* population of ~ 500 cells revealed variations in free zinc concentrations among the cells. These variations

may reflect various physiological conditions of the cell. This work demonstrated that these genetically encoded sensors are powerful tools for studying zinc homeostasis in bacteria.

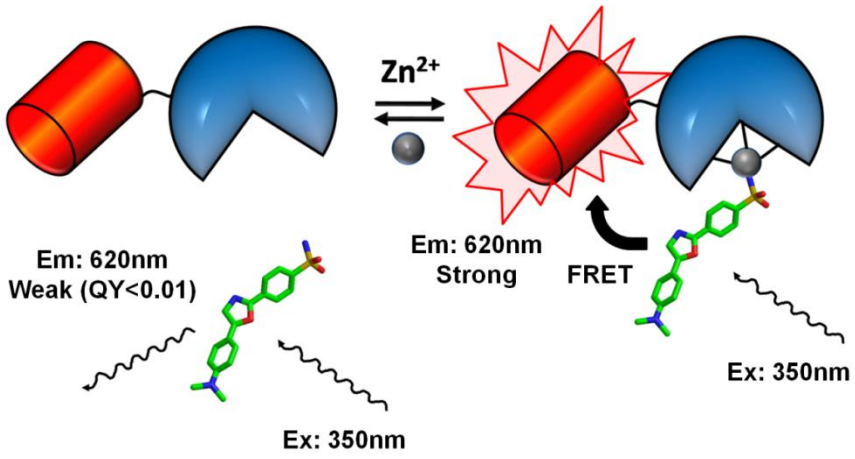

Figure 2.1. Schematic illustration of a genetically encoded CA-based ratiometric zinc sensor. A red fluorescent protein (RFP, shown as a red barrel) is fused to carbonic anhydrase (CA, shown as the blue moiety). An aryl sulfonamide inhibitor of carbonic anhydrase, dapoxyl sulfonamide (DPS, shown in stick stucture) selectively binds to holo-CA through coordination of the active site zinc (shown as a gray sphere). CA-bound DPS emits strongly at 530nm and acts as a FRET donor to RFP in this case. The UV-excited FRET signal is normalized to the emission from the directly excited RFP only (FP channel, not shown). Free zinc concentration is proportional to the ratio of FRET emission to directly excited RFP emission and can be read from a suitable calibration curve (see Fig. 2.3 and Fig. 2.6) under equilibrium conditions.

2.2 MATERIALS AND METHODS

2.2.1 Construction of CA_RFP Sensors

To construct the CA_RFP fusion protein, the human carbonic anhydrase II gene was sub-cloned from the vector pACA[207]; DsRed2, TagRFP and mCherry genes were cloned from the vectors pDsRed2 (Clontech), pTagRFP-N (Evrogen) and pRSET-mCherry (a gift from the Roger Tsien lab), respectively. The genes containing CA fused with a C-terminal red fluorescent protein (CA_RFP) were constructed through overlap PCR with a 1-glycine or 3-glycine linker between CA and RFP. The fusion gene CA_RFP was inserted into the expression vector pET24a (Novagen) between the restriction sites NdeI and XhoI with a C-terminal 6×His Tag for purification. Another plasmid, pACA_DsRed2, was constructed for the expression of CA_DsRed2 by inserting the DsRed2 gene into the vector pACA after the CA gene with a one-glycine linker in between.

2.2.2 Protein Expression and Purification

E. coli BL21(DE3) cells transformed with each plasmid were grown in 2xYT medium with 50 μg/ml kanamycin to OD_{600}~0.8 and then expression of the fusion protein was induced by addition of 250 μM IPTG. After incubation at 30˚C for 3 hours, protease inhibitors (7.4 μg/mL phenylmethanesulfonyl fluoride (PMSF) and 0.92 μg/mL tosyl-L-argininyl-methyl ester (TAME)) were added into the cultures. After another 3 hours of incubation, the cells were harvested and lysed using a Microfluidizer (Microfluidics). After removal of cell debris by centrifugation, nucleic acids were precipitated using 1% streptomycin sulfate and the lysate was clarified by centrifugation. The supernatants containing CA_mCherry-His_6 and CA_TagRFP-His_6 were dialyzed against Buffer C (30 mM HEPES, pH 8.0, 2 mM imidazole, 250 mM NaCl) overnight, loaded onto a Ni-

coated Chelating Sepharose column (GE Healthcare), washed with Buffer C and eluted with a 0.05 - 0.5 M imidazole gradient. Purified fractions of all three proteins were dialyzed against 10 mM MOPS, pH 7.0 before use or storage. CA_DsRed2 was purified using an alternate method. A clarified cell lysate containing CA_DsRed2 was dialyzed against Buffer A (10 mM Tris-SO_4, pH 8.0, 0.2 mM ZnSO4, 1 mM tris(2-carboxyethyl) phosphine hydrochloride (TCEP)) overnight and applied to a DEAE Sepharose (GE Healthcare) column equilibrated with this same buffer. The majority of CA_DsRed2 did not bind to the resin and was collected in the flow through. This CA_DsRed2 solution was then dialyzed against buffer B (10 mM MES, pH 7.0, 0.1 mM $ZnSO_4$ and 1 mM TCEP) overnight, loaded onto an SP Sepharose (GE Healthcare) column, and eluted with a 0.05 - 0.5 M $(NH_4)_2SO_4$ gradient. The CA_DsRed2 protein appeared in the fractions containing 0.1 - 0.25 M $(NH_4)_2SO_4$ as verified by SDS-PAGE. The purified protein was dialyzed against 10 mM MOPS buffer, pH 7.0 before storage at -80°C.

2.2.3 Synthesis of Dapoxyl Sulfonamide:

10 mg dapoxyl sulfonyl chloride (Molecular Probes/Invitrogen) was dissolved in 2 mL dry acetonitrile and placed in a 10 mL pre-dried reaction flask. Anhydrous ammonia gas was run through a condenser with a dry ice/acetone bath and liquid ammonia was dripped into the dapoxyl sulfonyl chloride solution over a 30 min period. Upon addition of ammonia, the reaction mixture turned yellow-green. At the end of the reaction, excess ammonia was evaporated slowly by gently blowing N_2 gas into the reaction vial. The reaction mixture was dried down using a speed vacuum and the resulting powder was re-dissolved in 1.5 mL 1:1 methanol/acetonitrile. The product was

purified by preparatory C18 reverse-phase HPLC (CH_3CN/H_2O-0.1% TFA, 5% - 100% over 60 min, 5 mL/min, 350 nm detection, t_R = 42 min). Dapoxyl sulfonamide was confirmed by comparison to known samples using thin layer silica chromatography (R_f ~ 0.8), liquid chromatography-mass spectrometry (LC-MS: m/z (M+H) single peak at 344.0) and fluorescence spectroscopy with an emission peak at 535 nm when excited at 350 nm in the presence of zinc-bound wild type carbonic anhydrase[203].

2.2.4 *In Vitro* Characterization of CA_RFPs

For the *in vitro* metal analysis experiments, all solutions were pre-incubated with Chelex® resin for several hours to remove contaminating metal ions. Metal ions, including the active site zinc ion, were removed from the purified CA_RFP proteins by dialysis in 10 mM MOPS, pH 7.0, 50 mM dipicolinic acid at 25˚C overnight. Excess dipicolinic acid was then removed by running the protein solution through a PD-10 desalting column (GE Healthcare). The Zn/protein ratio was < 0.03 (i.e. <3% holo-CA), verified by ICP-MS. For spectral characterization and microscope calibration, 1 µM metal-free sensor protein was incubated with NTA-chelated zinc buffers (10 mM MOPS, 2 mM NTA and various concentrations of $ZnSO_4$ at pH 7.0, as previously described[208]) at 25˚C overnight, then DPS dissolved in DMSO was added into the solution to a final concentration of 2 µM; control samples contained an equal concentration of DMSO. The spectra were taken on a Cary Eclipse fluorescence spectrophotometer (Varian Medical Systems). For microscope calibration, the solution was placed into a 96-well plate, and the fluorescence images were taken under the optical settings described in the fluorescence microscopy section.

2.2.5 Growth Conditions of *E. coli*

E. coli strain BL21 (DE3) transformed with a CA_RFP plasmid was cultured in a chemically defined (CD) MOPS minimal medium[209]. This medium is mainly buffered by 40 mM MOPS; the phosphate concentration is sufficiently low (1.32 mM) to minimize precipitation at high zinc levels. The overnight culture was diluted 1: 100 into 5 mL MOPS medium in a 125 mL flask. Protein expression was induced by addition of 50 µM IPTG at OD_{600} ~ 0.3, and the culture was incubated at 30˚C overnight to allow maturation of the fluorescent protein. Then 0.5 mL of this culture was harvested, the cells were washed twice with MOPS medium without IPTG, and then resuspended into 5 mL MOPS medium. Cells were incubated at 30˚C for 2 ~ 3 doubling times to OD_{600} 0.3 - 0.6 before microscopic analysis.

2.2.6 Fluorescence Microscopy and Data Analysis

E. coli cells were placed on a poly-L-lysine coated 96-well glass bottom plate (MatriCal Bioscience), incubated with 2 µM DPS in 100 µl MOPS medium for 20 min, then the excess DPS solution was removed and MOPS medium was added back before imaging. For *in situ* calibration, the cells in the 96-well plate were first incubated with 100 µl 1 mM EDTA in 10 mM metal-free MOPS buffer, pH 7.5 for 10 min. This solution was removed and the cells washed with 100 µl MOPS buffer. Finally, the cells were incubated for 20 min with 100 µl MOPS-NTA-Zn buffers containing 30 µM digitonin (made fresh from 30 mM stock in DMSO) and 2 µM DPS (made fresh from 200 µM stock in DMSO). 20 min is sufficient to reach equilibrium as experiments

conducted under longer incubation (30 and 40 min) generate the same results. The cells were then washed once with MOPS-NTA-Zn buffers without digitonin and DPS and imaged.

	FRET Ex. Filter	Exposure Time	FP Ex. Filter	Exposure Time	Dichroic Mirror	Em. Filter
CA_DsRed2	D350/50x	500ms	HQ 530/25x	500ms	550 dcxru	HQ 620/60m
CA_TagRFP	D350/50x	200ms	HQ 530/25x	500ms	550 dcxru	HQ 620/60m
CA_mCherry	D350/50x	50ms	HQ 575/50x	500ms	605 lpxru	HQ 625/30m

Table 2.1. Fluorescence imaging filter sets for different CA_RFP sensors.

Samples of cells or solution were photographed using a Nikon Eclipse TE2000-U inverted epifluorescence microscope through a Nikon Plan Fluor 100×/1.3 NA objective with a Photometrics CoolSNAP HQ cooled CCD camera. Fluorescence images of protein solution and live cells were acquired using the software MetaMorph (Molecular Devices). The filter sets for fluorescence imaging are summarized in Table 2.1. All filters and dichroic mirrors were purchased from Chroma Technology Corp. The images were analyzed using the software ImageJ. Background fluorescence was subtracted from the FRET and FP channel images. The average fluorescence intensity from the FRET images of pET24a cells plus DPS was also measured and subtracted from the FRET images with CA_RFP sensors to correct for the background from membrane bound DPS. A ratio image of I_{FRET}/I_{FP} was then created, and the average intensity in each cell was calculated to determine the free zinc concentration based on the *in situ* calibration curve.

2.3 RESULTS

2.3.1 Construction of CA_RFP Zinc Sensors

To develop a genetically encoded ratiometric zinc sensor, we fused a fluorescent protein (FP) to the C-terminus of CAII, replacing the chemical fluorophore covalently attached to CAII in the previously described sensor[44]. The fluorescent protein serves as both a FRET acceptor and as an intrinsic marker to track the location and concentration of the sensor. The CAII-FP zinc sensor is an excitation ratiometric sensor where fluorescence emission due to FRET between the donor (CAII-bound dapoxyl sulfonamide) and the acceptor (FP) (I_{FRET}) reflects the concentration of zinc-bound carbonic anhydrase while the fluorescence emission from excitation of the FP (I_{FP}) represents the total concentration of the sensor (Fig. 2.1). The I_{FRET}/I_{FP} ratio reflects the zinc-bound fraction of carbonic anhydrase. The concentration of readily exchangeable zinc is then determined from a calibration curve of the fluorescence intensity ratio I_{FRET}/I_{FP} at various concentrations of zinc measured under equilibrium conditions, as described in detail later.

The first step in developing a genetically encoded CAII_FP sensor is to determine which fluorescent protein to fuse to CAII. The following criteria were particularly important: (1) good spectral overlap with CA-bound DPS (Em = 530 nm) which limits the choice to orange-red fluorescent proteins; (2) high extinction coefficient and quantum yield to allow for detection at low concentrations; and (3) fast maturation under the experimental conditions. After testing several red fluorescent proteins fused to the C-terminus of CAII, including DsRed2, mRFP, mOrange, mCherry and TagRFP[210-212], we

chose TagRFP as the FP with the best balanced set of properties for our experiments. The properties of TagRFP, DsRed2 and mCherry are compared in Table 2.2. TagRFP is a bright, monomeric protein that matures faster than DsRed2[212] and has better FRET efficiency than mCherry (Fig. 2.2). As shown in the FRET spectra of CA_DsRed2, CA_TagRFP and CA_mCherry in the presence of DPS (Fig. 2.2), all three sensors respond readily to increases in free zinc concentrations with an enhanced FRET signal.

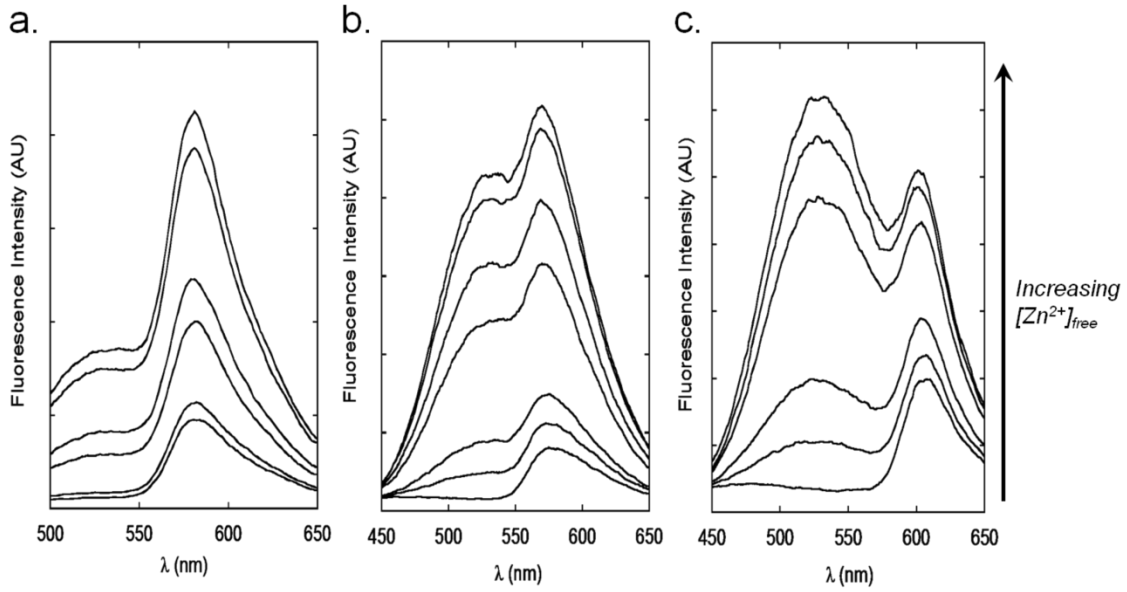

Figure 2.2. FRET emission spectra of CA_RFPs under various zinc concentrations. (a). CA_DsRed2; (b). CA_TagRFP; (c). CA_mCherry. 1 µM of apo-CA_RFP was incubated with NTA-chelated zinc buffers at various free zinc concentrations ($[Zn]_{free}$ from 0.002 pM to 5 nM). 2 µM DPS was added to the solution and emission scans were taken using an excitation wavelength of 350 nm. Emission peaks for CA-bound DPS and the fused DsRed2, TagRFP and mCherry are 530 nm, 587 nm, 584 nm and 610 nm, respectively.

Protein	Ex. (nm)	Em. (nm)	E.C. (M^{-1} cm^{-1})	Q.Y.	Brightness (%DsRed2)	Structure	$t_{0.5}$ (h) Maturation	$t_{0.5}$ (s) Photobleach	pKa
DsRed2	561	587	43,800	0.55	100	Tetramer	6.5	>100	4.5
TagRFP	555	584	100,000	0.48	134	Monomer	1.6	100	<4.0
mCherry	587	610	72,000	0.22	40	Monomer	0.25	96	4.5

Table 2.2. Comparison of the red fluorescent proteins used in CA_RFP zinc sensors[211-213].

To cover a wider dynamic range of zinc concentrations and select the sensor with the appropriate affinity, a series of four CA_TagRFP variants containing mutations in CAII (E117A, Q92A, T199A, or H94N) that were previously shown to alter the zinc binding affinity and/or kinetics[182, 183] were individually engineered in the sensor. We also prepared a CA_TagRFP variant where the single glycine residue linking the CAII and TagRFP proteins was replaced with three glycine residues to test whether altering the linker length could tune the apparent affinity and/or spectral properties.

2.3.2 *In Vitro* Calibration of CA_RFP Sensors

The apparent zinc affinities of the engineered CA_RFP sensors were measured *in vitro* by equilibration with nitrilotriacetate (NTA)-buffered zinc solutions to maintain an exchangeable zinc pool with known free zinc concentrations[208]. After equilibration of apo-CA_RFP with the zinc buffers, dapoxyl sulfonamide was added and the ratio of the emission intensity measured at 620 nm after excitation at either 530 nm (I_{FP}, FP channel, 575 nm for mCherry) or 350 nm (I_{FRET}, FRET channel) was calculated. The fluorescence

intensity ratio (I_{FRET}/I_{FP}) has a hyperbolic dependence on the zinc concentration (Fig. 2.3) which is well-described by a single binding isotherm (Eq. 2.1) where: $R = I_{FRET}/I_{FP}$, R_{min} is determined in the absence of zinc, and R_{max} is measured at saturating free zinc concentrations.

$$R = R_{\min} + \frac{(R_{\max} - R_{\min}) \times [Zn]_{free}}{[Zn]_{free} + K_{D,app}^{Zn}} \qquad \text{Eq. 2.1}$$

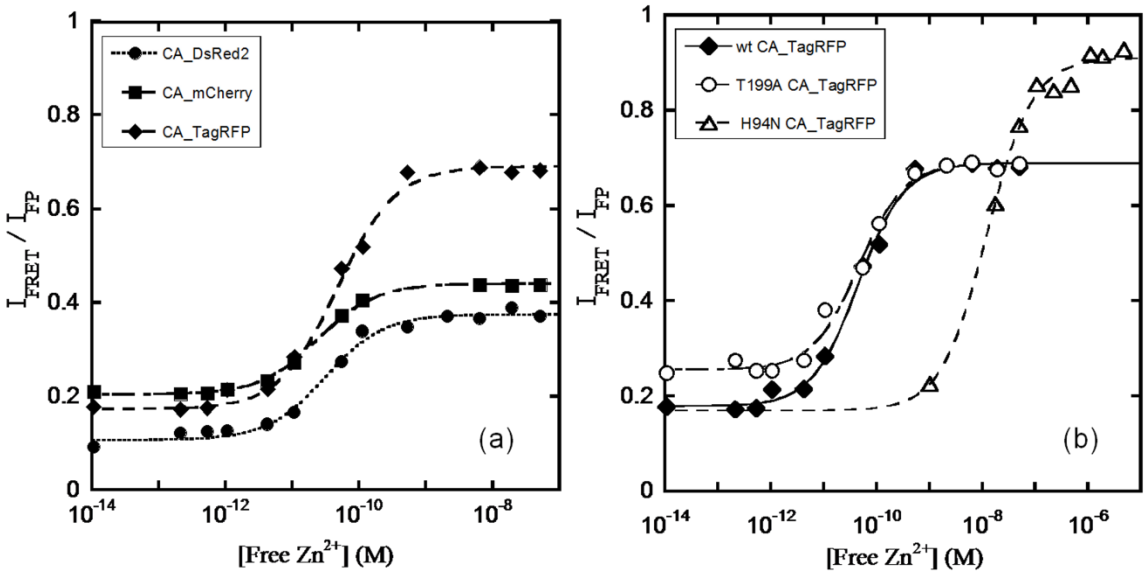

Figure 2.3. ***In vitro*** **calibration curves of CA_RFP sensors.** 1 µM apo-CA_RFP sensor was pre-equilibrated with NTA-chelated zinc buffers (pH 7.0) and 2 µM DPS, and then the excitation fluorescence intensity ratio was measured with filter sets detailed in Table 2.1 using 96-well plates on a Nikon TE2000 inverted fluorescence microscope. (a). *in vitro* calibration curves of CA_DsRed2 (filled circle), CA_mCherry (filled square) and CA_TagRFP (filled diamond). The calibration curve of CA_TagRFP with a Gly_3 linker is similar to that of CA_TagRFP with a single Gly linker but with a slightly higher $K_{D,app}^{Zn}$ (Table 2.3). (b). Examples of *in vitro* calibration curves of CA_TagRFP sensors with mutations in CA, including T199A (open circle) and H94N (open triangle) CAII. The *in vitro* $K_{D,app}^{Zn}$ values for all of the sensors are listed in Table 2.3.

The measured values of $K_{D,app}^{Zn}$ (apparent K_D for zinc) for the wt CA_FP sensors are 24 – 44 pM, depending on the identity of the red fluorescent protein (Table 2.3). When the linker between the CA and TagRFP proteins is increased from 1 to 3 glycine residues, the apparent zinc dissociation constant increases to 100 pM. These apparent affinities are significantly weaker than the previously reported zinc affinity of CAII (~1 pM [214]), perhaps due to subtle structural alterations of the zinc site caused by fusion of the red fluorescence protein to the C-terminus. Additionally, the apparent zinc affinities may also be affected by the optical properties of the microscope, as previously reported[44].

	Reported K_D^{Zn} of CA variants[183, 214]	*In vitro* $K_{D,app}^{Zn}$ pH 7.0 (Fig. 2.3)	*In situ* $K_{D,app}^{Zn}$ pH 7.0 (Fig. 2.6)	*In situ* $K_{D,app}^{Zn}$ pH 7.6 (Fig. 2.7)
wt CA_mCherry	1 pM	24 ± 1 pM	130 ± 55 pM	N.D.
wt CA_DsRed2		31 ± 5 pM	N.D.	N.D.
wt CA_TagRFP		44 ± 5 pM	140 ± 50 pM	32 ± 20 pM
wt CA_TagRFP - 3G linker		99 ± 2 pM	150 ± 70 pM	N.D.
Q92A CA_TagRFP	18 pM	76 ± 9 pM	150 ± 80 pM	7 ± 5 pM
E117A CA_TagRFP	40 pM	44 ± 6 pM	N.A.	N.A.
T199A CA_TagRFP	60 pM	60 ± 4 pM	200 ± 67 pM	11 ± 6 pM
H94N CA_TagRFP	40 nM	12 ± 2 nM	300 ± 90 nM	9 ± 6 nM

Table 2.3. Zinc dissociation constants for CAII and CA_RFP sensor variants.

The $K_{D,app}^{Zn}$ values measured *in vitro* for the CA_TagRFP variants containing mutations in the second shell ligands in CAII increase < 2-fold compared to that of wt CA_TagRFP. These changes in affinity are significantly smaller than expected (18 ~ 60 fold[183]) consistent with a subtle alteration in the structure of the zinc site in the CA_FP fusion protein. Mutation of a direct zinc binding ligand, H94N, in CAII reduces the apparent zinc affinity of the CA_TagRFP by > 250-fold, comparable to the effect of this substitution in CAII[182].

The zinc-dependent increase in the I_{FRET}/I_{FP} ratio is 3.5- and 4.5-fold for wt CA_TagRFP and H94N CA_TagRFP, respectively. These responses are significantly larger than the 50% increase observed for the previously described CA_AF594 sensor[202] due mainly to a reduction of fluorescence from direct excitation of the acceptor at 350 nm. The magnitude of the signal change observed for the CA_TagRFP sensor is also larger than the eCALWY zinc sensors (2-fold change in signal)[45], making it the most sensitive genetically-encoded zinc sensor with an affinity in the picomolar range. This improvement in the signal amplitude substantially enhances the sensitivity and accuracy of the measurement of zinc concentrations using CA-based fluorescent sensors.

2.3.3 Applying CA_RFP Zinc Sensors in *E. coli*

Although the level of free zinc in *E. coli* has been estimated[41], the readily exchangeable zinc concentration has not yet been directly measured in this organism or any other prokaryote. Therefore, we chose to use our expressible sensors to measure zinc levels in *E. coli* BL21(DE3) using the controllable T7 expression system to optimize the sensor concentration and maturation. Since it is not yet known how the intracellular free

zinc concentration varies with environmental factors and nutritional constraints, we used a chemically defined minimal medium to provide stringent control and reproducibility of these parameters[209]. The total zinc concentration in this medium is ~ 40 nM, measured by inductively coupled plasma emission mass spectroscopy (ICP-MS), and > 90% of the zinc is not chelated by components of the medium, calculated using the MINEQL+ program (Environmental Research Software).

One obstacle to using fluorescent protein-based sensors to measure analytes in *E. coli* is that the doubling time is comparable to or shorter than the half-time for maturation of the fluorescent proteins. In rich media, wild-type *E. coli* cells can divide as rapidly as every 30 min at 37 °C[215], while TagRFP and mCherry require 3 hrs and 1.5 hrs, respectively, to achieve 90% maturation at 37°C[211, 212]. To tackle this issue, we developed an expression-dilution strategy. After growing BL21(DE3) cells containing a plasmid encoding the CA_FP sensor to mid-log phase in chemically defined medium, expression of the sensor was induced by addition of isopropyl β-D-1-thiogalacto-pyranoside (IPTG), and the cells were incubated overnight at 30 °C to allow sufficient time for the red fluorescent protein to both express and mature. The cells were then harvested, washed once with fresh medium, diluted into fresh medium without IPTG and incubated at 30 °C for several doubling times before imaging. Under these conditions, little additional recombinant CA_FP is synthesized after dilution. However the bacterial cells retain sufficient CA_FP sensor with mature red fluorescent protein to measure the readily exchangeable zinc concentrations. Allowing sufficient time for maturation of the fluorescent protein is an essential step since sensors containing immature red fluorescent

protein have altered optical properties. This procedure also provides time for cells to adjust their zinc concentrations to accommodate the expressed zinc sensors.

E. coli cells were imaged using a fluorescence microscope, as described in the Materials & Methods. We first carried out a number of control experiments to demonstrate that the I_{FRET}/I_{FP} ratio measures zinc-bound CA_FP with bound DPS. First, images of *E. coli* cells expressing the parent vector only (pET24a) in the presence of DPS exhibit minimal background fluorescence in the FRET channel (Fig. 2.4(c)), caused mainly by the long wavelength tail of membrane-bound DPS emission which peaks at 450 nm. This minor background fluorescence was averaged and subtracted from the FRET intensity measured in cells expressing the CA sensor. This background signal correction altered the ratio measurements < 5%. Second, we imaged *E. coli* cells expressing the CA_RFP sensor in the absence of DPS and observed significant fluorescence in the FP channel (Fig. 2.4(e)) with a low baseline in the FRET channel (Fig. 2.4(f)). The I_{FRET}/I_{FP} ratio in cells expressing CA_TagRFP is 0.19 ± 0.03, which is comparable to the I_{FRET}/I_{FP} ratio observed in the *in vitro* calibration at very low zinc concentrations (0.18 ± 0.01; Fig. 2.3(a)). A significant increase in the FRET channel emission was observed when DPS was added to cells expressing CA_TagRFP (Fig. 2.4(i)). To verify that the signal increase was specifically caused by DPS binding to holo-CA, ethoxzolamide, a non-fluorescent inhibitor with a much higher affinity for holo-CA affinity (dissociation constant of 1.6 nM compared to 0.1 μM for DPS[203, 216]) was added to the DPS-treated cells. Upon addition of ethoxzolamide, the FRET channel emission decreased and the I_{FRET}/I_{FP} ratio returned to the baseline level (0.19 ± 0.03) (Fig. 2.4(l)), validating the specificity of the FRET signal to the DPS-bound CA_RFP sensor.

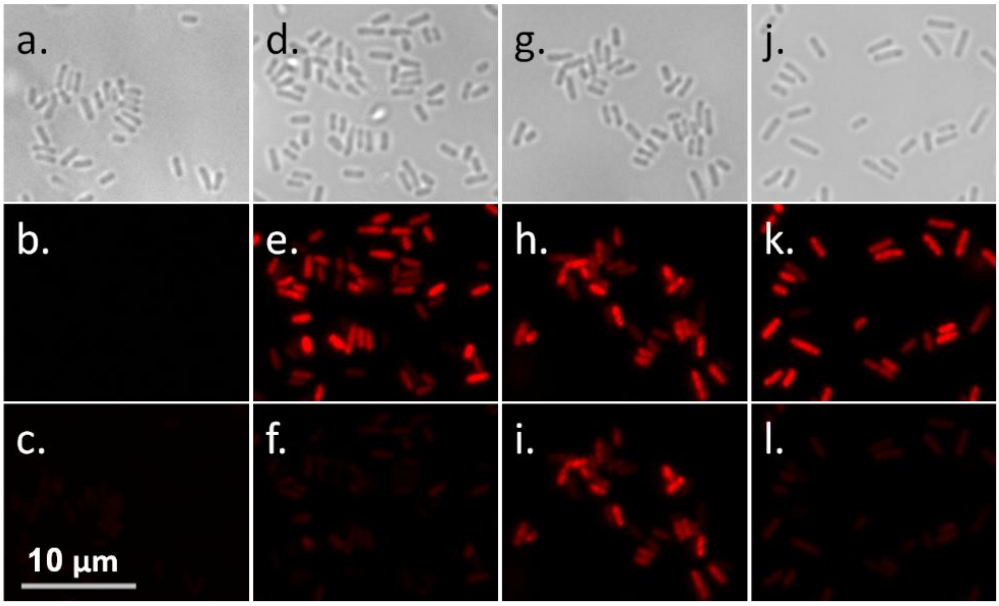

Figure 2.4. Fluorescence signal of the CA_TagRFP sensor in *E. coli*. Top row: Brightfield images; middle row: FP channel: Ex 530/ Em 620, exposure time 200 ms; bottom row: FRET channel: Ex 350/Em 620, exposure time 500 ms; (a) (b) (c), *E. coli* with void pET24a vector plus 2 µM DPS; (d) (e) (f), *E. coli* expressing CA_TagRFP without added DPS; (g) (h) (i), *E. coli* expressing CA_TagRFP with added 2 µM DPS. (f) (k) (l). *E. coli* expressing CA_TagRFP plus 2 µM DPS and 30 µM ethoxzolamide, a ligand that competes with DPS for binding to the active site of carbonic anhydrase.

To further examine the behavior of the CA_RFP expressible sensor in *E. coli*, the intracellular free zinc concentration was altered (Fig. 2.5). First, *E. coli* cells expressing the sensor were incubated with the transition metal-specific chelator N,N,N',N'-tetrakis(2-pyridylmethyl)ethylenediamine (TPEN). The I_{FRET}/I_{FP} ratio decreased to the baseline level (0.19 ± 0.04) within 10 min after addition of 50 µM TPEN, indicating that the sensor rapidly re-equilibrates with the lower intracellular zinc concentration. In contrast, incubation with the membrane impermeable chelator EDTA did not alter the fluorescence

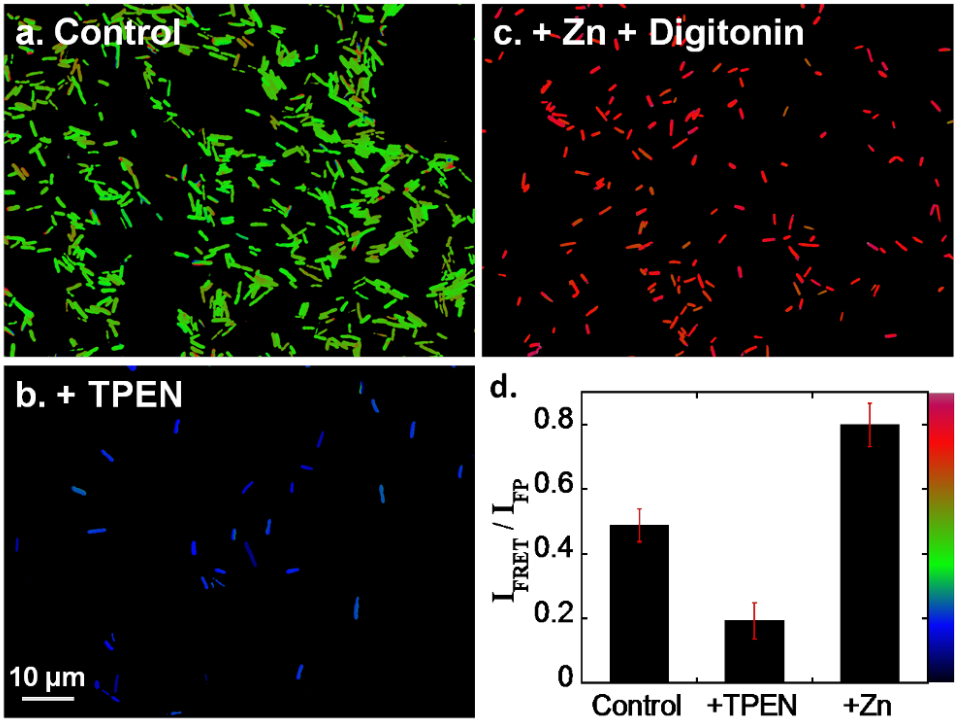

Figure 2.5. Fluorescence ratio changes with alterations of the intracellular zinc level. *E. coli* cells were grown in minimal media as described in materials and methods and the cells imaged after a 10-min incubation in either: (a) minimal medium; (b) 50 µM TPEN or (c) 30 µM Digitonin + 100 µM $ZnSO_4$. The fluorescence in the FP and FRET channels were determined as described in the legend of Fig. 2.4. The I_{FRET}/I_{FP} ratio images are shown in RGB color and the average values are shown in the bar graph in panel d.

ratio (I_{FRET}/I_{FP} ratio = 0.53 ± 0.06 after a 20-min incubation with 1 mM EDTA). Incubation of the *E. coli* cells expressing the sensor with the membrane permeabilizing compound digitonin[46] and 100 µM $ZnSO_4$ increases the I_{FRET}/I_{FP} ratio to ~ 0.8, slightly higher than the ratio at the high end of the *in vitro* calibration curve using wt CA_TagRFP, suggesting that the sensor is saturated with zinc under this condition. The modest discrepancy in the endpoint values between the *in vitro* and *in vivo* experiments

could be explained by either differential effects of the aqueous solution and intracellular environment on the fluorescent properties and FRET efficiencies, or the presence of a small amount of immature red fluorescent protein, which could lower the FP intensity relative to the FRET intensity, thus increasing the I_{FRET}/I_{FP} ratio. These data demonstrate that in *E. coli*, the CA_RFP sensor responds readily to changes in the cellular zinc concentration and is therefore suitable for monitoring dynamic processes in these cells.

2.3.4 *In Situ* Calibration of CA_RFP Sensors

Differences in the cellular milieu and optical properties could cause discrepancies in the I_{FRET}/I_{FP} ratio between the calibration curve measured in buffers and the measurement of zinc in the cells. Thus an *in situ* calibration curve is desirable to determine the response of CA_RFP sensors to alterations in readily exchangeable zinc concentrations in the cell. *E. coli* is a gram-negative bacterium that has an outer membrane to act as an extra barrier against the perfusion of divalent ions. To equilibrate the zinc buffers across the cell membranes, first the outer membrane is weakened through a brief incubation with EDTA to destabilize the lipopolysaccharide structure[217] and facilitate permeabilization by chelating divalent ions bound to LPS. After washing, the cells are incubated with the membrane permeabilizer digitonin[46] and zinc buffers. Since the zinc affinity of CAII is pH dependent[187], it is important to carry out the *in situ* calibrations at a pH close to the physiological pH of the *E. coli* cytosol. Previous data indicate that in minimal medium with an extracellular pH of 7.4, the intracellular pH in *E. coli* is ~ 7.6 [218].

The *in situ* calibrations were carried out using BL21(DE3) cells containing mature CA_RFP sensor, which were first briefly incubated with EDTA, and then incubated for 20 min with NTA-chelated zinc buffers plus digitonin and DPS to equilibrate. Doubling the incubation time with the zinc buffers had no effect on the fluorescent ratio indicating that the system readily equilibrates within this time frame. Consistent with this, the measured fluorescent ratio in the *in situ* calibration cell samples at both low and high concentrations of free zinc are comparable to the values measured for the *in vitro* calibration. It is worth noting that the response time of the expressed CA_TagRFP sensor to changes in free zinc concentration under both *in vivo* and *in situ* conditions is faster than predicted from the measured *in vitro* zinc equilibration rate constants ($k_{ex} \sim k_{on}[Zn]_{free} + k_{off}$) for wild-type CAII; the zinc dissociation rate constant has been estimated as 8×10^{-8} s^{-1} [214]. However, the CA_FP fusion proteins likely have faster dissociation rates consistent with the higher values of $K_{D,app}^{Zn}$. Zinc exchange *in vitro* can be enhanced by the addition of small molecule chelators, such as dipicolinate[185] and *in vivo* CAII zinc equilibration may also be catalyzed.

In situ calibrations were carried out using buffered solutions at both pH 7.0 and pH 7.6. The cells were imaged to measure the I_{FRET}/I_{FP} ratio at various free zinc concentrations maintained using NTA buffers (Fig. 2.6) and the values for the *in situ* $K_{D,app}^{Zn}$ were calculated by fitting a binding isotherm to these data, as summarized in Table 2.3. At pH 7.0, the values determined for *in situ* $K_{D,app}^{Zn}$ are similar for all of the CA_RFP variants (133~200 pM) except H94N CA_TagRFP (300 ± 90 nM). In all

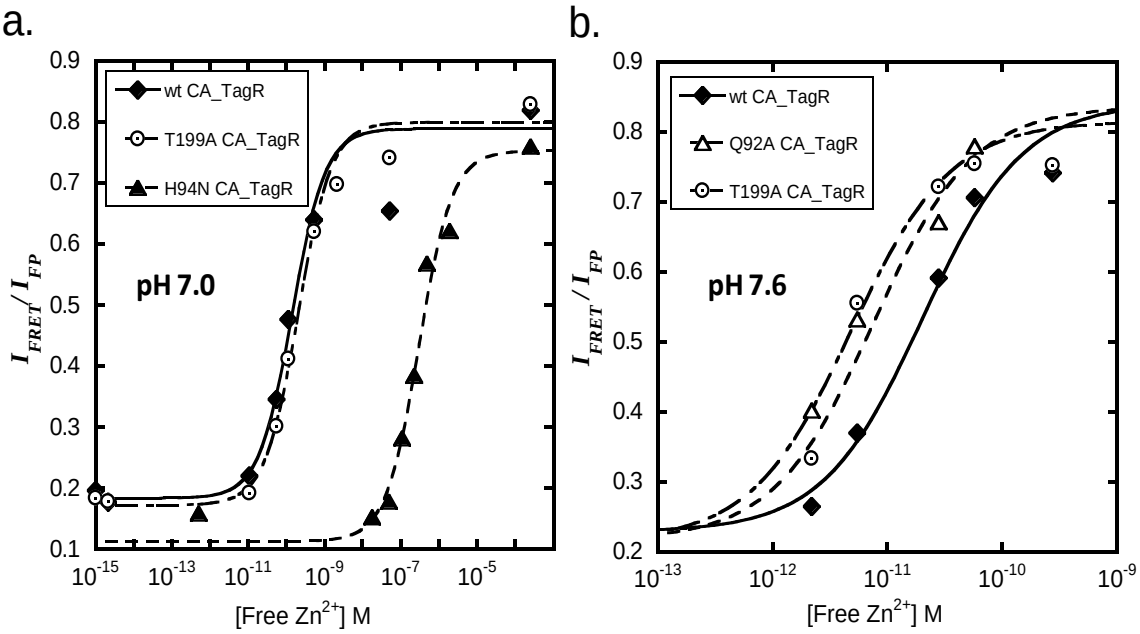

Figure 2.6. *In situ* calibration of CA_RFP zinc sensors at pH 7.0 and pH 7.6. *E. coli* cells pre-treated with membrane disruptor (EDTA and digitonin, as described in the Materials and Methods) were incubated with NTA-chelated zinc buffers with various free zinc concentrations at pH 7.0 (a) and pH 7.6 (b). The I_{FRET}/I_{FP} value averaged over all of the cells on the ratio images was determined at various concentrations of $[Zn^{2+}]_{free}$ and the apparent $K_{D,app}^{Zn}$ values are listed in Table 2.3.

cases, the value of *in situ* $K_{D,app}^{Zn}$ is larger than the value determined from the *in vitro* calibrations for reasons that are unclear. At pH 7.6, the value of $K_{D,app}^{Zn}$ for wt CA_RFP decreases 4-fold to 32 pM consistent with the pH dependence of the zinc affinity of wt CAII[187]. Two sensors, containing the Q92A or T199A mutations, have higher apparent zinc affinities ($K_{D,app}^{Zn}$ = 7 pM and 11 pM, respectively) than wild type at pH 7.6, consistent with the higher zinc-water pK_a values for these mutants[219]. These variations in the affinity of these sensors allow both measurement of a wider dynamic range of

intracellular free zinc concentrations (5 pM ~ 50 nM) and confirmation of the zinc concentration using sensors with different values of $K_{D,app}^{Zn}$.

2.3.5 Measurement of Intracellular Free Zinc Concentration in *E. coli*

The intracellular free zinc concentration of *E. coli* cultured in the MOPS-buffered minimal medium at log phase was measured using wt CA_TagRFP for comparison to the *in situ* calibration at pH 7.6 (Fig. 2.7(a)). The average I_{FRET}/I_{FP} ratio within single *E. coli* cells was measured to calculate the intracellular free zinc concentration. The standard deviation of the I_{FRET}/I_{FP} ratio from single pixels within a single cell (300 ~ 500 pixels/cell) was less than 5%, which is well within the normal error range of fluorescence imaging. These data indicate that there is no significant differential distribution of readily exchangeable zinc concentration within a cell. However, some variability in the readily exchangeable zinc concentration was observed among the cell population. An analysis of a sample of ~500 cells revealed that the majority of the cells (~80%) had intracellular free zinc concentrations within the 10 - 30 pM range (Fig. 2.7). Around 10% of the cells exhibited higher intracellular free zinc concentration (40 – 80 pM) and ~1.5% of the cells had zinc concentrations higher than 100 pM. We speculate that the cells with the significantly higher concentrations may be damaged or dying and therefore unable to correctly regulate their zinc concentration. The median intracellular readily exchangeable zinc concentration among this population of cells was 20 pM. This number was confirmed by measuring the intracellular free zinc concentration using the Q92A and T199A CA_TagRFP expressible sensors. For both mutants, the average I_{FRET}/I_{FP} ratio

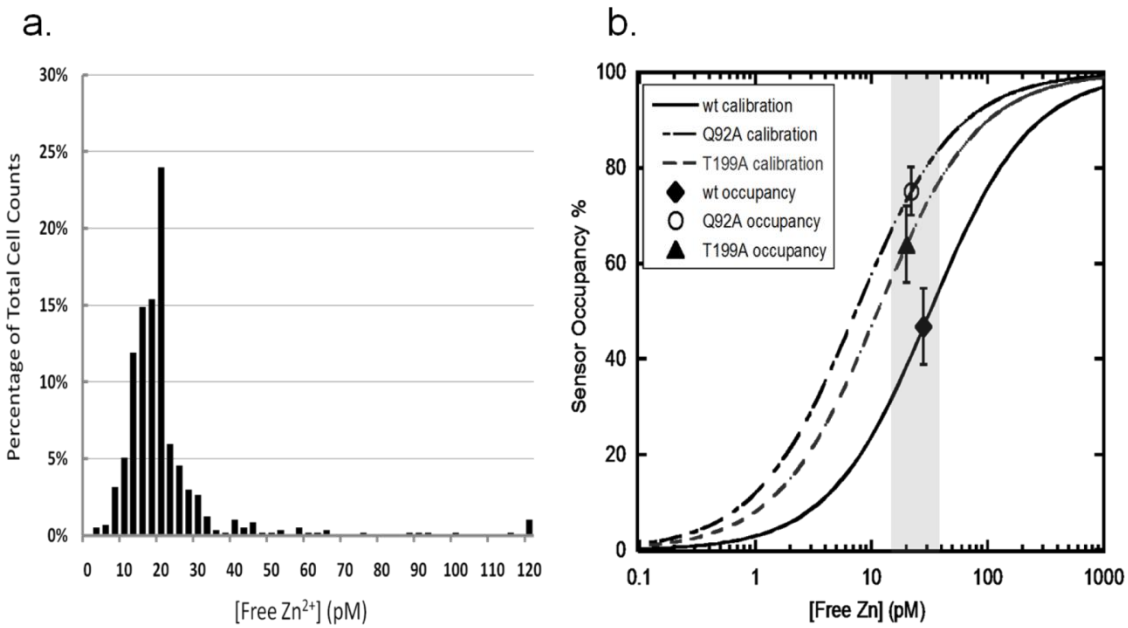

Figure 2.7. Measurement of *E. coli* intracellular free zinc concentrations. (a). Distribution of intracellular readily exchangeable zinc concentration among *E. coli* cells. Average I_{FRET}/I_{FP} ratio within a single cell was measured to calculate the corresponding intracellular free zinc concentration based on the *in situ* calibration at pH 7.6. ~ 500 *E. coli* cells were imaged and analyzed. The percentage of cells with each intracellular free zinc concentration is shown in Fig. 2.7(a). The intracellular readily exchangeable zinc concentrations of the majority of the cells (>80%) fall within the 10 - 30 pM range with the median at 20 pM. (b). Average occupancies of CA_TagRFP sensors in *E. coli* cells and the corresponding average free zinc concentrations calculated from the *in situ* calibration curves are shown. The average sensor occupancies of wild type, Q92A and T199A CAII are 46 ± 8%, 74 ± 5% and 64 ± 8%, respectively, corresponding to the free zinc concentration of 15 ~ 40 pM. The range of the measured free zinc concentration is shaded in gray.

for the cell population was higher than that observed for wt CA_TagRFP, consistent with the higher zinc affinity of these sensors. The measured average occupancies of the three sensors are placed on the *in situ* calibration curves in Fig. 2.7(b), demonstrating that all three sensors report an intracellular free zinc concentration in the range of 15 to 40 pM. The comparability of the results using different sensors with altered zinc affinities and

zinc equilibration rates also provides evidence that the zinc sensors readily equilibrate with the intracellular zinc concentration.

One important assumption of this method is that the binding of zinc to carbonic anhydrase does not change the intracellular readily exchangeable zinc concentration significantly. For measurements in the cells, the sensor concentration is maintained at a low level compared to the capacity of the total zinc pool by inducing expression of the sensor (incubation with 50 μM IPTG), harvesting the cells and then incubating in fresh medium (without IPTG) for several doubling times. We estimated by fluorescence and gel quantification that the sensor concentration is 10 ~ 20 μM, which is only a small fraction of the total zinc content of 200 μM as measured by ICP-MS. Furthermore, we altered the sensor expression level more than 10-fold by changing the concentration of IPTG used to induce expression (Fig. 2.8). The I_{FRET}/I_{FP} ratio was independent of the sensor concentration even when the concentration approaches the total zinc content (measured in cells without overexpressed CAII). Here we hypothesize that in contrast to a closed system, *E. coli* can actively import zinc from the medium to meet the need of newly synthesized metalloproteins and maintain cellular zinc levels.

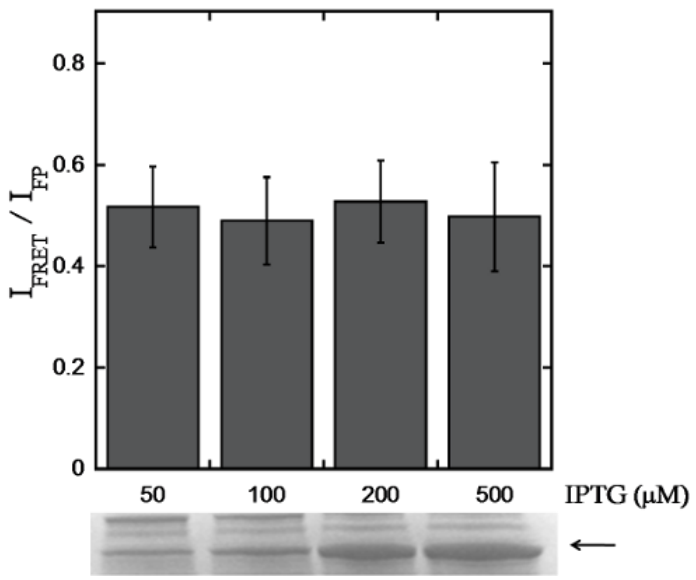

Figure 2.8. I_{FRET}/I_{FP} ratio is independent of the sensor concentration. *E. coli* cells transformed with wild type CA_TagRFP were induced with various concentrations of IPTG overnight, then diluted into fresh medium and grown for 3 hr at 30°C. When OD_{600} ~ 0.6, samples were taken for both imaging and protein analysis. The SDS-PAGE gel shows the varied CA_TagRFP expression levels; the arrow denotes the CA_TagRFP protein band. The I_{FRET}/I_{FP} ratio is constant as the sensor level varies.

2.4 DISCUSSION

2.4.1 The Development of CA_RFP Sensors and Application in *E. coli*

In this work, we developed a series of genetically encoded ratiometric sensors using carbonic anhydrase as the zinc binding scaffold. In these excitation ratiometric sensors, a red fluorescent protein, TagRFP, was fused to the C-terminus of CA as the FRET acceptor and used dapoxyl sulfonamide (DPS) bound to the active site of CA as the donor. Various mutations at the active site of CA were introduced to generate sensors

with different zinc affinities. These sensors were calibrated in the cell and successfully applied for free zinc measurements in *E. coli*.

The CA_RFP sensors have picomolar to nanomolar affinities, suitable for measurements of the low levels of intracellular free zinc under normal conditions. Mutations on the active site of CA generate a series of sensors with various affinities. T199A, Q92A and WT CA_TagRFP exhibit picomolar apparent affinities for zinc as measured *in situ* at pH 7.6, and are very sensitive for detection of subtle differences in intracellular free zinc concentrations (Fig. 2.7(b)). H94N CA_TagRFP has a low nanomolar affinity that can be used to monitor higher concentrations of intracellular free zinc fluctuations (Fig. 2.6(a)). Interestingly, the apparent affinities of CA_RFP variants do not readily correspond to those measured in CA alone. The zinc affinities appear to be lower in CA_RFP sensors, possibly reflecting a subtle structural alteration of CA after fusion with the red fluorescent proteins, or different optical properties on the microscope. In the case of a possible structural disturbance upon RFP fusion, switching RFP to the N-terminus of carbonic anhydrase may reduce these possible effects as the N-terminus is more flexible compared to the C-terminus. However, this flexibility could potentially reduce the FRET efficiency, resulting in lower sensitivity. Increase in the linker length from 1 Gly to 3 Gly, which could increase the flexibility, appears to reduce the apparent K_D by potentially decreasing the FRET efficiency.

CA_RFPs are the first zinc sensors used in bacteria to measure resting levels of intracellular free zinc known so far. We have optimized methods for sensor expression and calibration in the fast growing Gram negative bacteria *E. coli*. The expression-dilution method enabled measurements of free zinc in cells in the log phase with bright

mature sensors, and the *in situ* calibration eliminated the artifacts associated with *in vitro* calibrations. One key assumption of *in vivo* zinc measurements using the CA_RFP sensors is that the sensors are in equilibrium with the cellular zinc pool. This hypothesis was supported by the following data: (1) alteration of the sensor concentration *in vivo* has no significant effect on the measured zinc concentration; (2) application of CA sensors with different zinc affinities provides comparable zinc concentrations; and (3) measurement of the intracellular free zinc concentration is independent of equilibration time, indicating that the sensor equilibrates with the intracellular zinc concentration within minutes. The equilibrium time of CA_RFP sensors in the cell was much faster than that *in vitro*[190], similar to that previously seen in mammalian cells[195]. It is possible that zinc exchange is catalyzed in the cell.

Compared to other protein-based sensors developed so far, one major advantage of the CA_RFP sensors is the insensitivity to oxidation as the zinc ligands in CA are His instead of Cys in other sensors. The calibration of sensors with Cys ligands are complicated by their oxidation in air, and reliable measurements were difficult to achieve even in the presence of high concentration of reducing agents such as DTT[174]. These sensors are not suitable for detecting free zinc changes under oxidative conditions in the cell. CA-based sensors remain stable upon exposure to 1 mM hydrogen peroxide (data not shown), and therefore can be used for study zinc changes under oxidative conditions.

The CA_RFP sensors are pH sensitive, a major drawback of all protein-based sensors known to date, but to a lesser extent under physiological pH compared to other sensors with Cys as the zinc binding ligand. As expected, the zinc affinities of these sensors are pH-dependent. *In situ* calibration of the sensors at pH 7.6 shows higher

apparent zinc binding affinities compared to when the sensors are calibrationed at pH 7.0. The pH could complicate the application of these sensors if not well controlled. In the case of *E. coli*, the pH is controlled by the buffers in the minimal medium, creating a relatively stable pH environment for free zinc measurements. For applications in the cell, especially in cellular organelles, carefully controlled cellular environment and calibration is needed for zinc quantification.

2.4.2 Intracellular Free Zinc Concentration in *E. coli*

Using the CA_RFP sensors, we have measured the intracellular free zinc in *E. coli* BL21(DE3) grown in MOPS minimal medium at 20 ± 15 pM. A value of 20 pM readily exchangeable zinc in an *E. coli* cell corresponds to <1 "free" zinc ion per cell (calculated using a cell volume of 1.8×10^{-15} liter); the intracellular free zinc concentration has to be at least 1 nM to ensure 1 free zinc ion in each cell[41]. However, since the total zinc concentration in these cells is ~200 μM (measured by ICP-MS), the intracellular zinc measurements are consistent with the existence of an exchangeable zinc pool in the cell chelated by numerous metal ligands, including proteins, nucleic acids and small molecules, that function as a "zinc buffer". The expressed CA sensors form a portion of the zinc buffering capacity in the cell and equilibrate with the readily exchangeable zinc pool, as indicated by the lack of dependence of the fluorescence ratio on the sensor concentration. This principle is general for all fluorescent indicators used to measure analyte concentrations in cells. A similar analogy is the measurement of pH; pH indicators equilibrate with various proton-binding species in the solution to reach a steady level of protonation, and to

provide a readout of the ensemble proton level in the system. Similarly, we are measuring the pZn level using the expressed CA sensors.

Previous *in vitro* measurements have shown that the transcription factors that regulate the zinc transporter expression in response to changes in zinc concentration, ZntR and Zur, have femtomolar affinity for zinc[41, 109], leading to the proposal that cellular free zinc levels were in the fM range. One possible explanation for the apparently paradoxical higher cellular concentrations reported by the CA sensors (20 pM) is that the zinc occupancy of these transcription factors may not rapidly equilibrate with the readily exchangeable intracellular zinc pool when the concentration is in the pM range, consistent with their slow zinc dissociation rates[220]. However, high extracellular zinc concentrations that lead to rapid induction of Zn-dependent transcription[221] also increase the intracellular zinc concentration to the nanomolar range (see next section). This increase in the readily exchangeable zinc concentration will accelerate the cellular response to zinc stress that is slow at lower zinc concentrations. For example, the dissociation constant of the transcription factor ZntR is 10^{-15} M [109] and reasonable assumptions for the association and dissociation rate constants for Zn^{2+} are 10^{7} $M^{-1}s^{-1}$ and 10^{-8} s^{-1}. Therefore zinc equilibration is estimated to have a half-time of ~ 1 hr at 20 pM zinc and ~ 5 s at 20 nM zinc.

Many native Zn^{2+} enzymes typically have K_D^{Zn} values of 1 - 10 pM (measured *in vitro*)[109], so they should be saturated at 20 pM zinc. Other metalloproteins have lower affinities for zinc suggesting either that: zinc is not the native cofactor *in vivo*; the readily exchangeable cellular zinc concentration can vary depending on growth conditions (as proposed by Eide[6]), and/or that the zinc occupancy of these proteins

does not equilibrate readily with the free zinc pool (as proposed by Outten and O'Halloran[41]). Recent results also demonstrate that some metalloenzymes alter their native metal cofactor in response to changes in metal availability[222].

In summary, we have successfully developed a series of genetically encoded ratiometric zinc sensor and applied them for quantifying the intracellular rapidly exchangeable zinc concentration in the fast growing model organism *E. coli* at log phase in minimal medium; the median zinc concentration is 20 pM with a range of 10 to 40 pM observed in the majority of the cells. These measurements provide evidence for the availability of a "zinc pool" in *E. coli* where the excess total zinc is buffered by ligands and the sensor equilibrates with the low free zinc concentration without significantly disturbing the system. The cells maintain very low intracellular free zinc concentration with almost no free zinc ions in the cell statistically. These results demonstrated that CA-based sensors are powerful tools for studying the regulation of zinc homeostasis.

CHAPTER III

REGULATORY MECHANISM OF ZINC DETOXIFICATION IN *E. COLI* UNDER ZINC SHOCK

3.1 INTRODUCTION

Bacteria constantly face the challenge of changes in environmental metal concentrations. They have developed an extensive regulatory system for metal homeostasis to maintain the zinc content optimal for growth and proliferation. In *E. coli*, zinc homeostasis is regulated primarily through a network of zinc influx and efflux pumps[7, 223]. The influx systems include the constitutively expressed ZupT, a member of the ZRT/ IRT-like protein (ZIP) transporter family[97, 98], and the high affinity importer ZnuABC, an ATP-binding cassette (ABC) transporter complex that is up-regulated by the transcription factor Zur under zinc depletion conditions[90, 95]. The efflux systems include ZitB, a cation diffusion facilitator (CDF)[110, 224], and ZntA, a P-type ATPase transporter that is up-regulated by the transcription factor ZntR at high zinc concentrations[104, 107]. Many other transporters have also been proposed to facilitate translocation of zinc ions under various conditions, including low specificity iron transporters, inorganic phosphate transporters, and multidrug efflux systems[7, 94, 113-115].

The redundancy of this zinc regulation network raises the question of what are the distinctive functions of each component under specified conditions. In the case of ZitB and ZntA, biochemical and genetic studies have previously provided insight into their roles in zinc detoxification. ZntA consumes ATP to catalyzed zinc export while ZitB transport is driven by the transmembrane proton gradient[111]. Genetic studies have shown that ZntA is critical for the survival of *E. coli* in the presence if high environmental zinc, as knock-out of the *zntA* gene results in accumulation of high concentrations of total Zn(II) in the cell and renders the cells hypersensitive to zinc stress[104]. In contrast, the Δ*zitB* deletion strain has a doubling time for growth that is similar to the wild type strain in culture medium with high zinc concentrations, possibly due to adaptation by overexpression of ZntA; the Δ*zitB*Δ*zntA* strain shows a slight growth disadvantage at high zinc compared to the Δ*zntA* strain[110]. ZntA has an apparent *in vitro* K_m for zinc transport of 9 μM zinc, while the apparent K_m for zinc transport by ZitB was measured at 1.4 μM and 105 μM using everted *E. coli* membrane with over-expressed ZitB and reconstituted ZitB proteoliposomes, respectively[104, 111, 225]. These values are orders of magnitude higher than the proposed free zinc concentrations in the cell, which range from fM to nM[41, 226]. Neither the genetic nor the biochemical studies provide a clear paradigm how ZntA and ZitB carry out its functions in regulating the intracellular free zinc concentrations.

The transcriptional response of ZitB and ZntA under zinc stress poses additional questions. The transcription of ZitB was reported to be induced at 50 - 100 μM extracellular zinc in minimal salt medium using a Φ*(zitB-lacZ)* operon fusion on the bacterial chromosome[225]. In *E. coli* the transcription of *zntA* is regulated by ZntR, a

MerR-like transcription factor that is activated by zinc[107]. *In vitro* measurements indicate that ZntR has an apparent femtomolar affinity for zinc and zinc-dependent activation of transcription in TPEN-chelated zinc buffers[41, 109]. Two distinct models of zinc homeostasis were proposed in light of this extreme affinity. One proposal is that there are essentially no free zinc ions in the cell and zinc is trafficked within the cell bound to putative metallochaperones, as in the case of copper[227, 228]. This model assumes that ZntR equilibrates with the intracellular zinc concentration, which is unlikely to occur rapidly at the low cellular concentrations. An alternative proposal for zinc regulation, suggested by David Eide, depicts a scenario in which the cell undergoes cycles of intracellular zinc depletion and repletion[6]. Excess intracellular zinc activates transcription factors that induce the production of exporters to lower cellular zinc while metal import is activated when the efflux leads to a cellular zinc deficiency. This model provides an attractive explanation for zinc regulation through high affinity transcription factors, however, experimental evidence in bacterial cells is lacking.

To advance the understanding of bacterial metal regulation, we have developed a series of genetically-encoded fluorescent ratiometric zinc sensors with carbonic anhydrase (CA) as the scaffold to measure intracellular free zinc concentrations in *E. coli* as described in the previous chapter[226]. Using these ratiometric fluorescent sensors, we demonstrated that the median intracellular free zinc concentration in *E. coli* strain BL21(DE3) grown in MOPS minimal medium is ~ 20 pM [226]. In this work, we used these sensors to investigate how the exporter systems function in zinc detoxification. We observed a transient increase in intracellular free zinc after sudden exposure to high environmental zinc ("zinc shock"). We quantified the free zinc concentrations after zinc

shock using a fast equilibrating sensor H94N CA_TagRFP that has a DPS affinity ~ 0.08 μM (data not shown) and an apparent zinc affinity ~ 9 nM (Table 2.3) in both wild type *E. coli* and the zinc exporter knock-out strains Δ*zitB* and Δ*zntA*. The changes of intracellular free zinc concentrations in these strains differ in both timing and magnitude, highlighting the temporal coordination of *in vivo* regulatory mechanisms and suggesting that ZitB functions as a constitutive, first-line defense while ZntA is up-regulated for sustainable zinc detoxification. Furthermore, time-dependent changes in transcription of *zitB* and *zntA* after zinc shock reveal that the ZntR transcription factor up-regulates *zntA* transcription in response to nanomolar concentrations of free zinc, significantly higher than the previously measured *in vitro* activation by femtomolar zinc[41]. These results are consistent with a simple kinetic model where the ZntR transcription factor is activated by fluctuations in the intracellular free zinc concentration.

3.2 MATERIALS AND METHODS

3.2.1 *E. coli* Strains and Growth Conditions

E. coli strains from the Keio Knockout Collection were obtained from the *E. coli* Genetic Stock Center of Yale University[229]. The parent strain of this single knock-out collection, BW25113 {F-, *Δ(araD-araB)567, ΔlacZ4787*(::rrnB-3), *& lambda*$^{-}$, *rph-1, Δ(rhaD-rhaB)568, hsdR514*} was derived from *E. coli* K-12, and considered "wild type" in this work. Δ*zntA* (JW3434-1), Δ*zitB* (JW0735-1) and Δ*zntR* (JW3254-5) strains were constructed from BW25113 by replacing the target gene with a kanamycin insert[229]. *E. coli* cells were cultured in MOPS minimal medium supplemented with thiamine (1

μg/ml) and uracil (20 μg/ml)[209]. The doubling time (T_G) for growth of these cells was determined by a fit of Equation 3.1 to the growth curves (OD_{600} versus time).

$$OD_{600,t} = OD_{600,initial} \times 2^{(t/T_G)} \quad \text{Eq. 3.1}$$

3.2.2 Measurement of Intracellular Total Zinc

E. coli cells with the plasmid pTH_H94N_CA_TagRFP (see 2.3 for plasmid construction) were diluted 1:50 from an overnight culture into MOPS medium without antibiotics and grown at 25ºC to OD_{600} ~ 0.3 and then a final concentration of 50 μM $ZnSO_4$ was added to the flask. An aliquot (1 ml) of the cell culture was centrifuged (13,500 rpm, 1 min) at various time points. The pellets were washed twice with 500 μl ice-cold MOPS medium without additional zinc and once with 1 ml ice-cold ddH_2O. The pellets were then dissolved in 200 μl of 35% ultra pure nitric acid (VMR), and incubated at 37ºC overnight. The total metal content in these samples was measured by inductively coupled plasma mass spectrometry (ICP-MS), and the total zinc concentration per cell was calculated through dividing the total metal content by the total cell volume. The total cell volume was derived by multiplying the estimated average cell volume of 0.5×10^{-18} m^3 with the total number of cells as measured by OD_{600}. The number of cells per OD_{600} (~ 1.3×10^9) was calibrated by plating the cells and counting the colonies. The volume per cell of 0.5×10^{-18} m^3 was derived from the average dimensions of a *E. coli* cell of 2 μm length and 0.5 μm diameter (both strains have similar cell dimensions as observed by microscopy).

3.2.3 Measurement of Intracellular Free Zinc

Intracellular free zinc concentration was measured using carbonic anhydrase-based zinc sensors, described in the previous chapter with slight modifications[226]. The sensor expression vectors pTH_CA_TagRFP and pTH_H94N_CA_TagRFP were constructed by inserting the DNA sequence of wild type CA_TagRFP or H94N CA_TagRFP fusion genes between the restriction sites NcoI and KpnI after the trc-lac promoter on the vector pTrcHisa (Invitrogen). *E. coli* cells chemically transformed with one of these expression vectors were grown in MOPS minimal medium with 100 µg/ml ampicillin to OD_{600} ~ 0.3 at 30ºC then induced by addition of 1 mM isopropyl β-D-1-thiogalactopyranoside (IPTG). The induced cultures were incubated at 30ºC overnight allowing expression and maturation of the sensor. The culture was then diluted 1:20 into fresh MOPS medium without antibiotics and incubated at 30ºC allowing the cells to recover and grow to log-phase. At OD_{600} ~ 0.3, samples (2 µl) of the culture were placed on a poly-L-lysine-coated 96-well glass bottom plate (Matrical) and incubated with 100 µl 2 µM dapoxyl sulfonamide (DPS)[203] in MOPS medium for 20 min at room temperature. Then excess DPS was removed and 100 µl MOPS medium was added. Before imaging, 11 µl of various 10× $ZnSO_4$ stock solutions were added to the imaging medium to make the final total zinc concentrations at 10 µM, 50 µM and 100 µM for zinc shock experiments. Each culture sample was repeated in 5 separate wells, and a maximum of 2 images was taken from each well to limit photobleaching. Images were acquired at room temperature on a Nikon TE2000U inverted fluorescence microscope from two channels: FRET channel (Ex 350 nm/Em 620 nm, exposure time 500 ms) and FP channel (Ex 530 nm/Em 620 nm, exposure time 200 ms). The average I_{FRET}/I_{FP} ratio was compared to the *in situ* calibration curve of the sensor to calculate the intracellular

free zinc concentration. *In situ* calibrations of the sensors were carried out by incubating the cells with NTA-chelated zinc buffers plus digitonin and DPS as described previously[226].

3.2.4 mRNA Preparation and Quantification

E. coli cells with the plasmid pTH_H94N_CA_TagRFP were grown to OD_{600} ~ 0.3 in MOPS medium without antibiotics at 37ºC, cooled for ~ 20 min to room temperature (~ 25ºC), and then various concentrations of $ZnSO_4$ (0, 10, 50, and 100 µM) were added. A 0.5 ml sample of the cell culture was collected at various times, and diluted into 1 ml of RNeasy Bacteria Protect (Qiagen) solution. The mixture was vortexed for 5 s, incubated at room temperature for 5 min, and centrifuged for 10 min at 8,000 rpm. The cell pellets were flash frozen in a dry ice-ethanol bath, and then stored at -80ºC. Total mRNA was extracted from the cell pellets using the RNeasy Mini Kit (Qiagen) according to the manufacturer's instructions. On-column DNase I treatment was conducted to eliminate the residual DNA during the extraction. The purified total RNA was then re-incubated with DNase I for 30 min using the DNA-free DNase treatment and removal reagents (Ambion). Total mRNA concentration was measured using the NanoDrop spectrophotometer (Thermo Scientific) and an extinction coefficient of 27 $(ng/ml)^{-1}cm^{-1}$.

mRNA transcripts of the *zntA* and *zitB* genes were quantified by RT-PCR. Template cDNA was synthesized using the SuperScript III Reverse Transcriptase Kit (Invitrogen) using total mRNA as the template and random hexamers as the primers. ~ 50 ng of the synthesized first strand cDNA was used as template in the 20 µl RT-PCR

reaction. The PCR primers for the *zntA*, *zitB* and the housekeeping gene *rrsD* (16S ribosomal RNA of *rrnD* operon) were designed using the software Primer3. These primers clone a ~ 200 bp DNA sequence within each gene. The primer sequences are: *rrsD*-5' CTCAAAGGAGACTGCCAGTGATAA; *rrsD*-3' ACGATTACTAGCGATTCCGACTTC; *zntA*-5' AGTACGTAACGATGACGTGCTTG; *zntA*-3' GTCACCGCTTTGACTTTATCTTCC; *zitB*-5' AATTACTTGAAGGTGCACCGGTAT; and *zitB*-3' ATCCATCAGGTAGTGTTGGATCTG. The RT-PCR experiments were set up in triplicate and conducted using the SYBR Green qPCR SuperMix (Invitrogen) on a Mastercycler® ep realplex real time PCR machine (Eppendorf).

3.3 RESULTS

3.3.1 Growth Rates of WT, Δ*zntA* and Δ*zitB*

To evaluate the functions of the zinc exporters ZntA and ZitB in zinc detoxification, we first measured the effects of high zinc on the growth rates of wild-type and *zntA* and *zitB* single knock-out strains (Fig. 3.1). Overnight cultures of three *E. coli* strains derived from K-12, BW25113 (wild type, WT), JW3434-1 (Δ*zntA*) and JW0735-1 (Δ*zitB*) were diluted into MOPS minimal medium with or without addition of 100 μM $ZnSO_4$, and the optical density (OD_{600}) was recorded at various time points. The doubling times, T_G, were determined from a fit of Eq. 3.1 to these growth curves. The addition of 100 μM $ZnSO_4$ to cells grown in MOPS minimal medium had little effect on the doubling time for both WT (63 ± 2 min vs. 67 ± 2 min with Zn) and the Δ*zitB* (64 ± 3 min vs. 61 ± 3 min with Zn) strains, suggesting that critical zinc detoxification

mechanisms are functional in these cells. However, addition of 100 µM extracellular zinc increases the doubling time for Δ*zntA* by almost 2-fold (71 ± 3 min vs. 122 ± 15 min with Zn), indicating a significant increase in sensitivity to zinc toxicity. Consistent with previous results[104, 110], these data demonstrate that the ZntA exporter plays a major role in cellular zinc detoxification.

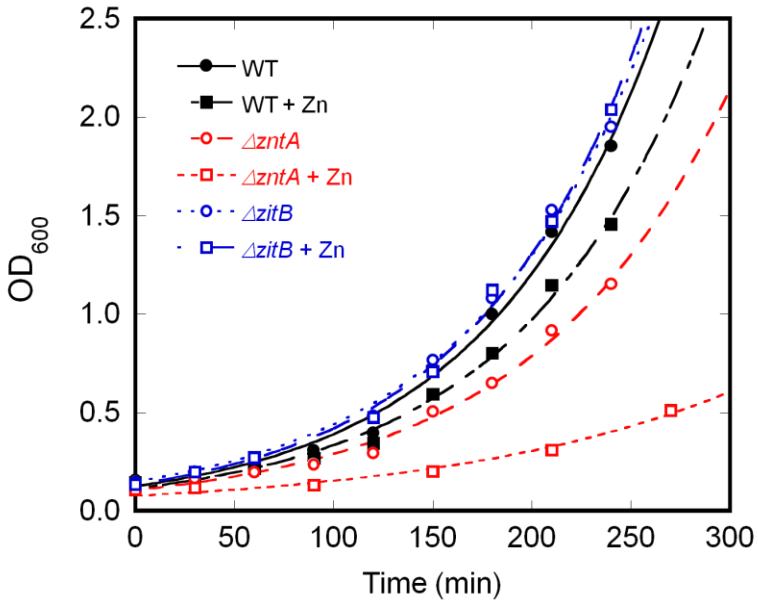

Strain/Condition	T_G (min)
WT	63 ± 2
WT+Zn	67 ± 2
Δ*zntA*	71 ± 3
Δ*zntA* + Zn	122 ± 15
Δ*zitB*	64 ± 3
Δ*zitB* + Zn	61 ± 3

Figure 3.1. Growth curves of WT, *ΔzntA* and *ΔzitB* strains. Overnight *E. coli* cultures were diluted into MOPS minimal medium with either 100 µM $ZnSO_4$ or no zinc added. The optical density at 600 nm was measured as a function of time. The doubling times (T_G) calculated from a fit of Eq. 3.1 to the growth curves are listed in the table on the right. The Δ*zntA* strain exhibits significant growth defects under high zinc, while the growth of the Δ*zitB* strain is similar to that of WT.

3.3.2 Accumulation of Total Zinc in Δ*zntA*

The detrimental effects of the *zntA* knock-out on *E. coli* growth in high zinc concentration are predicted to be related to a significantly elevated intracellular zinc level

due to impaired export. To examine this we monitored the time-dependent intracellular changes in both total zinc and free zinc (next section) in *E. coli* after zinc shock. In MOPS minimal media the total zinc concentrations of both the WT and Δ*zntA* strains are estimated at ~ 200 μM (Fig. 3.2), comparable to previous measurements[41]. After zinc shock, the total zinc concentration increases to a peak of 800 μM in WT cells (at ~5 min) and 1300 μM in Δ*zntA* cells (at ~15 min). This temporary increase is followed by a decline in zinc concentration, potentially as a result of both up-regulation of zinc export and down-regulation of zinc import systems. After zinc shock, the total zinc concentration in the WT strain persists at a higher level after 1 hr (360 μM vs. 180 μM),

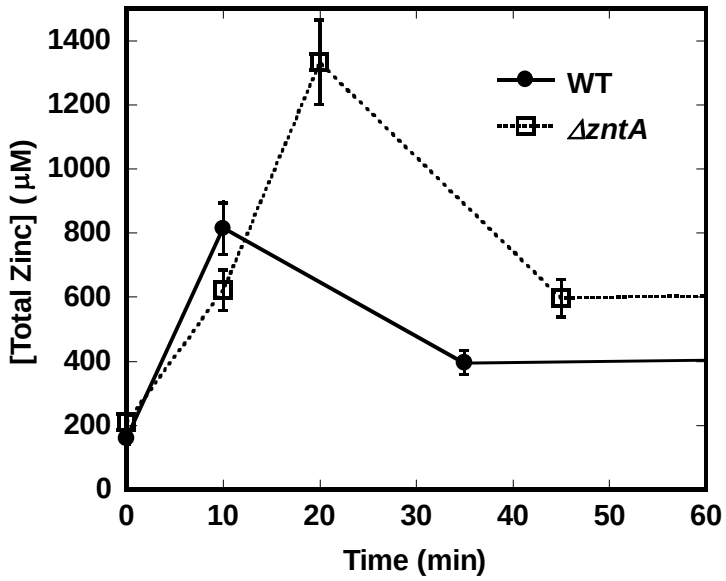

Figure 3.2. Changes in total intracellular zinc after zinc shock. 50 μM $ZnSO_4$ was added to the *E. coli* cell culture at log phase and samples were prepared in duplicate as described in the Experimental section. The total zinc in the cells from 1 ml of culture was measured by ICP-MS, and adjusted by the total cell volume, which was calculated by multiplying the number of cells by the average volume of an *E. coli* cell.

consistent with the differences in metal content previously reported for cells grown in medium with variable zinc concentrations[105]. Significantly higher total zinc remains in the Δ*zntA* strain compared to the WT strain after 1 hr (600 μM vs. 360 μM), as previously reported[110]. Overall, the Δ*zntA* cells exhibit a more dramatic increase and a sustained higher level of intracellular total zinc compared to the WT strain. These factors likely contribute to the growth defect of the *zntA* knock-out strain in high zinc.

3.3.3 Intracellular Free Zinc in WT, Δ*zntA* and Δ*zitB* Cells

In cells, the majority of the total zinc is bound to a variety of ligands, including proteins, nucleic acids and small molecules. Therefore, the concentration of readily exchangeable (or "free" zinc), rather than total zinc, likely has the largest contribution to cell toxicity. Previously, we measured the intracellular free zinc concentration of *E. coli* BL21(DE3) cells grown in MOPS minimal medium at ~20 pM using a genetically-encoded fluorescent ratiometric zinc sensor (CA_TagRFP)[226]. Here we applied this sensor to measure the intracellular free zinc concentrations in WT, Δ*zntA* and Δ*zitB* strains, at 42 ± 15 pM, 50 ± 15 pM and 106 ± 27 pM, respectively (Fig. 3.3). These cells were grown in MOPS minimal medium with uracil supplement (total zinc concentration ~ 200 nM). The increased free zinc concentration in the wild-type BW25113 strain compared to BL21(DE3) likely reflect differences in the genetic background. Under these growth conditions with moderate environmental zinc exposure, the intracellular free zinc in the Δ*zntA* and wild-type strains are comparable while the Δ*zitB* strain has a modestly higher concentration of free zinc. Under these conditions the intracellular free zinc concentration does not correlate with the doubling time since the Δ*zntA* cells grow

slightly more slowly than the WT and Δ*zitB* strains in MOPS medium (Fig. 3.2). One possible explanation is that alterations in cellular components that are required to maintain a healthy level of free zinc in the Δ*zntA* cells also lead to a decreased growth rate.

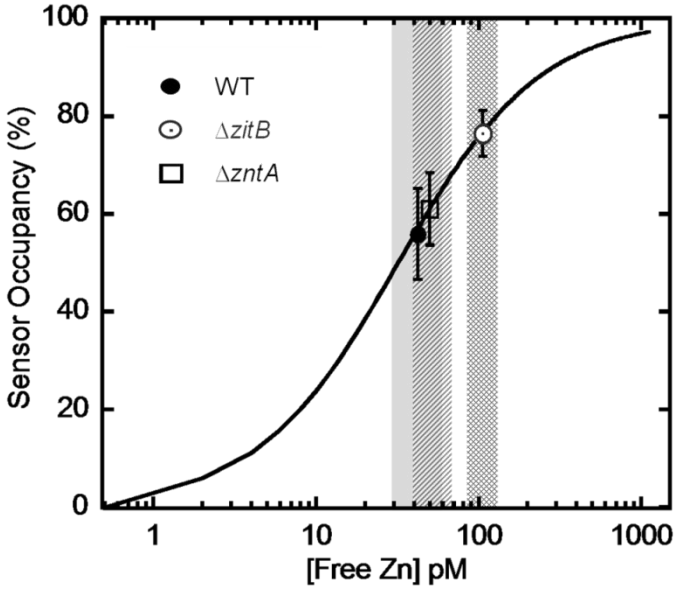

Figure 3.3. Measurement of intracellular free zinc concentrations using wild type CA_TagRFP sensor. *E. coli* strains BW25113, Δ*zntA* and Δ*zitB* transformed with pTH_CA_TagRFP (K_{Zn} ~ 30 pM) were grown in MOPS minimal medium and the cells were imaged at log phase after addition of DPS to measure the fluorescence intensity ratio I_{FRET}/I_{FP}. The sensor occupancy and the free intracellular zinc concentration were determined by comparison to an *in situ* calibration curve of wt CA_TagRFP, as described previously [226]. The intracellular free zinc as an average of ~100 cells in each sample and the error range are illustrated as follows: WT (filled circle, solid gray), Δ*zntA* (open square, dash), Δ*zitB* (open circle, cross hatch).

3.3.4 Role of *zntA* and *zitB* in Regulating Intracellular Free Zinc

The intracellular free zinc concentration is proposed to be tightly controlled within a very narrow range; here we observed a dramatic transient increase in

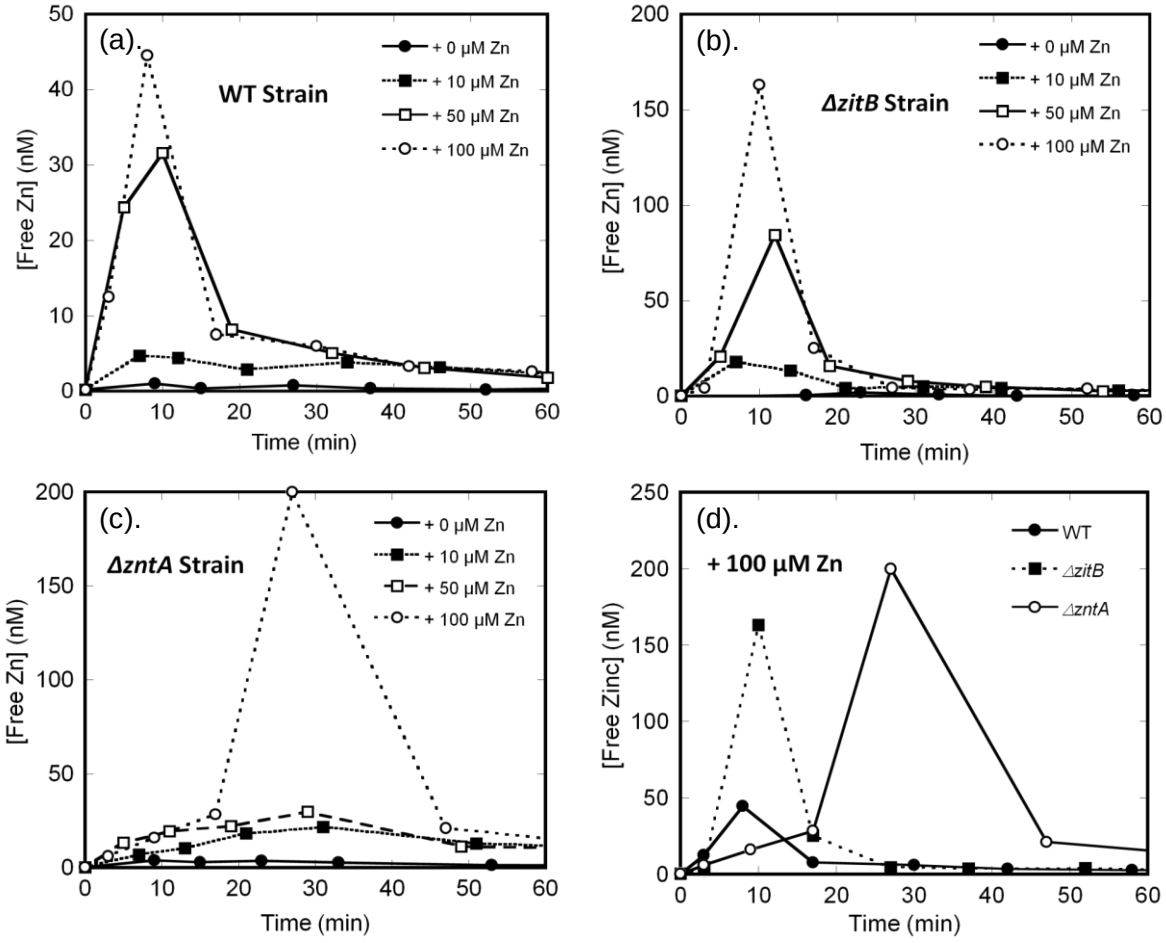

Figure 3.4. Changes in intracellular free zinc in *E. coli* WT, Δ*zitB* and Δ*zntA* strains after zinc shock. *E. coli* cells expressing the H94N CA_TagRFP (K_{Zn} ~ 9 nM) sensor were grown in MOPS minimal medium, and imaging samples were prepared by incubation with DPS as described in the Experimental section. Various concentrations of $ZnSO_4$ (0 – 100 μM) were added to the imaging medium and the cells were imaged to measure the fluorescence intensity ratio I_{FRET}/I_{FP} as a function of time. The sensor occupancy and the free intracellular zinc concentration were determined by comparison to an *in situ* calibration curve of H94N CA_TagRFP, as described previously [226]. Free zinc concentrations for cells grown in MOPS minimal medium without zinc (as measured in Fig. 3.3) are used as the baseline level at time zero. (a).(b).(c). The intracellular free zinc changes over time after addition of varying external zinc concentrations in wild type, Δ*zitB*, and Δ*zntA*.

intracellular free zinc in *E. coli* cells after sudden exposure to high environmental zinc (Fig. 3.4). This transient increase may play important roles in triggering the defensive response in *E. coli*. Using the fast equilibrating sensor H94N CA_TagRFP, we examined the time-dependence of the fluctuation in intracellular free zinc, and explore the functions of ZntA and ZitB in regulating intracellular free zinc.

In *E. coli* BW25113 (WT) cells, after zinc shock the intracellular free zinc increases dramatically (up to 10^3-fold) to nanomolar levels within 5 min, reaching a maximal concentration at ~ 10 min (Fig. 3.4(a)). The magnitude of the change in free zinc increases with the external zinc concentration; for addition of 10 μM, 50 μM and 100 μM $ZnSO_4$ to the medium, the intracellular free zinc concentration peaks at 5 nM, 30 nM and 45 nM, respectively. This pattern of temporary increase is similar to the observed changes in total zinc, although the magnitude of the alteration in free zinc concentration is much higher than the total zinc increase (2- to 4-fold, Fig. 3.2), indicative of the limited buffering capacity of an *E. coli* cell facing an abrupt zinc challenge. In a second phase, the zinc concentration decreases rapidly over the next 10 to 20 min followed by a slower decrease in zinc to nanomolar or lower levels at 1 hr. Transcriptional and/or translational up-regulation of efflux systems, down-regulation of zinc importers, and/or changes in the capacity of zinc buffers in *E. coli* can occur within this time frame to reduce the intracellular free zinc concentration.

To examine the role of zinc exporters in zinc homeostasis, we monitored the intracellular free zinc changes in the *zntA* and *zitB* single knock-out strains after zinc shock (Fig. 3.4). In the Δ*zitB* knockout strain, the intracellular free zinc peaks at a level that is ~ 3-fold higher than the WT maximal zinc concentration (Fig. 3.4 (a),(b),(d)),

suggesting an impairment in the initial zinc efflux. However, after reaching this peak, the zinc concentration declines within a time frame that is comparable to the WT strain, indicating that efflux mechanisms other than ZitB are deployed to lower the free zinc concentration. The de-coupler carbonylcyanide-p-trifluoromethoxyphenylhydrazone (FCCP) inhibits ZitB by disrupting the proton gradient across the membrane[225]; addition of 10 μM FCCP to the wild-type strain leads to an enhanced free zinc peak after zinc shock, mimicking the results obtained in the *zitB* knock-out strain (Fig. 3.5(a)). Although no significant growth defects in the presence of high extracellular zinc concentrations have been observed in the Δ*zitB* compared to the WT strain[110] (Fig. 3.1), the intracellular zinc measurements demonstrate that ZitB plays an important role in alleviating the initial zinc accumulation that potentially minimizes cellular toxicity caused by the sudden zinc influx.

The Δ*zntA* strain exhibits a distinct temporal pattern in the intracellular free zinc changes after zinc shock compared to the WT and Δ*zitB* strains (Fig. 3.4(c)(d)). The initial increase in free zinc (within 10 min) is not as dramatic as that observed in the Δ*zitB* and even WT strains at high zinc. This slower increase in the free zinc concentration after zinc shock is likely due to accommodations that the Δ*zntA* strain makes prior to the zinc shock, such as up-regulation of zinc exporters or down-regulation of importers, to compensate for the loss of ZntA for growth in the presence of even moderate zinc concentrations in the medium. Consistent with this, we measured a significantly higher transcript level of *zitB* in the Δ*zntA* strain compared to WT, while the mRNA levels of the zinc importers *zupT* and *znuC* (the ATP binding component of zinc import complex ZnuABC) remain similar to those in the WT strain (Fig. 3.6(a)). The

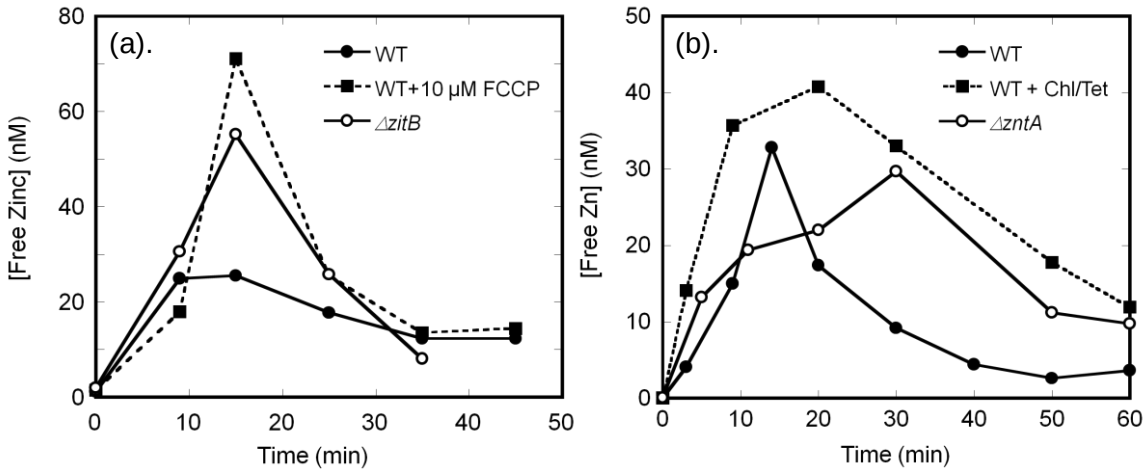

Figure 3.5. The de-coupler FCCP and protein synthesis inhibitors alter the intracellular free zinc fluctuations after zinc shock. *E. coli* cells expressing the H94N CA_TagRFP sensor were grown in MOPS minimal medium and imaging samples were prepared as described in Experimental 2.3. (a). The de-coupler FCCP inhibits the function of the ZitB exporter. 50 µM $ZnSO_4$ was added to WT (solid circle, solid line) and Δ*zitB* (open circle, solid line) cells, or 50 µM $ZnSO_4$ and 10 µM FCCP were added to WT cells (solid square, dashed line) in imaging medium at time zero. The effects of FCCP on the free zinc fluctuations in *E. coli* after zinc shock mimic the effects of the *zitB* knock-out. (b). Incubation of *E. coli* cells with protein synthesis inhibitors lead to prolonged high zinc levels after zinc shock. WT *E. coli* cells were incubated either with 170 µg/ml chloramphenicol and 50 µg/ml tetracycline for 10 min (solid square, dashed line), or without inhibitors (solid circle, solid line), then 50 µM $ZnSO_4$ was added and the fluorescence intensity ratio was measured. The time dependence of the free zinc levels in the Δ*zntA* (open circle, solid line) strain after zinc shock was measured in the absence of inhibitors.

peak intracellular zinc level in the Δ*zntA* strain occurs at 30 min, rather than 10 min, and is 4-fold higher than the maximal free zinc level observed in the WT strain at 100 µM zinc in the medium. Furthermore, at 30 min the intracellular zinc concentration in the WT and Δ*zitB* strains decreases to a sub-nanomolar level. In the Δ*zntA* strain the free zinc concentration begins to decrease after 30 min but remains at 10 nM even 90 min after zinc shock (Fig. 3.4; data not shown). The rapid decrease in the free zinc

concentration in the WT and Δ*zitB* strains compared to the Δ*zntA* strain suggests that expression of ZntA is induced under these conditions leading to the decrease in zinc concentration. To test this proposal, we measured the effect of biostatic protein synthesis inhibitors (chloramphenical and tetracycline) on the intracellular zinc concentration in the WT strain after zinc shock (Fig. 3.5(b)). Under these conditions, the WT strain is unable

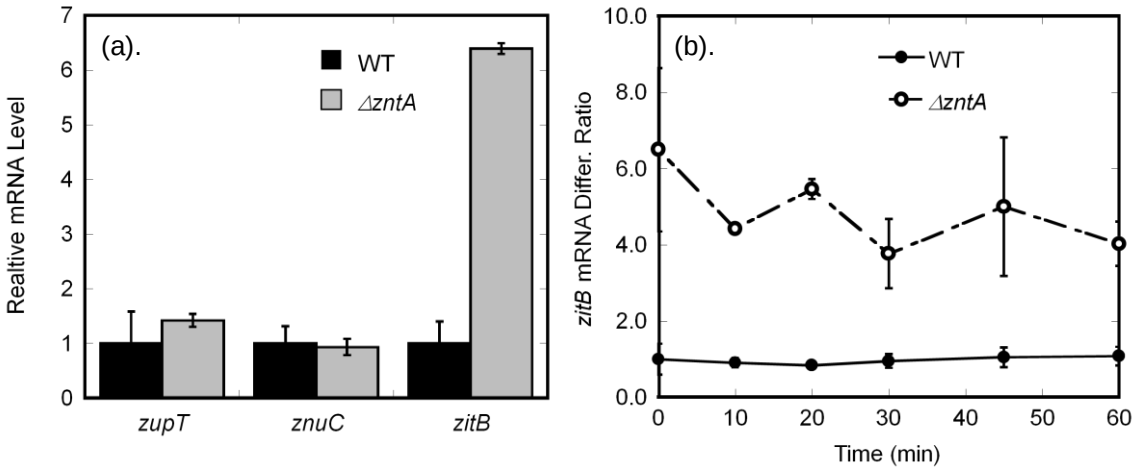

Figure 3.6. *zitB* mRNA level is up-regulated in Δ*zntA* but remains relatively constant upon zinc shock. Relative mRNA levels were measured by RT-PCR, and normalized by the level of the housekeeping gene transcript, *rrsD*, a 16S ribosomal RNA of the *rrnD* operon. (a). The mRNA level in WT is set as 1 (black bar), and the relative levels of *zupT*, *znuC* and *zitB* transcripts in Δ*zntA* are shown (gray bar). While transcription levels of zupT and znuC stay relatively constant, the mRNA level of *zitB* is increased more than 6-fold in the Δ*zntA* strain compared to that in WT. (b). *E. coli* cells (WT, solid circle; Δ*zntA*, open circle) were grown in MOPS minimal medium and 100 μM $ZnSO_4$ was added at OD_{600} ~ 0.3, samples were taken at various time points thereafter. The *zitB* transcript level in WT before adding zinc is set as the base level 1. The mRNA level of *zitB* in Δ*zntA* is normalized against the baseline (before adding zinc) *zitB* mRNA level in WT. The level of the *zitB* transcript remains relatively constant over 1 hr after zinc shock with less than two-fold changes.

to rapidly reduce the zinc concentration leading to elevated zinc concentrations even after 1 hr, mirroring the slower zinc detoxification rate of the Δ*zntA* strain. The sustained high free zinc concentrations observed in the Δ*zntA* cells negatively impact cell growth and viability (Fig. 3.1), potentially by inhibiting a variety of cellular enzymes[109, 222], demonstrating the vital function of ZntA for survival of *E. coli* grown in high environmental zinc.

3.3.5 Transcriptional Response of Zinc Exporters and Importers

zntA Transcription. The previous data demonstrate that rapid and sustained detoxification of zinc relies on the expression of ZntA. Transcription of *zntA* is up-regulated by the transcription factor ZntR under high zinc stress[230]. ZntR was previously reported to have a femtomolar apparent affinity for zinc binding and transcriptional activation in *in vitro* experiments[41]. For this high zinc affinity, ZntR should be saturated at the picomolar free zinc concentrations observed using the CA-based zinc sensor if ZntR rapidly equilibrates with the buffered free zinc pool. To examine the zinc-dependence of intracellular ZntA expression, we measured the time-dependence of *zntA* mRNA levels in WT, Δ*zntR* and Δ*zitB* strains after zinc shock using RT-PCR. In the wild-type strain, the peak *zntA* mRNA levels increase (10- to 130-fold) roughly linearly in response to intracellular free zinc concentrations up to 50 nM (Fig. 3.7(a)); no increase in *zntA* mRNA after zinc shock is observed in the Δ*zntR* strain. These data indicate that ZntR enhances transcription in response to nanomolar, rather than femtomolar, levels of free zinc *in vivo*. In the Δ*zitB* strain, the *zntA* mRNA level after zinc shock is increased by ~ 600-fold (Fig. 3.7(b)), consistent with the increased

free zinc peak concentration in this strain (Fig. 3.4). This result provides an explanation for the lack of an effect of the single gene knock-out of *zitB* on the growth and viability of *E. coli* as the loss of ZitB-catalyzed zinc efflux is readily compensated by the increased expression of ZntA.

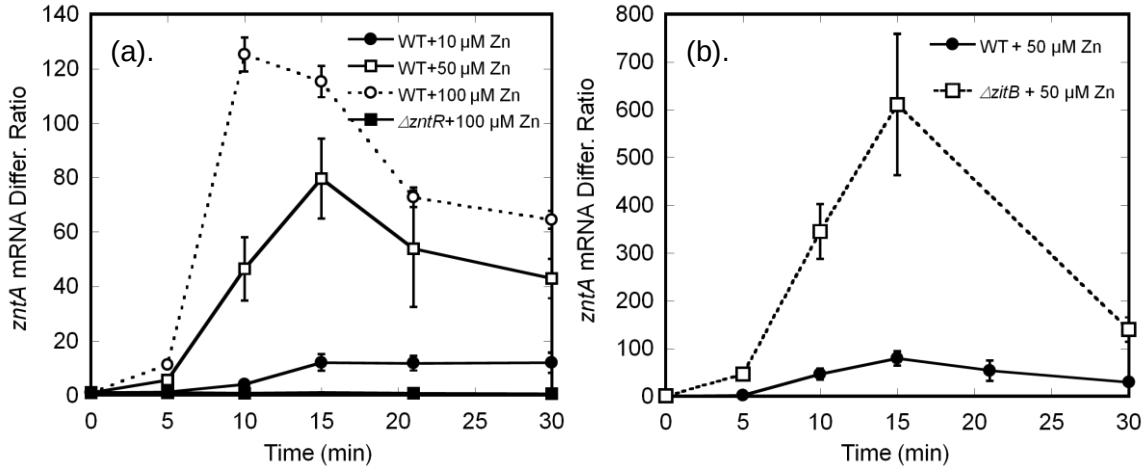

Figure 3.7. Transcription of *zntA* is strongly induced upon zinc shock. Relative mRNA levels were measured by RT-PCR, and normalized by comparison to *rrsD*. (a). mRNA level of *zntA* in wild type (100 μM Zn, open circle; 50 μM Zn, open square; 10 μM Zn, solid circle) and in Δ*zntR* (100 μM Zn, solid square) at various extracellular zinc concentrations. The transcription levels increase as the zinc concentration increases. (b). mRNA level of *zntA* in wild type (solid circle) and Δ*zitB* (open square) strains at 50 μM extracellular zinc. The level of *zntA* mRNA in the Δ*zitB* strain is significantly higher than in the WT strain due to the higher intracellular zinc concentrations upon zinc shock (shown in Fig. 3.4).

zitB Transcription. In contrast to the increase in *zntA* transcription, we observed no dramatic changes in the *zitB* mRNA levels, as measured by RT-PCR, in both the WT and Δ*zntA* strains within one hour after addition of 100 μM $ZnSO_4$ (Fig. 3.6(b)). This indicates that *zitB* expression is not directly responsive to increases in cellular free zinc

concentrations in this time frame. These data indicate that ZitB is constitutively expressed in *E. coli*, consistent with a role as a first-line defense against excess zinc. A similar lack of increase in *zitB* mRNA transcripts 3 hours after zinc addition was reported previously[221]. However, one previous study showed that the reporter β-galactosidase activity increased by 3- to 5-fold after exposure to 50 - 100 μM zinc for 3 hrs in minimal salt medium using a Φ*(zitB-lacZ)* operon fusion on the bacterial chromosome[110]. The authors proposed that *zitB* transcription was induced at high zinc, contrary to our observations. The reason for this discrepancy is not clear; one possible explanation is that high zinc concentration alters protein synthesis and degradation, leading to a modest accumulation of the reporter enzyme.

3.4 DISCUSSION

3.4.1 Regulation of Intracellular Free Zinc Fluctuations

Upon zinc shock, temporary increases in both the intracellular total and free zinc are observed; however, the increases in free zinc are much larger (Figs. 3.2 and 3.4). The dramatic increase in intracellular free zinc is caused by a sudden increase in the zinc influx due to the increased extracellular concentration coupled with a lack of sufficient intracellular ligands to rapidly sequester and buffer all of the excess zinc. While ZnuABC is the primary zinc transporter in zinc-depleted conditions, many metal transporters are proposed to catalyze zinc import under zinc-replete conditions, including ZupT (a ZIP family transporter), Pit (phosphate transporter), and other metal transporters with relatively low specificities [7, 99]. A dramatic increase in the extracellular zinc concentration disrupts the established metal gradient across the cell membrane and leads

to zinc influx via multiple transporters. These increases in total intracellular zinc overwhelm the zinc buffering capacity of *E. coli;* the lack of an abundant intracellular ligand similar to metallothionein may exacerbate the initial accumulation of free zinc ion in the cytosol after zinc shock. However, even under these conditions the total zinc concentration is more than 10^3-fold higher than the free zinc concentration (800 μM vs. 30 nM in the WT strain at 50 μM extracellular zinc), indicating that the majority of zinc is chelated. A similar transient increase in cytosolic zinc content after zinc shock has been proposed to occur in *S. cerevisiae*; in this case, zinc is transported into the cell, causing a temporary increase in the cytosolic zinc concentration, before the zinc concentration is reduced mainly by sequestration into the vacuole[231]. In *E. coli* the alterations in the zinc concentrations observed in the Δ*zitB* and Δ*zntA* strains indicate that both of these exporters play important roles in reducing cytosolic free zinc. In addition to up-regulation of zinc exporters, a variety of other mechanisms could play a role in reducing free zinc concentrations, such as down-regulation of zinc importers, and synthesis of small molecule metal ligands, such as cysteine and glutathione, to enhance the intracellular buffering capacity[232].

3.4.2 Role of ZntA and ZitB in Zinc Detoxification after Zinc Shock

The differential patterns of intracellular free zinc changes in the WT, Δ*zitB* and Δ*zntA* strains reveal the diverse functions of ZitB and ZntA in zinc detoxification. ZitB is constitutively expressed and not up-regulated under high zinc conditions, thereby functioning as a first-line defense against the initial zinc influx to minimize the toxic effects. The expression of ZntA is induced dramatically in a zinc concentration-

dependent manner to provide the sustained efflux needed to achieve and maintain the required low levels of intracellular free zinc. Therefore, the redundancy of the detoxification systems of *E. coli* ensures that the cells can adapt to abrupt and extreme environmental challenges in zinc concentration. Furthermore, these data imply that additional zinc detoxification systems function in *E. coli*. Even in the *zntA* knock-out strain, the cells are able to reduce the intracellular zinc levels (Figs. 3.2 and 3.4), albeit with a weakened response and prolonged high intracellular zinc. Although *zitB* mRNA level is elevated in Δ*zntA* compared to WT (Fig. 3.6(a)), this decline is unlikely solely due to export catalyzed by ZitB for two reasons: (1) the transcription level of *zitB* was not significantly elevated upon zinc shock in Δ*zntA* (Fig. 3.6(b)) and (2) the Δ*zntA*Δ*zitB* strain exhibits a zinc resistance level similar to that of Δ*zntA*[110]. Other transporters may play additional roles in zinc detoxification. For example, YiiP, a CDF family transporter, has demonstrated zinc transport activity *in vitro*[113, 114] even though its over-expression or deletion did not appear to alter the cells' sensitivity to zinc[110]. Furthermore, some multidrug resistance efflux systems are up-regulated in high zinc medium and knock-out of these transporters impact the growth of enterobacteria under high zinc stress[115, 221]. Additionally, zinc importers such as ZnuABC are down-regulated under high zinc[232], helping to maintain low intracellular zinc levels by decreasing zinc influx.

The elevated intracellular zinc levels after zinc shock demonstrate the ability of *E. coli* cells to tolerate high levels of extracellular zinc by both accommodating higher intracellular concentrations for short periods of time in addition to detoxifying zinc by energy-consuming efflux. Cells could potentially adapt to a high zinc environment over a longer period of time by up-regulating synthesis of periplasmic and intracellular zinc

ligands to enhance the buffering capacity of the cell, such as the periplasmic zinc-binding protein ZraP and the cysteine synthesis pathway[119, 232]. Ribosomes have been proposed as a major zinc storage pool under normal conditions[233 234]; under zinc deficient conditions zinc is released from ribosomes for use in other metalloproteins[91]. However, the importance of ribosomes in buffering zinc under excess zinc is unknown. Additional mechanisms in *E. coli* zinc tolerance remain to be investigated.

3.4.3 Intracellular Free Zinc Spikes Accelerate a Transcriptional Response

The temporary intracellular peak in free zinc may be important for activating the zinc detoxification system in *E. coli*. Intracellular zinc concentrations lower than 1 nM, including the measured values of 20 – 50 pM, mean that there is less than one free zinc ion per *E. coli* cell, as originally discussed by O'Halloran and colleagues[41]. These low concentrations of free zinc can lead to slow equilibration of proteins with the total zinc pool even when zinc association is limited by diffusion. The zinc affinity of ZntR measured *in vitro* is in the femtomolar range[41]; however, the activation of *zntA* transcription *in vivo* occurs at nanomolar concentrations of free zinc (Fig. 3.7). This discrepancy suggests that ZntR may respond mainly to transient changes in zinc so that it is under kinetic, rather than thermodynamic, control. At 50 pM free zinc, there is <1 free zinc ion per cell; however, the total zinc concentration is 200 – 800 μM (Fig. 3.2) indicating that various ligands in the cytosol are capable of binding and buffering zinc to maintain the low free zinc ion levels. Assuming a reasonable zinc association rate constant of 10^7 $M^{-1}s^{-1}$ to ZntR[235], the half time for equilibration is ~ 20 min at 50 pM free zinc. Therefore, if ZntR only binds free zinc, equilibration with cellular zinc pools

should be slow under these conditions. However, the equilibration half time is accelerated to seconds when the free zinc concentration reaches the nanomolar range. Sudden exposure of *E. coli* to high concentrations of environmental zinc causes a transient fluctuation in the intracellular free zinc concentration to a value that is orders of magnitude higher than the resting level. This change in intracellular free zinc accelerates the association rate of zinc with ZntR which in turn enhances transcription of ZntR-responsive genes and initiates the regulated zinc detoxification process. This analysis suggests that kinetic control of ZntR is plausible and that fluctuation of intracellular zinc concentrations could lead to activation of expression systems that allow the cell to react and adapt to environmental changes. These data are consistent with the zinc homeostasis model proposed by David Eide[6], in which transcriptional responses are mediated by fluctuations in intracellular zinc.

3.4.4 The *In Vivo* Zinc Affinity of ZntR

In vitro zinc binding and transcription assays measured under equilibrium conditions demonstrated that ZntR responds to changes in free zinc in the femtomolar range[41]. Therefore, if ZntR equilibrates rapidly with the intracellular free zinc concentration under all conditions, then transcription of ZntR-responsive genes should be saturated even in low zinc media where $[Zn]_{free}$ is at picomolar levels (Fig. 3.3)[226]. The apparent rate for zinc association can be increased significantly by binding a zinc species chelated by small molecules or putative "zinc chaperones" as the concentrations of these complexes could be significantly higher since the total cellular zinc concentration is ~ 200 µM (Fig. 3.2). However, our data show that the *zntA* mRNA increases by 10- to 100-

fold as the intracellular free zinc concentration increases from ~ 50 pM to 5 - 80 nM (i.e. the availability of free zinc ions increases from <1 to 5 - 100 ions per cell) (Fig. 3.7). Therefore, ZntR-mediated transcription of zntA has an apparent $K_{1/2}$ for free zinc in the nanomolar range *in vivo*. Here we explore some possible explanations for the discrepancy between the apparent zinc affinity of ZntR under *in vivo* and *in vitro* conditions.

First, as proposed above, activation of ZntR by zinc could be kinetically controlled. If ZntR only binds free zinc ions it should not rapidly equilibrate with the pM levels of cellular free zinc. Increasing the free zinc concentration to nM levels accelerates the formation of zinc-bound ZntR and subsequent activation of *zntA* transcription. Therefore ZntR could be activated by free zinc in the nanomolar range as the apparent association rate is linearly dependent on the free zinc concentration. In this model, activation depends mainly on the zinc association rate constant, assuming that $k_{on}[Zn^{2+}] > k_{off}$, and theoretically the zinc dissociation constant could be either femtomolar or low nanomolar. On the other hand, if ZntR has a femtomolar affinity for zinc as reported previously, a simple model of kinetic control cannot explain the rapid decline in the *zntA* transcript level paralleling the decreases in intracellular free zinc (Fig. 3.8). Assuming a simple association reaction with diffusion-controlled zinc binding, the half-time for zinc dissociation for a femtomolar zinc binding site is estimated at >100 days; this half-time decreases to the minute range for a nanomolar affinity site. The *zntA* mRNA level is maximal at 10 to 15 min after zinc shock and then decreases over the next 30 min, paralleling the decline in the intracellular free zinc level (Fig. 3.8). Furthermore, the transcript level increases with the peak free zinc concentration up to nanomolar levels.

More complicated mechanisms, such as zinc-dependent enhancement of RNA degradation or proteolysis of zinc-bound ZntR, could contribute to the decrease in the ZntA mRNA levels.

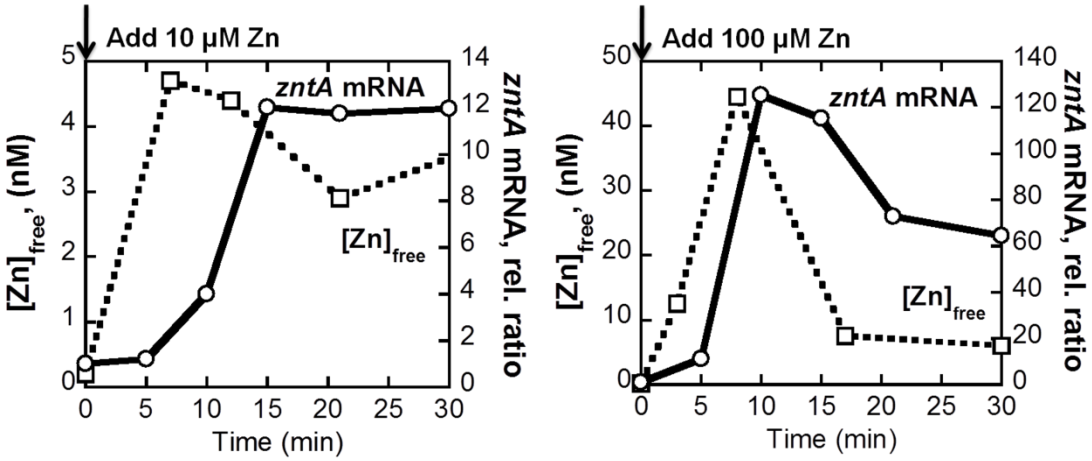

Figure 3.8. Correlating time course between intracellular free zinc changes and the transcription level of *zntA*. The changes in the transcript level of *zntA* mRNA largely follow the changes of intracellular free zinc with a 5 – 10 min time lag across various zinc concentrations. This correlation suggests that *zntA* transcription is regulated kinetically by the intracellular free zinc changes, and that ZntR has a nanomolar intracellular zinc affinity.

Second, all of the data can be easily explained if the ZntR-mediated transcription has a nanomolar, rather than femtomolar, apparent $K_{1/2}$ in the cell. In this case, transcription will readily respond to fluctuations in the intracellular free zinc concentration at nanomolar levels. A number of explanations for the apparent decrease in the zinc affinity of ZntR *in vivo* can be envisioned. For example, the $K_{1/2}$ for activation of ZntR by zinc could be increased from fM to the nM range due to competition with other ligands, oxidation of the cysteine ligands in ZntR and/or negative allosteric

regulation by other effectors in the cell. Alternatively, another component in the transcription complex could require nanomolar free zinc concentrations to activate transcription or zinc binding to ZntR could stabilize the protein and enhance the availability of ZntR in the cell, thereby regulating the transcriptional response[108].

In summary, exposure of *E. coli* cells to micromolar environmental zinc concentrations leads to a transient intracellular free zinc peak in the nanomolar range. If the zinc peak is short-lived, it has little effect on the growth rate and viability of *E. coli* cells. Several exporters, including ZitB and ZntA, function to decrease intracellular zinc concentrations. In particular, the transient intracellular zinc rise to nanomolar levels induces ZntR-mediated transcription of *zntA* as a cellular response to zinc detoxification. ZitB and ZntA exhibit distinct functions in regulating intracellular free zinc upon zinc shock. ZitB counteracts the initial zinc influx, acting as a first-line defense against zinc shock. In contrast, expression of the ZntA exporter is induced by the increase in free zinc and provides an efficient and sustainable detoxification mechanism to remove excess cellular zinc. This temporal pattern reveals that *E. coli* coordinates multiple mechanisms to reduce metal toxicity.

CHAPTER IV

FUNCTIONS OF BAE S/R REGULON IN ZINC HOMEOSTASIS IN *E. COLI*

4.1 INTRODUCTION

Although ZntA and ZitB are the best known zinc transporters, it has been proposed that other transporters may also be involved in zinc detoxification. Our results in the previous chapter showed that the cells are able to reduce the free and total zinc contents even with *zntA* knockout (Fig.3.2 and Fig.3.4). Genomic studies also showed up-regulation of transporter genes other than *zntA*, including *acrD, mdtA, mdtC, mdtD, yfiK,* and *amtB, etc*[221]. Among these transporters, *acrD, mdtA, mdtC* and *mdtD* are all controlled by the BaeS/R (bacterial adaptive response) two-component system[236], which implies that the BaeS/R regulon may play a role in zinc regulation.

BaeS/R two-component signal transduction system is one of the three extracytoplasmic stress response (ESR) systems in *E. coli* that controls the adaptive responses to changes in the environment[237]. BaeS is a membrane-bound histidine kinase that senses the environmental changes and transduces the information to the transcription factor BaeR through phosphorylation[236]. BaeR modulates the expression of eight genes, which encode three transporters, one periplasmic protein and the two-component system BaeS/R itself[120, 236] (Fig.4.1). These genes are involved in envelope stress response, drug

resistance, and metal resistance of *E. coli* and *Salmonella*. The BaeS/R regulon responds to a wide range of environmental stresses, including spheroplasting, and exposure to indole, tannin, flavonoid, sodium tungstate, and high levels of zinc or copper[221, 236]. Previous studies have focused on the involvement of BaeS/R regulon in drug resistance, while the role of the BaeS/R regulon in zinc detoxification and homeostasis regulation is still emerging[115]. The transporters and the periplasmic protein on the BaeS/R regulon are up-regulated upon exposure to high concentrations of zinc[221], and *Salmonella* strains lacking genes on this regulon exhibit significant growth defects under high zinc conditions[115]. Here we seek to further investigate the role of this gene cluster in zinc homeostasis and to understand the function of each component.

BaeS is an inner-membrane-bound histidine kinase containing a periplasmic sensing domain[238]. BaeR is a cytoplasmic transcription factor that can be phosphorylated by BaeS, which results in the activation of DNA binding of BaeR, leading to initiation of gene transcription. Genetic studies revealed a consensus BaeR binding sequence, 5'-TTTTTCTCCATDATTGGC-3' (where D is G, A, or T), in the promoter regions of the *mdtABCD-baeSR* operon, *acrD* gene and *spy* gene (Fig. 4.1)[120]. The *mdtABC* and *acrD* sequences encode components of two RND (Resistance-Nodulation-Cell Division)-type transporters, *mdtD* encodes a putative transporter that belongs to the major facilitator superfamily (MFS), and *spy* encodes a small periplasmic protein. Activation of the BaeS/R regulon results in a positive feedback loop as the expression of the two-component system BaeS and BaeR is also up-regulated. In addition to BaeS/R, the *mdtABCD*, *acrD* and *spy* genes are also proposed to be regulated by another envelope stress response two-component system, CpxA/R, as a consensus binding sequence for the

transcription factor CpxR can also be found upstream of the promoters in addition to the BaeR binding sequence[239]. However, the zinc-associated gene up-regulation is modulated through the BaeS/R system, not the CpxA/R system[115, 239].

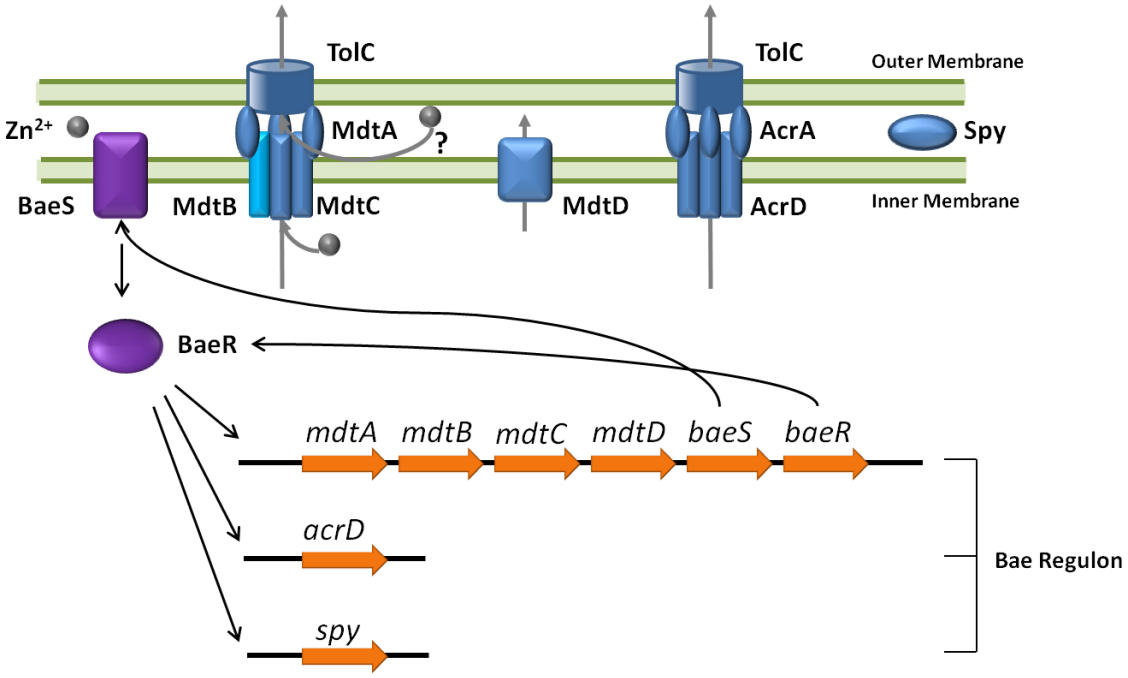

Figure 4.1. Schematic illustration of the BaeS/R regulon. The BaeS/R regulon encodes three transporters and one periplamic protein. The membrane-bound BaeS senses environmental signals and transduces them to the transcription activator BaeR, which up-regulates the expression of eight genes on this reguon including *baeR* and *baeS*. MdtABC forms a RND-type transenvelope efflux complex with TolC. MdtD belongs to the major facilitator family for metal transport. AcrD forms another RND-type efflux system in complex with AcrA and TolC. Spy is a periplsmic protein that exhibits ATP-independent chaperone activities *in vitro*. The regulator BaeS and BaeR are also up-regulated, forming a positive feedback loop to amplify the transcriptional response.

MdtA, MdtB and MdtC form a RND-type trans-envelope efflux multiplex with the outer membrane pore protein TolC in *E. coli*[116]. MdtB and MdtC form a

heterotrimeric proton-substrate antiporter across the inner membrane, which is connected to the outer membrane factor TolC through the membrane fusion protein MdtA. Exposure to 0.2 – 1 mM zinc resulted in a 2- to 3-fold increase in the transcription levels of *mdtA* and *mdtC* via regulation of BaeS/R[115, 221]. Over-expression of MdtABC confers resistance to drugs such as novobiocin (16-fold) and deoxycholate (32-fold)[240]. MdtB is not necessary for drug resistance as trans-expression of *mdtA* and *mdtC* are sufficient to induce the phenotypes in *E. coli*[116]. It is possible that the MdtB/MdtC heterotrimer may be replaced by an MdtC homotrimer in the transmembrane channel as MdtB shares ~ 50% amino acid sequence similarity with MdtC. Two models were proposed regarding the transport mechanisms: periplamsic transport, in which the substrates enter the efflux channel from the periplasmic space through interactions with the membrane fusion protein; and transenvelope efflux, in which the substrates enter the channel from cytosol[102]. Similar to all RND-type transporters in *E. coli* except the copper transporter CusABC, MdtABC requires TolC as the outer membrane factor to function[115].

mdtD, the fourth gene on the *mdtABCD-baeSR* operon, encodes a putative transporter that belongs to the major facilitator superfamily (MFS) based on sequence analysis[117]. The MFS transporters are single-polypeptide secondary carriers capable of transporting small solutes in response to chemiosmotic gradients[241]. They typically have 12 – 14 transmembrane domains. Similar to *mdtA/B/C*, exposure to high zinc resulted in an ~ 2-fold increase in *mdtD* transcription[221]. The transport mechanism and biological function of MdtD is unknown. There is no evidence that MdtD is involved in multidrug resistance; over-expression of MdtD does not confer resistance to two dozen drugs tested

in *E. coli* KAM3[240], and deletion of *mdtD* does not affect the drug resistance in cells overexpressing BaeR either[117].

acrD encodes an aminoglycoside efflux pump[242, 243] that is a homologue to the well-known multidrug resistance transporter, AcrB. Like AcrB, AcrD forms a trans-inner-membrane homotrimer which complexes with the membrane fusion protein AcrA and outer membrane channel TolC as an RND-type efflux pump[244]. The AcrD-mediated cross-membrane transport measured *in vitro* is activated by addition of AcrA[245]. Exposure to zinc caused a 4- to 6-fold increase in *acrD* transcription activated by BaeS/R[115]. Over-expression of AcrD in *E. coli* resulted in resistance to deoxycholate (>40,000-fold), sodium dodecyl sulfate (>400-fold), kanamycin (12.5-fold), and novobiocin (6.25-fold)[117].

Spy, another gene product modulated by the BaeS/R system, is a 12-kDa periplasmic protein that was first demonstrated to be up-regulated during spheroplasting[246]. In addition to spheroplast formation, denatured proteins and metal stress induce expression of Spy. Copper and zinc exposure lead to over-expression of Spy through regulation by CpxA/R and BaeS/R, respectively[89]. However, Spy does not demonstrate significant zinc binding affinity, even though its transcription is up-regulated 20- to 50-fold upon zinc exposure[87, 221]. Recent findings suggest that Spy functions as a periplasmic molecular chaperone to suppress protein aggregation and enhance protein folding under envelope stress conditions[247]. Spy may provide protection against zinc-induced protein denaturation and aggregation in the periplasm.

Although the BaeSR regulon is up-regulated upon high zinc exposure, the biological functions of the individual proteins are not clear. The roles of the BaeS/R-

regulated transporters in protecting cells against high zinc stress were first studied in *Salmonella enterica*[115]. The mutant strains Δ*acrD*Δ*mdtABC* and Δ*baeSR* are much more sensitive to zinc and copper stress than the wild type strain, while no changes in drug resistance were observed. These results implicate that the BaeS/R regulon may play an important physiological role in metal homeostasis, similar to the function of the RND-type copper transporter, CusABC, in copper resistance. In this chapter, we investigated the function of each component of BaeS/R regulon in the regulation of zinc homeostasis in *E. coli*. We demonstrate that deletion of *mdtC, mdtD* and *spy* result in slower cell growth rate at high cell density, as well as a temporary increase in the intracellular free and total zinc concentrations upon zinc shock. These results provide further evidence that components of BaeS/R are involved in the regulation of intracellular zinc homeostasis, in addition to a role in multidrug resistance.

4.2 METHODS AND MATERIALS

4.2.1 *E. coli* Strains and Growth Conditions

E. coli strains from the Keio Knockout Collection were obtained from the *E. coli* Genetic Stock Center of Yale University[229]. The parent strain of this single knock-out collection, BW25113 {F-, *Δ(araD-araB)567, ΔlacZ4787*(::rrnB-3), *& lambda*$^{-}$, *rph-1, Δ(rhaD-rhaB)568, hsdR514*} was derived from *E. coli* K-12, and is considered "wild type" in this work. Δ*mdtA* (JW5338-1), Δ*mdtB* (JW2060-1), Δ*mdtC* (JW2061-3) , Δ*mdtD* (JW2062-1), Δ*acrD* (JW2454-1), Δ*baeS* (JW2063-1), Δ*baeR* (JW2064-3), Δ*spy* (JW1732-1) strains were constructed from BW25113 by replacing the target gene with a kanamycin insert [229]. *E. coli* cells were cultured in MOPS minimal medium

supplemented with thiamine (1 µg/ml) and uracil (20 µg/ml) [209]. The doubling time (T_G) for growth of these cells was determined by a fit of Equation 4.1 to the growth curves (OD_{600} versus time).

$$OD_{600,t} = OD_{600,initial} \times 2^{(t/T_G)} \quad \text{Eq. 4.1}$$

4.2.2 Measurement of Intracellular Total Zinc

E. coli cells transformed with the plasmid pTH_H94N_CA_TagRFP (see 2.3 for plasmid construction) that encodes a carbonic anhydrase-based zinc senor were diluted 1:50 from an overnight culture with addition of 100 µg/ml ampicillin into MOPS medium without antibiotics and grown at 25ºC to OD_{600} ~ 0.3 and then a final concentration of 50 µM $ZnSO_4$ was added to the flask. An aliquot (1 ml) of the cell culture was centrifuged (15,000 g, 1 min) at various time points. The pellets were washed twice with 500 µl ice-cold MOPS medium without additional zinc and once with 1 ml ice-cold ddH_2O. The pellets were then dissolved in 200 µl of 35% ultra pure nitric acid, and incubated at 37ºC overnight. The total metal content in these samples was measured by inductively coupled plasma mass spectrometry (ICP-MS), and the total zinc concentration per cell was calculated through dividing the total metal content by the total cell volume. The total cell volume was derived by multiplying the estimated average cell volume for *E. coli* of 0.5×10^{-18} m^3 with the total number of cells as measured by OD_{600}. The number of cells per OD_{600} (~ 1.3×10^9) was calibrated by plating the cells and counting the colonies. The volume per cell of 0.5×10^{-18} m^3 was derived from the average dimensions of a *E. coli* cell of 2 µm length and 0.5 µm diameter[248, 249] (both strains have similar cell dimensions as observed by microscopy).

4.2.3 Measurement of Intracellular Free Zinc

Intracellular free zinc concentration was measured using carbonic anhydrase-based zinc sensors as described in the previous chapter with slight modifications [226]. The sensor expression vectors pTH_CA_TagRFP and pTH_H94N_CA_TagRFP were constructed by inserting the DNA sequence of wild type CA_TagRFP or H94N CA_TagRFP fusion genes between the restriction sites NcoI and KpnI after the trc-lac promoter on the vector pTrcHisa (Invitrogen). The CA_TagRFP genes were sequenced at the University of Michigan Sequencing Core facility. *E. coli* cells chemically transformed with one of these expression vectors were grown in MOPS minimal medium with 100 µg/ml ampicillin to OD_{600} ~ 0.3 at 30ºC then induced by addition of 1 mM isopropyl β-D-1-thiogalactopyranoside (IPTG). The induced cultures were incubated at 30ºC overnight allowing expression and maturation of the sensor. The culture was then diluted 1:20 into fresh MOPS medium without antibiotics and incubated at 30ºC allowing the cells to recover and grow to log-phase. At OD_{600} ~ 0.3, samples (2 µl) of the culture were placed on a poly-L-lysine-coated 96-well glass bottom plate (Matrical) and incubated with 100 µl 2 µM dapoxyl sulfonamide (DPS) [203] in MOPS medium for 20 min at room temperature. Then excess DPS was removed and 100 µl MOPS medium was added. Before imaging, 11 µl of various 10× $ZnSO_4$ stock solutions were added to the imaging medium to make the final total zinc concentrations 50 µM for zinc shock experiments. Each culture sample was repeated in 5 separate wells, and a maximum of 2 images was taken from each well to limit photobleaching. Images were acquired at room temperature on a Nikon TE2000U inverted fluorescence microscope from two channels:

FRET channel (Ex 350 nm/Em 620 nm, exposure time 500 ms) and FP channel (Ex 530 nm/Em 620 nm, exposure time 200 ms). The average I_{FRET}/I_{FP} ratio was compared to the *in situ* calibration curve of the sensor to calculate the intracellular free zinc concentration. *In situ* calibrations of the sensors were carried out by incubating the cells with NTA-chelated zinc buffers plus digitonin and DPS as described previously [226].

4.2.4 mRNA Preparation and Quantification

E. coli cells with the plasmid pTH_H94N_CA_TagRFP were grown to OD_{600} ~ 0.3 in MOPS medium without antibiotics at 37ºC, cooled for ~ 20 min to room temperature (~ 25ºC), and then various concentrations of $ZnSO_4$ (0, 10, 50, and 100 μM) were added. A 0.5 ml sample of the cell culture was collected at various times, and diluted into 1 ml of RNeasy Bacteria Protect (Qiagen) solution. The mixture was vortexed for 5 s, incubated at room temperature for 5 min, and centrifuged for 10 min at 5,500 g. The cell pellets were flash frozen in a dry ice-ethanol bath, and then stored at -80ºC. Total mRNA was extracted from the cell pellets using the RNeasy Mini Kit (Qiagen) according to the manufacturer's instructions. On-column DNase I treatment was conducted to eliminate the residual DNA during the extraction. The purified total RNA was then re-incubated with DNase I for 30 min using the DNA-free DNase treatment and removal reagents (Ambion). Total mRNA concentration was measured using the NanoDrop spectrophotometer (Thermo Scientific) and an extinction coefficient of 27 $(ng/ml)^{-1}cm^{-1}$.

mRNA transcripts of the *zntA* and *zitB* genes were quantified by RT-PCR. Template cDNA was synthesized using the SuperScript III Reverse Transcriptase Kit

(Invitrogen) using total mRNA as the template and random hexamers as the primers. ~ 50 ng of the synthesized first strand cDNA was used as template in the 20 µl RT-PCR reaction. The PCR primers for the *zntA*, *zitB* and the housekeeping gene *rrsD* (16S ribosomal RNA of *rrnD* operon) were designed using the software Primer3. These primers clone a ~ 200 bp DNA sequence within each gene. The primer sequences are listed in Table 4.1.

Gene	Primer Sequence
rrsD-5'	CTCAAAGGAGACTGCCAGTGATAA
rrsD-3'	ACGATTACTAGCGATTCCGACTTC
mdtA-5'	TTAATAATCAGGATGATGCGCTGT
mdtA-3'	CACCACTTTCTGACTGTCCTGAAT
mdtB-5'	CGGTTATGGTGTTTCTCGATTTTT
mdtB-3'	AGGTCAGCGAGATAATGGTAAAGC
mdtC-5'	TCCAGACCAATGATGAGCTAAAAA
mdtC-3'	TGTCAACCGTCTGGATAATATTGG
mdtD-5'	AGATTGACGGTGATGAAAATCGTA
mdtD-3'	GTAGTTCGGCATTAACAGCAATGT
baeR-5'	GAGTTACCAATCGACGAAAACACA
baeR-3'	CAGGGAGCATCAGATCTAACAGG
acrD-5'	ACTTCACCCATGAAAAAGACAACA
acrD-3'	CGATAACGCGAGCTTCTTTAATTT
spy-5'	AGGACATGATGTTCAAAGACCTGA
spy-3'	ATGTTAGCTTTGCGCTGTTCTTC

Table 4.1. Primers for quantification of gene transcripts by RT-PCR.

The RT-PCR experiments were set up in triplicate and conducted using the SYBR Green qPCR SuperMix (Invitrogen) on a Mastercycler® ep realplex real time PCR machine (Eppendorf).

4.3 RESULTS

4.3.1 Growth Rates of Bae Regulon Knockout Strains

We first examined the effects of single gene knockouts in the Bae regulon on the growth rate of *E. coli*. Overnight culture of *E. coli* strains *WT,* Δ*baeR,* Δ*baeS,* Δ*mdtA,* Δ*mdtB,* Δ*mdtC,* Δ*mdtD,* Δ*acrD,* and Δ*spy* were diluted to OD_{600} ~ 0.1 into MOPS minimal medium without additional zinc or with 300 μM $ZnSO_4$, and the OD_{600} of each sample was recorded. Eq. 4.1 was fit to this time course to calculate the average doubling time. As shown on Fig. 4.2, the *E. coli* cells exhibited biphasic growth curves. Cells grown in medium without additional zinc enter a distinctly slower growth phase after ~150 min, while cells grown in medium with high zinc enter a slower growth phase after ~ 250 min. The growth rates at different phases were obtained by fitting the growth curves to Eq. 4.1

$$OD_{600,t} = OD_{600,initial} \times 2^{\left(\frac{t}{T_G}\right)} \qquad \text{Eq. 4.1}$$

On the log scale plots (Fig. 4.2), the doubling time is reflected as the slope of the fitted growth curve. The doubling time values were also re-plotted in Fig. 4.3 to facilitate comparison among the various strains. In MOPS medium without additional zinc, no significant differences in growth rates were observed between WT and all of the single knockout strains in either early or late growth phase (Fig. 4.3(a)). This is not surprising given that Bae regulon is primarily responsible for the cell's adaptive response to environmental stress conditions, so its functions may not be essential under normal growth conditions. When grown in the presence of 300 μM zinc, slower growth rates are observed for the following single knockout strains: Δ*baeR* (T_G = 205 ± 34 min), Δ*baeS* (T_G = 243 ± 35 min), Δ*mdtA* (T_G = 253 ± 26 min), Δ*mdtC* (T_G = 264 ± 33 min), Δ*mdtD*

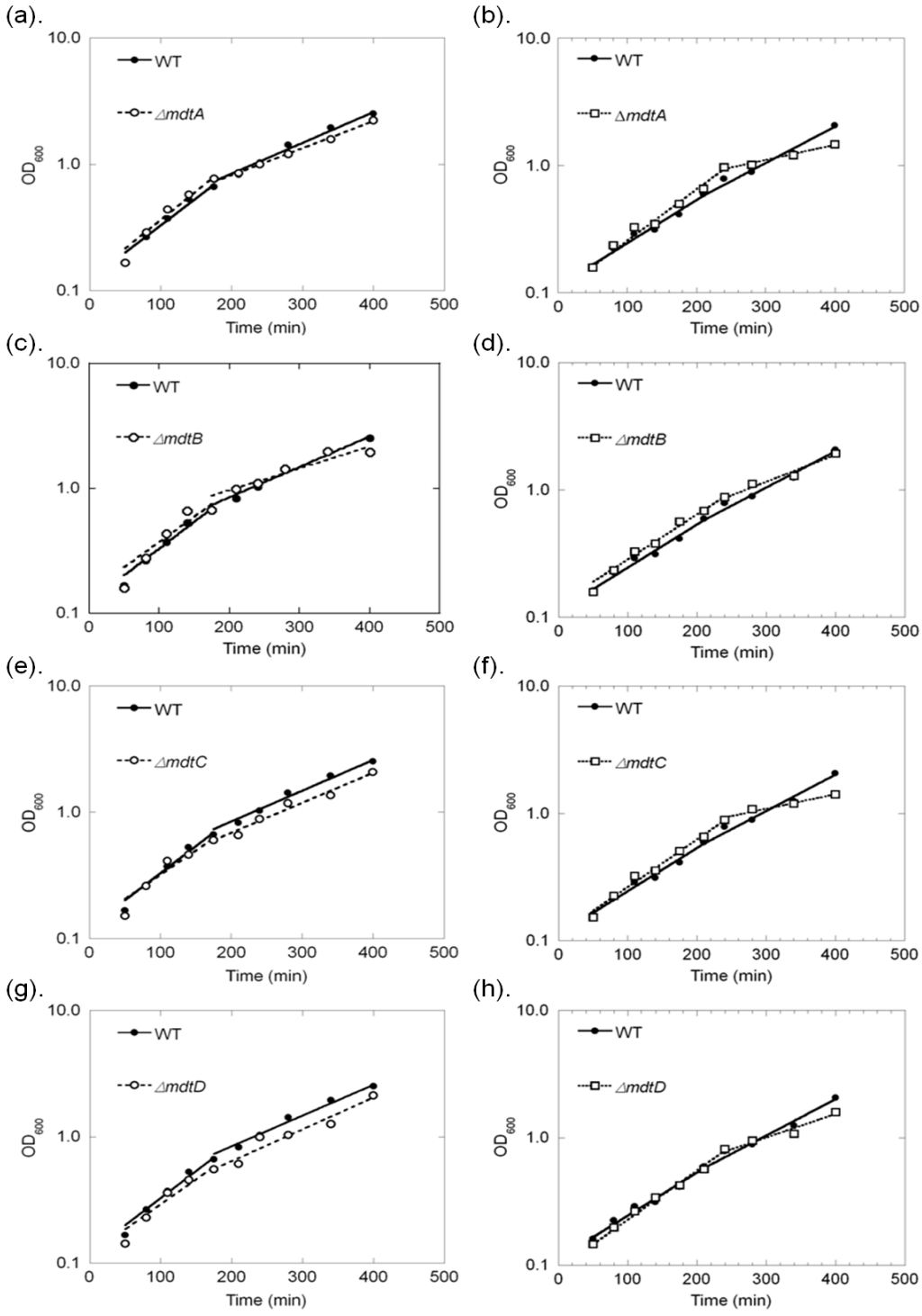
(a).
WT
ΔmdtA
OD600
Time (min)
(b).
WT
ΔmdtA
OD600
Time (min)
(c).
WT
ΔmdtB
OD600
Time (min)
(d).
WT
ΔmdtB
OD600
Time (min)
(e).
WT
ΔmdtC
OD600
Time (min)
(f).
WT
ΔmdtC
OD600
Time (min)
(g).
WT
ΔmdtD
OD600
Time (min)
(h).
WT
ΔmdtD
OD600
Time (min)

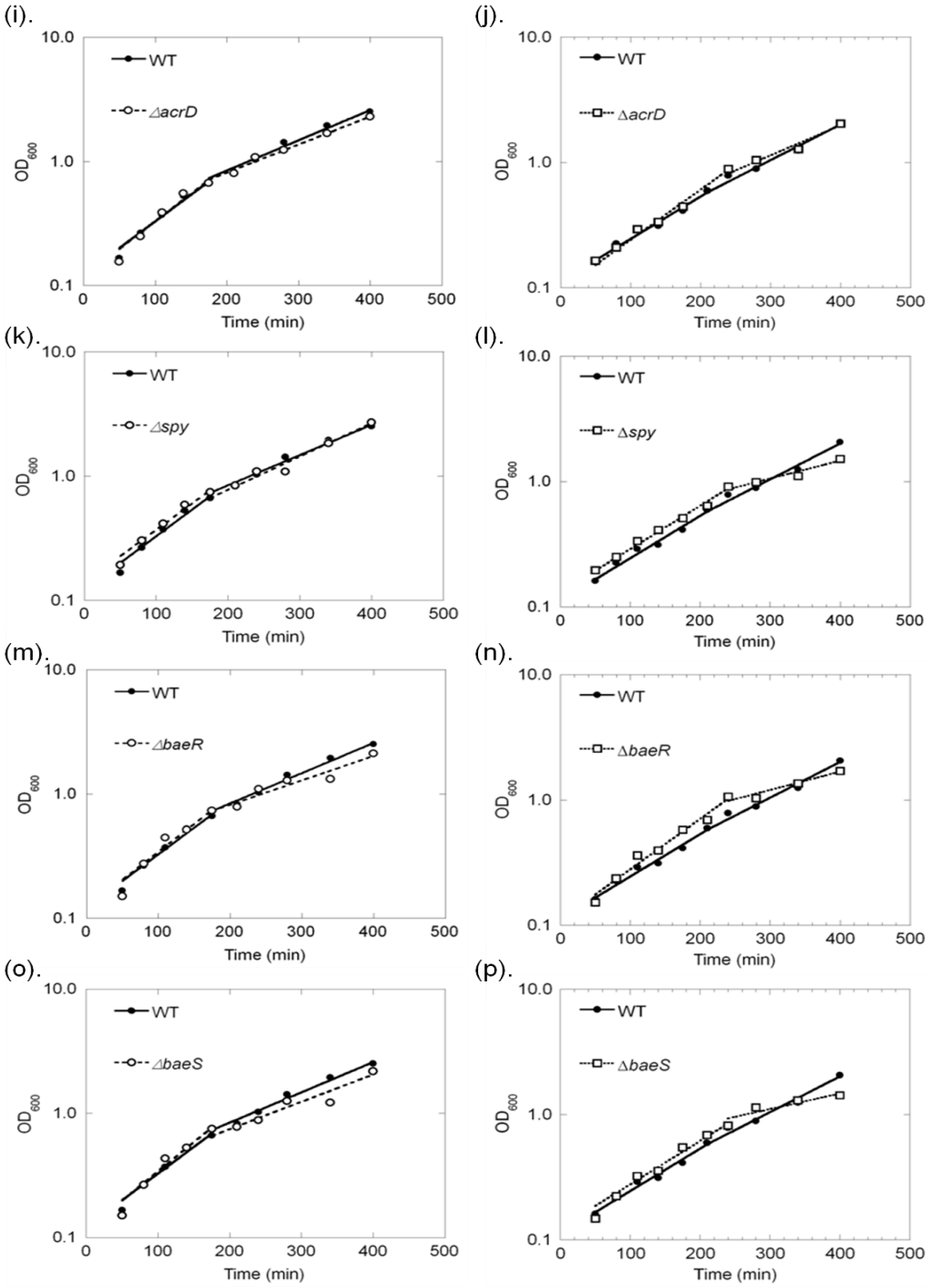

Figure 4.2. Growth curves of BaeS/R regulon single gene knockout strains. OD_{600} is plotted on a log scale on the y-axis. Growth curves in medium without zinc are presented on the left, and those in the presence of 300 μM zinc are on the right. The growth curves are fitted to Eq. 4.1.

(a).

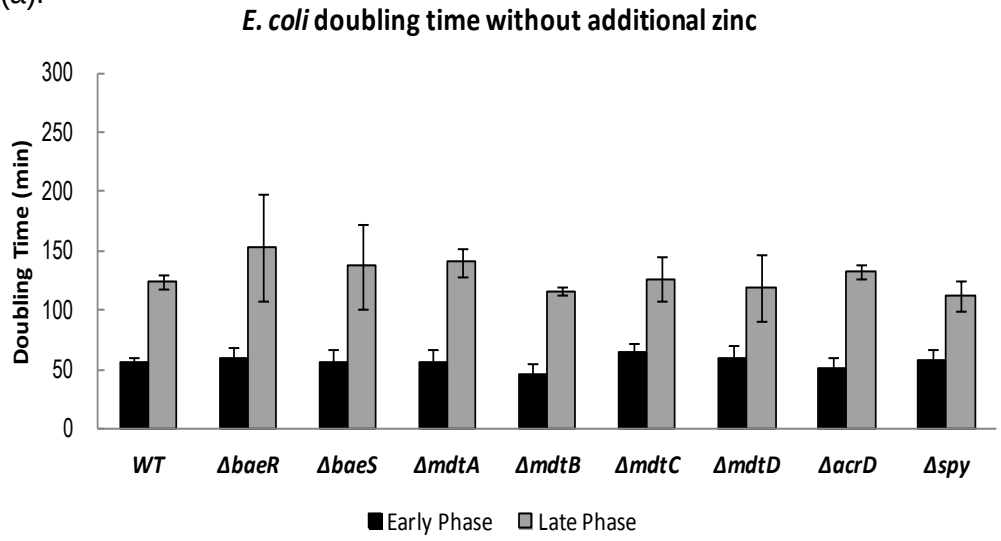

(b).

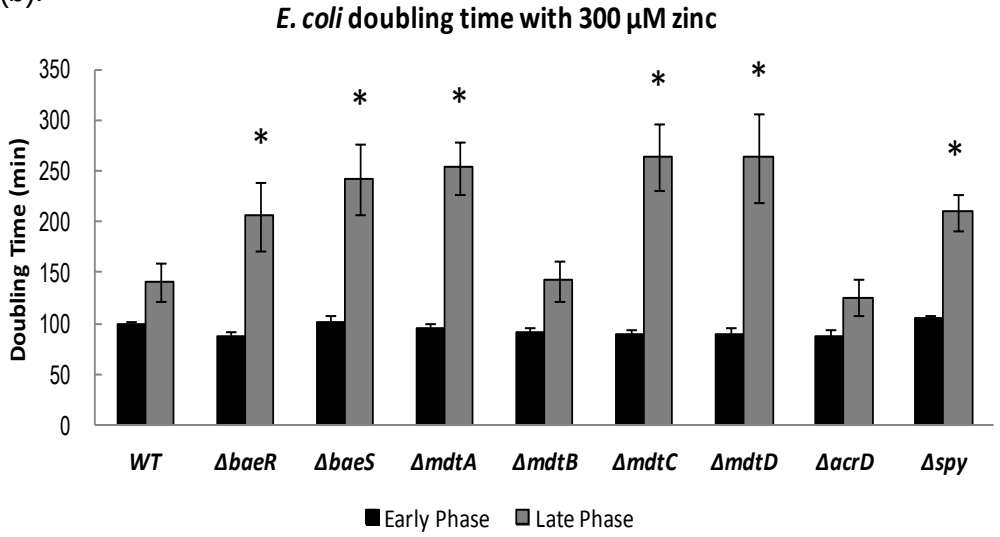

Figure 4.3. Doubling time of *E. coli* cells with and without zinc. Cultures of *E. coli* strains were diluted into MOPS minimal medium with or without zinc. OD_{600} were monitored over time and fitted into Eq 4.1 to calculate early and late stage average doubling time. (a). Cells grown in MOPS medium without additional zinc. No significant differences in doubling time were observed between the mutant strains and WT in either early phase or late phase. (b). Cells grown in MOPS medium with 300 µM $ZnSO_4$. No significant differences were observed between mutant strains and WT in early stage. In the late stage, Δ*baeR*, Δ*baeS*, Δ*mdtA*, Δ*mdtC*, Δ*mdtD* and Δ*spy* (labeled with stars) exhibited slower growth rates (T_G > 200 min) than WT (T_G ~ 140 min).

(T_G = 263 ± 43 min) and Δ*spy* (T_G = 209 ± 17 min), compared to the growth rate of the WT strain (T_G = 142 ± 19 min) in the late phase, but not in the early phase. These results indicate that the proteins encoded by the Bae regulon are involved in zinc detoxification when the cells are in the late growth phase under both nutrition and energy constraints. This result suggests that these proteins complement other energy dependent detoxification mechanisms that may not function well at this growth stage to alleviate the zinc stress.

The single knockouts Δ*mdtB* and Δ*acrD* did not exhibit significant growth defects even upon addition of 300 μM zinc. Previous experiments have demonstrated that MdtB can be replaced by an MdtC in the transmembrane heterotrimer[117]. Therefore, Δ*mdtB* may not exhibit any phenotype due to this functional complementation by MdtC. The lack of growth defects observed with the strain Δ*acrD* indicates that AcrD may not play a significant role in protection against metal stress.

4.3.2 Free Zinc Changes after Zinc Shock in Bae Regulon Deletion Strains

To understand the functions of the BaeS/R regulon components in regulating intracellular zinc contents, the changes in intracellular free zinc upon zinc shock were examined in these single knockout strains using the H94N CA_TagRFP sensor. Cells grown in MOPS minimal medium at log phase (OD_{600} ~ 0.3 – 0.4) was sampled on the microscope and 50 μM $ZnSO_4$ was added to the well before imaging.

The intracellular zinc concentration increased dramatically after zinc shock in the Δ*mdtA* and Δ*mdtC* cells (> 200 nM, which is beyond the dynamic range of the sensor), substantially higher than that of the WT strain (~ 50 nM) (Fig. 4.4(a)). The initial high

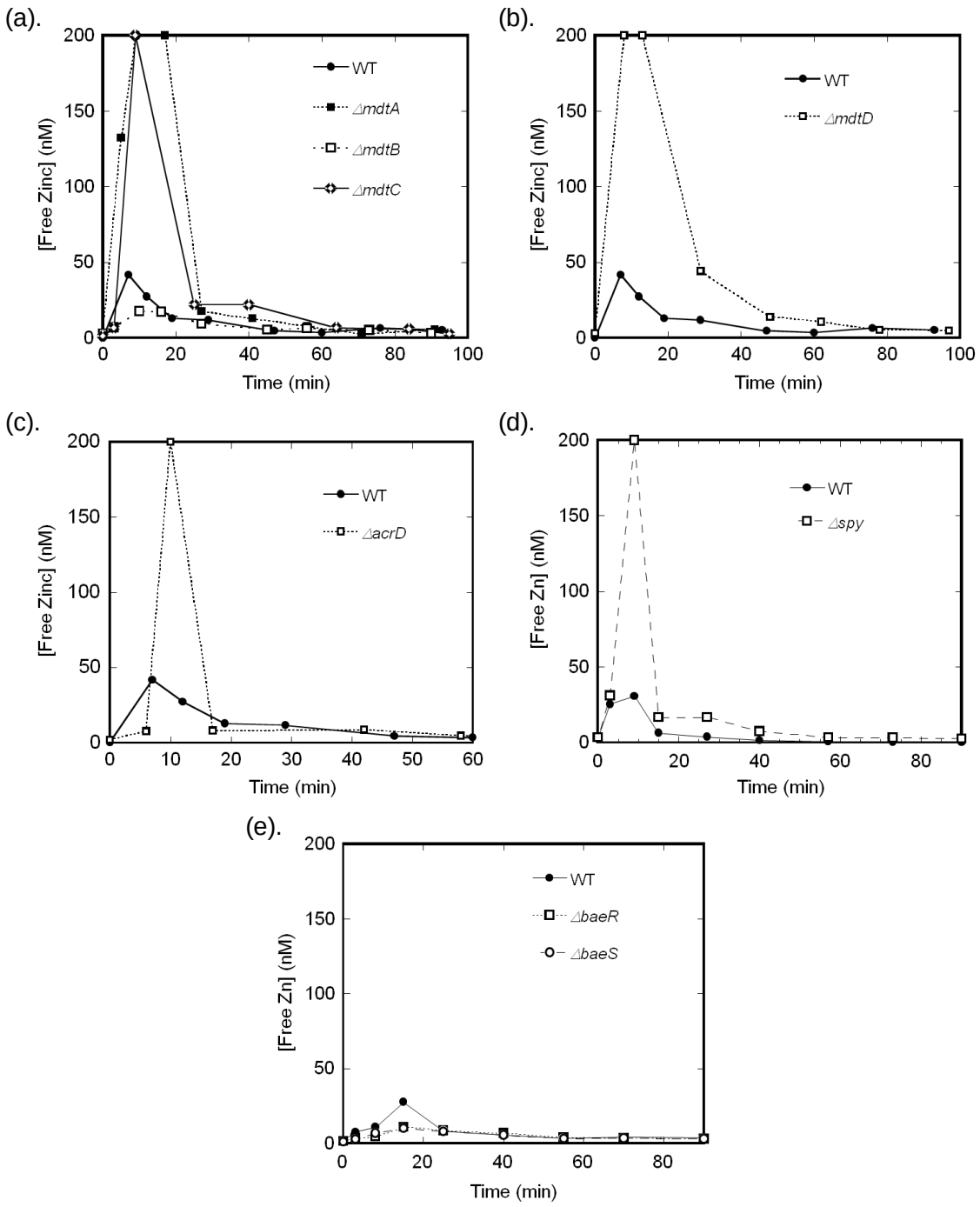

Figure 4.4. Intracellular free zinc changes after zinc shock. *E. coli* cells grown in MOPS minimal medium were sampled on microscope as described in Section 4.2.3. 50 µM ZnSO4 was added to the imaging medium and free zinc concentrations were measured over time using the H94N CA_TagRFP sensor.

zinc dropped to ~ 20 nM within ~ 25 min, and then gradually subsided to a level similar to the WT concentration within 1 hr. There was little change in Δ*mdtB* as expected, consistent with the previous observation of no growth defects under zinc stress. The free zinc changes in Δ*mdtD* are similar to that of Δ*mdtA* and Δ*mdtC* except that the high zinc level lasted for slightly longer (still at ~ 50 nM at 30 min after zinc shock) (Fig. 4.4(b)). These free zinc increases coincide with the observation that the mutant strains Δ*mdtA,* Δ*mdtC* and Δ*mdtD* grow slower under high zinc stress. These results indicate that MdtABC may participate in zinc detoxification by lowering intracellular free zinc initially when the cells encounter zinc stress.

A very brief increase in the intracellular free zinc peak was observed in Δ*acrD* as well (Fig. 4.4(c)), even though the knockout strain did not exhibit significant growth defects. Free zinc levels increased to >200 nM at 10 min and then rapidly dropped to below 10 nM within 15 min, and was comparable to that of WT thereafter. The short burst of high free zinc may not cause any substantial damage to the cell; therefore, AcrD's role in the response to zinc toxicity may be more opportunistic rather than obligatory.

Interestingly, a similar short burst of free zinc increase (>200 nM at 10 min) is occurred in the Δ*spy* knockout strain (Fig. 4.4(d)), even though there is no evidence that this protein is directly involved in zinc transport. Free zinc dropped precipitately to ~ 15 nM at 15 min and plateaued for ~15 min before decreasing to a similar level of zinc in WT. Two possible explanations for the free zinc peak in Δ*spy* include: (i). some of the zinc exporters may require Spy for proper folding, and its absence weakens the constitutive metal transport system, resulting in higher initial zinc; and (ii). Spy may

function to decrease the free zinc concentration in the periplasm, reducing the initial zinc influx.

Unexpectedly, the *baeS* and *baeR* knockouts barely affect the intracellular free zinc after zinc shock (<10 nM) (Fig. 4.4(e)) compared to the wild-type strain, even though Δ*baeS* and Δ*baeR* had slower growth rates in high zinc medium. It is possible that the basal level expression of various components of the BaeS/R regulon was sufficient for initial defense of zinc stress. It is also possible that deletion of *baeS* and *baeR* may result in over expression of other protective mechanisms against metal stress that compensate for the impairment of the Bae regulon function.

4.3.3 Total Metal Changes after Zinc Shock in Bae Regulon Deletion Strains

We then measured the total metal changes using ICP-MS in the Δ*mdtC,* Δ*mdtD* and Δ*spy* knockout strains, which exhibited both late stage growth defects and substantial free zinc increases upon zinc shock. These single knockout strains showed increase in both total zinc and copper compared to the wild type strain (Fig. 4.5). No significant alterations in total iron, calcium and magnesium contents were observed in these strains (data not shown). Previous studies have demonstrated that the Bae regulon can be up-regulated by addition of Cu(II) as well as zinc, and that the Δ*mdtABC*Δ*acrD* and Δ*baeS*Δ*baeR* mutants grow much more poorly than wild type in the presence of high copper in the medium[115]. However, it is interesting that exposure to external zinc can cause significant increase in the intracellular copper homeostasis in these single knock-out mutants. The increased copper levels may contribute to the growth defects observed under zinc stress conditions.

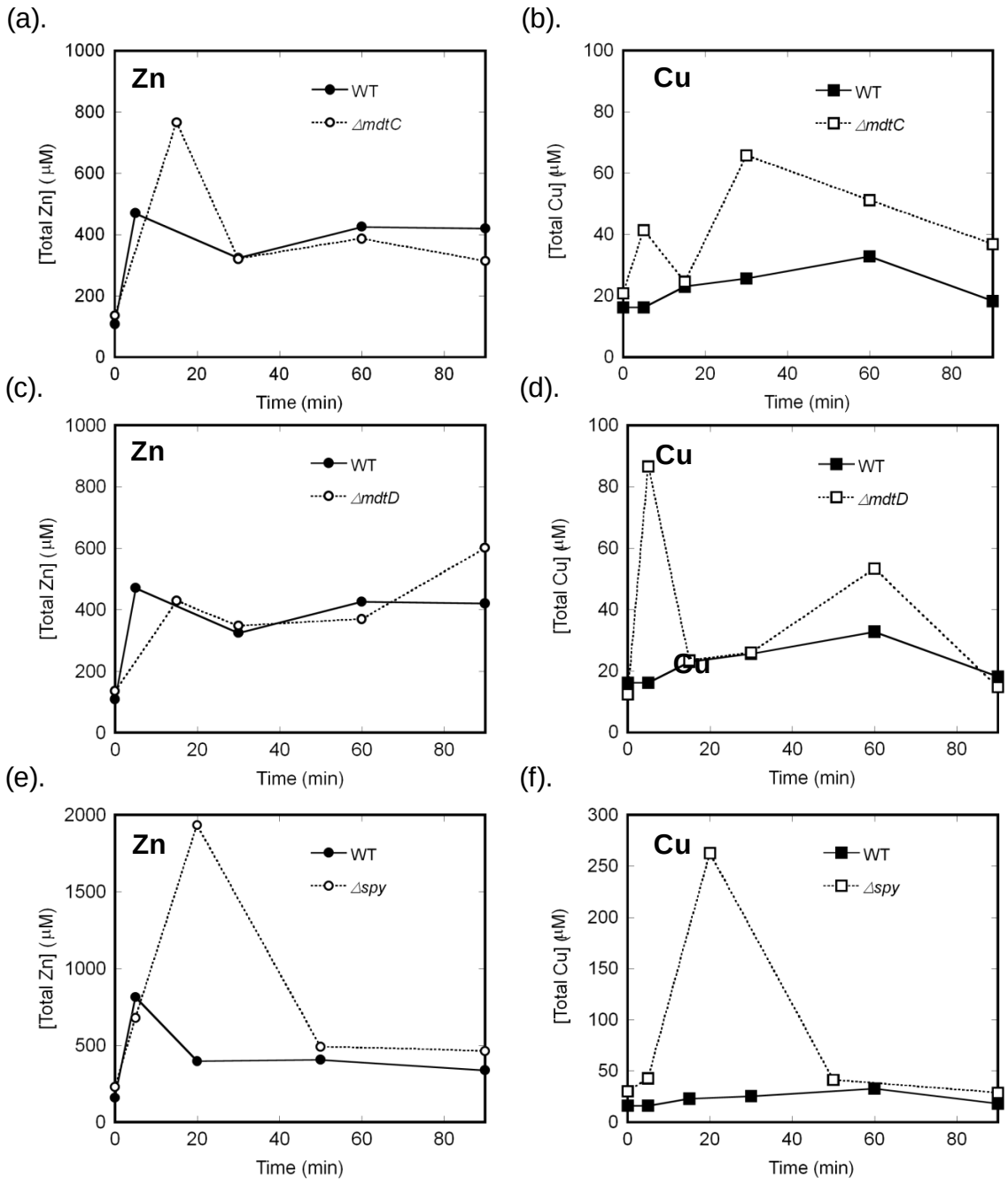

Figure 4.5. Total zinc and copper changes after zinc shock. *E. coli* cells grown at log phase were exposed to 50 μM ZnSO4, and total cellular metal concentrations were measured by ICP-MS as described in Section 4.2.2. (a)(b). Both total zinc (circle) and copper (square) levels are much higher in Δ*mdtC* than that of WT. (c)(d). No significant differences between Δ*mdtD* and WT, but transient increase in total copper level were observed at 5 min and 60 min. (e)(f). Both total zinc and copper increased dramatically (>10-fold) in Δ*spy*, highlighting its importance in metal homeostasis.

In the Δ*mdtC* strain, the total zinc concentration increased by 2-fold at ~ 20 min which then subsided to a level similar to that of wild type at 30 min, coinciding with the observed changes in free zinc (Fig.4.4(a) and Fig.4.5(a)). In the WT cells, exposure to zinc caused a modest increase in total copper (20 – 30 μM) which then decreased to the initial level at 90 min. While in the Δ*mdtC* cells, the intracellular total copper content increased by 2- to 3-fold in multiple waves and remained ~ 2-fold higher than the baseline level even after 90 min (Fig. 4.5(b)). In Δ*mdtD*, little to no alteration in total zinc concentration compared to WT is observed (Fig.4.5(c)). This was unexpected because the free zinc concentrations increased enormously after zinc shock (Fig.4.4(b)). It is possible that this mutant alters the cell membrane permeability such that zinc dissociates from the cell during the washing steps. However, in Δ*mdtD* substantial changes in copper content were observed in two waves (Fig.4.5(d)). The copper level increased by ~ 4-fold at 5 min in the first wave followed by a decrease to wild-type level at 20 min, and by ~ 2.5-fold in the second wave at ~ 60 min. It is worth noting that the copper efflux system, CusABC, a RND-type transporter, was significantly up-regulated upon exposure to zinc in a previous study[221], implying that the cells somehow need to export copper under high zinc stress. It is possible that MdtABC and MdtD have copper efflux functions similar to CusABC under these conditions.

In the Δ*spy* knockout strain, dramatic increases in both total zinc (~ 10-fold) and copper (~ 12-fold) were observed at ~ 20 min (Fig. 4.5(e)(f)). The patterns of zinc and copper changes overlay very well temporally. Furthermore, the time-dependent changes in total zinc conincide with the observed changes in free zinc (Fig.4.4(d)). These data suggest that the loss of Spy may result in global defects in transition metal transport.

Previous evidence suggested that Spy functions as a molecular chaperone and plays important roles in protecting the membrane and periplasmic proteins against zinc stress. In this case, it is likely that the absence of Spy impaired the integrity of the transporters and/or periplasmic proteins that have important functions in metal detoxification, resulting in elevated cellular levels of zinc and copper.

4.3.4 Transcriptional Response to Zinc Shock of Bae Regulon Deletion Strains

The Bae regulon had previously been shown to be up-regulated to various degrees upon exposure to high zinc stress[115, 221]. Here we monitored the time course of the transcription of various genes on the regulon to gain further insight into their functions. RT-PCR revealed that genes on all three operons (*mdtABCD-baeSR, acrD* and *spy*) were up-regulated in the WT strain upon exposure to ~ 100 µM $ZnSO_4$ at log phase (Fig. 4.6). The *spy* mRNA increased the most with an almost 50-fold increase after 30 min, followed by the *acrD* mRNA at 18-fold. The *mdtABCD-baeSR* operon exhibited only a moderate increase, with transcripts of *mdtA* and *baeR* increasing by ~ 7-fold and ~ 2-fold, respectively. These increases in transcription are consistent with previous results[115, 221]. The zinc induced increase in transcription was proven primarily through regulation of BaeR not CpxR, as the transcriptional response was abolished in a Δ*baeSR* strain in a previous study[115].

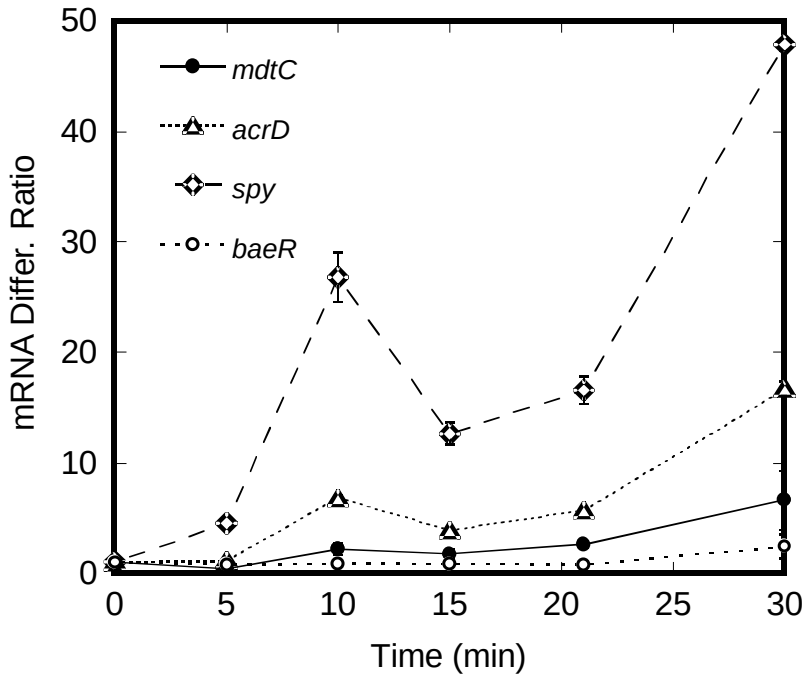

Figure 4.6. Transcriptional response of BaeS/R regulon upon exposure to zinc. Wild-type *E. coli* cells were exposed to 100 μM $ZnSO_4$, and the transcripts level of each gene were measured by RT-PCR at various time points after zinc exposure. The first phase of the transcriptional increase peaked at 10 min, and then decreased with the free zinc level. The transcript level then jumped substantially after 20 min, possibly from the positive feedback effects of BaeS and BaeR amplification. The transcript increases are 6.6-fold, 16.7-fold, 47.8-fold and 2.5-fold for *mdtC, acrD, spy* and *baeR* at 30 min, respectively.

Interestingly, the transcription of Bae regulon exhibited two distinct peaks. The transcript levels peaked at ~ 10 min after zinc shock, and then declined afterwards at 15 min. In this phase, the changes in the transcript levels coincide nicely with the increases in intracellular free zinc levels (Fig.4.4 and Fig.4.6). Therefore, it is possible that the BaeS/R system directly senses and responds to changes in intracellular free zinc levels. However, unlike the transcription of *zntA* that plateaus or decreases as the free zinc level subsides (Fig.3.8), a second phase of increasing transcript level was seen in all four of the

genes on the BaeS/R regulon tested. The mRNA level increased slightly at 20 min compared to the low point at 15 min, and then jumped almost 2 – 3 times at 30 min. Two possible explanations to this second phase of transcriptional increase include: (i) the BaeS/R two-component system may sense tertiary stress signals that escalate overtime under prolonged exposure to high zinc concentrations to trigger the stress response transcription; and (ii) the second phase of transcriptional increase could result from the intrinsic positive feedback loop of the BaeS/R system[120]. Increases in the BaeS and BaeR protein levels at 15 – 20 min in response to the free zinc levels could amplify the stress signals and activate additional transcription.

4.4 DISCUSSION

The BaeS/R regulon is responsible for envelope-related stress responses[237]; however, the functions of each of its components remain unclear. Past explorations of the function of MdtABC has focused on its role in multidrug resistance. However, over-expression of MdtABC only exhibits minor enhancement in drug resistance compared to other major drug resistance associated transporters, and the Δ*mdtABC* knockout strain did not alter the cell's drug resistance profile[115]. On the other hand, in *Salmonella* knockout of *mdtABC/acrD* or *baeS/R* dramatically reduced the cells viability under zinc and copper stress dramatically[115]. This observation, together with the fact that BaeS/R regulon is up-regulated under exposure to zinc, led to the proposal that BaeS/R regulon may play important roles in defense against metal stresses. In this chapter, I explored the effects of single knockouts of the genes of the BaeS/R regulon in *E. coli* on the growth, free zinc

and total zinc changes after zinc shock to evaluate the functions of these transporters and periplasmic protein in zinc homeostasis.

My results demonstrated that the RND-type transporter MdtABC is involved in zinc homeostasis, in addition to its drug efflux function, especially under energy constraints and zinc shock conditions. The three knockout strains Δ*mdtA*, Δ*mdtB*, and Δ*mdtC*, exhibited different patterns in growth rate, and free and total zinc changes, coinciding with the proposed function of each component based on previous studies[116, 117]. MdtC is the trans-inner-membrane antiporter that drives efflux of a substrate into the periplasmic space through proton exchange[117]. Over-expression of MdtC alone confers mild drug resistance while over-expression of MdtA and/or MdtB alone has no effects, confirming the central role that MdtC plays in this system[240]. The Δ*mdtC* knockout produced a growth defect in the late phase (Fig. 4.2(f)) and a dramatic transient increase in cytosolic free zinc (Fig. 4.4(a)), total zinc and total copper levels (Fig. 4.5(a)(b)). This indicates that loss of *mdtC* leads to accumulation of zinc and copper content in the cell. Under energy constraint conditions, this can leads to a lower growth rate as the metal stress cannot be effectively alleviated. MdtA is a membrane fusion protein that links the trans-inner-membrane trimer with the outer-membrane pore, TolC, to facilitate efficient extrusion of substrates to the outside of the cells[116, 117]. Growth defects and increases in cytosolic free zinc in Δ*mdtA* were similar to that of Δ*mdtC*. Loss of MdtA could potentially reduce the cells' ability to lower the zinc concentration in the periplasm as MdtC cannot form a trans-envelope complex with TolC to efficiently extrude zinc ions to the outside. This buildup of periplasmic zinc can be toxic by interfering with periplasmic metalloptoteins or osmotic levels. Higher periplasm zinc levels also correlate with higher

intracellular zinc level due to enhancement of zinc influx via transporters. No significant growth defects or changes in free zinc were observed in Δ*mdtB* (Fig. 4.2(d), Fig. 4.4(a)), which is consistent with the previous proposal that the MdtB-MdtC heterotrimer can be substituted with MdtC homotrimer without significant loss of function[116].

Bioinformatic analysis indicates that the function of MdtABC may be different from both other characteristic *E. coli* drug efflux and metal efflux RND-type transporters. Although MdtABC is classfied as a hydrophobic and amphiphilic efflux RND-type (HAE-RND) transporter, MdtC does not share high sequence identity with other known RND-type multidrug resistance transmembrane proteins (except for MdtB) in *E. coli*, including AcrB, AcrF, and MdtF (28%, 29%, and 30%, respectively)[240]. In contrast, the sequence similarities among AcrB, AcrF, AcrD and MdtF are fairly high (60 – 80%). On the other hand, MdtC also has low sequence homology with the heavy metal efflux RND-type transporter CusA (23%), which transport Cu(I) through a series of methiones pairs employing a stepwise shuttle mechanism[102]. Interestingly, MdtC does share 73% identity with a putative cation/protein antiporter, CvrA, that is proposed to be involved in coping with osmotic pressure changes and regulation of cell volume[242]. These analyses indicate that MdtABC may employ a different transport mechanism than other types of RND transporters.

Whether MdtABC exports zinc in the form of free ions or in a ligand complex is unclear. This exporter transports several structurally unrelated amphilitic molecules (novobiocin, SDS, doxycycline and cholates, etc.), as extrapolated from the observed drug resistance in cells over-expressing MdtABC[116, 117, 236, 240]. This is similar to other drug resistance RND-type transporters that have unspecific substrate binding sites[250, 251].

Therefore, it is possible that MdtABC exports zinc in a ligand-complex form from the cytosol and/or the periplasm to lower the total zinc content. However, the observation of a dramatic increase in intracellular free zinc content in the Δ*mdtC* and Δ*mdtA* knockout strains suggests that MdtABC may reduce the intracellular free zinc concentration by extruding free zinc ions from the cytosol. Overall, our results revealed that MdtABC transporter is involve in lowering cellular zinc contents, and plays important role in cell survival under high zinc stress.

MdtD is an uncharacterized member of the major facilitator superfamily (MFS) of transporters[238]. MFS members are functionally diverse, transporting a wide range of molecules from inorganic phosphate to organic drug compounds[241]. Although proposed as a putative multidrug transporter, MdtD does not seem to be involved in drug resistance, as neither deletion of *mdtD* nor over-expression affect cellular drug resistance[115, 116, 240]. Here I showed that MdtD is involved in zinc homeostasis in *E. coli*. The *mdtD* knockout resulted in a moderately decreased growth rate at higher cell density (Fig.4.2(h)), and a dramatic increase in the intracellular free zinc concentration after zinc shock (Fig.4.4(b)). Though no significant changes in total zinc content were observed in Δ*mdtD*, copper homeostasis is disturbed upon zinc shock (Fig. 4.5(c)(d)). These results indicate that MdtD is involved in zinc and copper homeostasis under metal stress conditions. Since no known MFS family members transport divalent cations[241], it is likely that zinc and/or copper is co-transported in a complex with other ligands that are substrates of MdtD.

The function of AcrD seems to be primarily in drug resistance rather than zinc homeostasis. AcrD shares 66% and 63% sequence identity with the well-known drug resistance transporters, AcrB and AcrF[240]. Furthermore, AcrD transports

aminoglycosides *in vitro* in the presence of the membrane fusion protein AcrA[243, 245]. My results showed that the Δ*acrD* knockout had a very short, transient effect on free zinc (Fig. 4.4(c)), which is not sufficient to lower the cell growth (Fig. 4.2(j)). However, the transcription of *acrD* increases up to 17-fold after zinc shock, a more dramatic increase than the transcription level of *mdtC* (7-fold) (Fig. 4.6). The implication of this increase in transcription is unclear. One speculation is that up-regulation of AcrD may be a response to secondary effects caused by elevated zinc and/or copper levels. One clue is that AcrD is involved in L-cysteine efflux from the cell[252], and exposure to high zinc could lead to over-production of cysteine as shown in a previous study[232]. Therefore, up-regulation of AcrD could be responding to the high cysteine level.

Spy, an ATP-independent molecular chaperone in the periplasmic, is involved in metal-associated stresses. The Δ*spy* knockout exhibited slower growth rate under high zinc stress (Fig. 4.2(i)), and a temporary increase in free zinc (Fig. 4.4(d)), and total zinc/copper upon zinc shock (Fig. 4.5(e)(f)). Spy is aggressively up-regulated upon zinc exposure, mediated by the BaeS/R system[89]. Spy may be indirectly associated with defense against zinc stress as a molecular chaperone to facilitate the folding and to protect the integrity of newly-synthesized transmembrane and periplasmic transporters for zinc detoxification.

Overall, I have shown that the BaeS/R regulon plays an important role in *E. coli*'s defense against high zinc stress. The MdtABC and MdtD transporters are involved in the initial efflux of zinc, possibly in the form of a small molecule ligand bound complex. Spy possibly acts as a periplasmic chaperone to facilitate the folding of the newly synthesized zinc detoxification machinery. Deletion of key components of this regulon

renders the cells more sensitive to zinc toxicity, especially under high cell density with energy constraints, highlighting their functions in defense against zinc that are complementary to the ATP-driven exporters, such as ZntA.

To put the metal resistance function of the MdtABC and MdtD in context, they are not the primary detoxification transporters since deletion of these components does not have as significant an effect on cell growth as deletion of *zntA*. However, the impact of these transporters on cell growth and zinc content changes is more substantial that the impact of ZitB, a known constitutive metal transporter. Our data showed that MdtABC and MdtD are important parts of a a first-line defense network that functions to lower the intracellular metal contents upon zinc stresses, similar to ZitB. Furthermore, they are also up-regulated upon zinc exposure, making them share some similarity with ZntA in its responsiveness to metal stress. Overall, these attributes are imporatnt in achieve their functions in zinc detoxification.

CHAPTER V

SUMMARY AND FUTURE DIRECTIONS

5.1 DEVELOPMENT OF CARBONIC ANHYDRASE-BASED SENSORS

5.1.1 Summary of CA-based Ratiometric Sensor Development

In this work, I developed a suite of genetically encoded carbonic anhydrase-based ratiometric zinc sensors. These sensors were constructed by fusing a red fluorescent protein to carbonic anhydrase to form a FRET pair with the DPS bound to holo-CA. *In vitro* and *in situ* characterization demonstrated that the FRET signal increases readily with the free zinc concentration, resulting in a 2 – 4 -fold enhancement in fluorescence. Sensors with various zinc affinities were created through mutations in the active site of carbonic anhydrase, covering a dynamic range from 1 pm to 10 nM. These CA_RFP sensors are highly selective, sensitive and quantitative. They are also less prone to oxidation given that the metal ligands are histidines instead of cysteines, a major advantage over other protein-based sensors developed so far.

These CA_RFP sensors were successfully applied in *E. coli* to measure the intracellular free zinc concentration. Methods for measuring free zinc concentration in the rapid growing gram-negative prokaryote were developed. The conditions for sensor expression were optimized through an expression-dilution method to achieve

measurements of intracellular free zinc at log phase with mature fluorescent protein-based sensors. Methods for *in situ* calibration were developed to effectively permeabilize the envelope of *E. coli* and equilibrate with free zinc. For free zinc measurement, the ratio I_{FRET}/I_{FP} in the cell was recorded and the free zinc was calculated by fitting the ratio to the *in situ* calibration curve. Using three sensors with different affinities (T199A, Q92A and WT CA_TagRFP), I determined that the median intracellular free zinc concentration in *E. coli* is ~ 20 pM. In addition, I also observed variations among cells in the *E. coli* population. The CA_RFPs were the first sensors applied in prokaryotes to quantify the intracellular free zinc concentration. These sensors have been proven to be powerful tools for studying zinc homeostasis in *E. coli* and will facilitate further investigation in this field.

5.1.2 Future Directions in Sensor Development

Further Sensor Optimization

Although we have successfully applied the carbonic anhydrase-based ratiometric sensors to measure the intracellular free zinc concentration in *E. coli*, there are several aspects of the sensors that can be potentially improved upon.

I constructed a series of sensors that theoretically can measure free zinc concentration in the range of 1 pM – 300 pM (using Q92A and WT CA_TagRFP) and 1 nM – 100 nM (using H94N CA_TagRFP). However, given the increasing errors when the analyte concentration approaches the upper or lower limits of the sensor's dynamic range, the free zinc concentrations that can be accurately measured using these sensors is narrower in practice. Therefore, the current suite of sensors does not adequately cover

the sub to low nanomolar range. To bridge this gap in the dynamic range, it would be useful to develop a sensor variant with subnanomolar apparent zinc affinity. I propose two ways to achieve this goal. One way is to further alter the linker length between CA and TagRFP since increasing the linker length from 1 Gly to 3 Gly increases the apparent zinc affinity *in vitro* at pH 7.0 by 3-fold. This could result from a to lower FRET efficiency in the zinc-bound state as the RFP is further away from DPS, or from changes in zinc binding affinity due to the altered structural interactions between CA and RFP. However, this apparent decrease in affinity is masked by other factors when the calibration was conducted *in situ*. If the linker is further lengthened, this effect may manifest itself *in situ* as well, resulting in a CA_RFP variant with a zinc affinity between those of WT and H94N CA_TagRFP. Another way to alter the zinc affinity is to fuse the RFP to the N-terminus of CA, however, the effects on apparent zinc affinity are unpredictable in this case. The N-terminus of CA appears to be more flexible than the C-terminus, therefore it could potentially lessen the structural interference of RFP on the zinc binding properties of CA; on the other hand, the switch could also alter the FRET efficiency in either direction.

Another drawback of the sensor is the utilization of UV light to excite the fluorophore. The FRET channel is excited at 350 nm for 500 ms. This UV excitation could be phototoxic to the cells. To solve this problem, we need to develop new fluorescent inhibitors of CA with a longer excitation wavelength to replace dapoxyl sulfonamide. Ideally, this new sulfonamide derivative fluorophore will have a low quantum yield in the free form, and have a significant increase in fluorescence intensity upon binding to CA. Depending on the spectra of this fluorophore, a matched fluorescent

proteins can be used to form an appropriate FRET pair. For example, if the spectrum of the new fluorophore is similar to fluorescein (Ex: 490nm / Em: 516 nm), this could be paired with mOrange (Ex: 548 nm / Em: 562 nm), a bright monomeric fluorescent protein[211], as the FRET acceptor. Alternatively, if the new fluorophore's excitation spectrum is in the red range, we could pair it with a green fluorescent protein (GFP) as the FRET donor. In this case, the FRET channel will be recorded at excitation of GFP and emission of the red fluorophore, while the FP channel will be recorded at excitation of GFP and emission of GFP. The ratio I_{FRET}/I_{FP} will still reflect the fraction of zinc-bound sensor as it does with the current sensors. We are currently collaborating with Richard Thompson's lab at the University of Maryland to improve the optical properties of the fluorophore. With these improvements, the CA sensors should be applicable for imaging zinc in live organisms such as *C. elegans* or zebra fish.

Applying CA_RFP Sensors in Yeast

One advantage of genetically encoded sensors is that it could be expressed in multiple organisms. *Saccharomyces cerevisiae* is the model organism for single cell eukaryotes, and extensive studies have been conducted to understand its metal homeostasis and regulation[5]. However, although some small molecule non-ratiometric sensors have been applied to detect the increase in intracellular zinc contents[55], the intracellular free zinc concentration in yeast has yet to be accurately measured because of the low affinities of these sensors. We are working on applying the CA_RFP sensors in *S. cerevisiae* for free zinc measurements and other studies of metal homeostasis. We have conducted some preliminary trials on developing the methods for sensor expression and

fluorescence quantification (results see Appendix I). Some initial observations and issues that need to be addressed are discussed below.

First, the sensor expression needs to be optimized in yeast. We tried two plasmid constructs for sensor expression in yeast, CA_mCherry on a pRS316 vector (low copy), and CA_TagRFP on a p426_Gal1 vector (high copy). The expression of the sensors was controlled by the Gal promoter on the vectors in both cases. However, the sensor expression level was low and highly variable among the population as measured by the microscopic fluorescence intensity (see Appendix I. Section 1). This is potentially due to the poor stability of carbonic anhydrase at acidic conditions (pH < 6). The intracellular pH of yeast varies with the extracellular pH, and the relationship has been experimentally determined[253]. As we can see from Fig. 5.1, the intracellular pH in yeast drops to ~ 6 when the pH in the medium is below 5. In my experiments, the medium became progressively acidic as the cells grew and dropped to ~ 4 by the time the samples were taken for imaging. In this case, the intracellular pH is ~ 6 as shown in Fig. 5.1, which is not ideal for the expression and folding of carbonic anhydrase. This low pH was also problematic for *in situ* calibration of the CA_TagRFP sensors – and any pH sensitive zinc sensors for that matter – to accurately measure the intracellular free zinc concentration. To optimize the methods in the future, the pH should be carefully controlled and monitored through addition of buffering agents suitable for yeast growth.

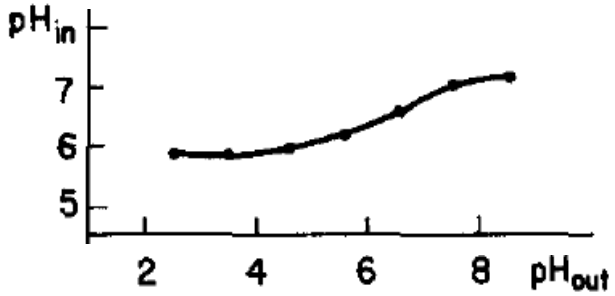

Figure 5.1. Yeast intracellular pH changes with environmental pH[253].

Another obstacle in using the CA sensors to image zinc in yeast is the high fluorescent background from membrane-bound DPS. The fluorescence of dapoxyl is sensitive to the polarity of the solvent, and increases dramatically in a hydrophobic environment[254]. The emission fluorescence spectrum of membrane-bound DPS, determined experimentally using a fluorometer with yeast cells plus DPS, peaks at 450 nm and has a long tail that can bleed through to the FRET channel at 620 nm (Fig. A1.2). This was not a significant issue in *E. coli* imaging due to the lack of intracellular membranes. However, when applied to eukaryotic cells, the intracellular membrane system (nucleus envelope, ER, Golgi, vesicles, vacuole, etc.) can generate significant background fluorescence in the FRET channel with bound DPS, interfering with the ratiometric measurements. To solve this problem, we set up a third channel, DPS channel, to correct for the background fluorescence. The channel set up will be elaborated in of the next section describing mammalian cell imaging.

Overall, several issues need to be addressed before the CA sensor can be used successfully in yeast. The pH needs to be carefully controlled, and the DPS background needs to be corrected. In addition, yeast cells do not adhere well on the poly-L-lysine

plates and other adhesive agents such as Concanavalin A (ConA), a lectin that binds to the sugar structures on the yeast cell wall[255], should be considered for fixation to the plates. Once these problems are adequately addressed, the CA_RFP sensors may be useful for applications in yeast.

Applying CA_RFP Sensors in Mammalian Cells

I have also been working on developing methods to apply the CA_RFP sensors to mammalian cells for intracellular free zinc measurements. We have optimized the expression of the sensor CA_DsRed2 in HEK293T cells, corrected the background from membrane-bound DPS, and generated quantifiable ratio images. However, further experiments need to be conducted to calibrate the sensors *in situ* for accurate zinc measurements. The preliminary results are described in Appendix I Section 2 and discussed below.

Like in yeast, fluorescence bleedthrough from membrane-bound DPS was also an issue in mammalian cells. We solved this problem by adding a third imaging channel to measure the intensity of bleedthrough from DPS and subtract it from the intensity in FRET channel, so that the measured $I_{FRET,adj}$ only reflects the fluorescence from the FRET between the CA-bound DPS and RFP (Fig. A1.2). This adjustment should generate background-free ratios for calculation of free zinc concentrations.

The $I_{FRET,adj}/I_{FP}$ was relatively evenly distributed within a single cell (Fig. A1.4), however, significant variations were observed among the cell population (Fig. A1.5). This observation is consistent with the previous work published by the Merkx group, in which the fluorescence ratio varied from cell to cell[45]. To quantify the sensor occupancy,

Merkx *et. al* obtained *in situ* endpoints at high and low zinc for individual cells by treating the cells with pyrithione plus zinc or TPEN[45]. We have experimented with various ionophores to permeabilize and equilibrate the cells with zinc buffers, including TPEN, alpha toxin[45], digitonin[46], pyrithione[153] and 4-BrA23187[256]. Unfortunately, none of these agents were able to induce any changes in the fluorescence intensity in the FRET channel or the $I_{FRET.adj}/I_{FP}$ ratio (data not shown). There are two possibilities to these results. First, it is possible that these ionophores failed to equilibrate the zinc concentration across the membrane. In this case, a set of control cells with other fluorescent zinc sensors could be used to test the zinc equilibration under the same conditions. However, it is highly unlikely that these agents would fail across the board since each of them has been applied successfully for other sensors. A second explanation is that the equilibration of zinc binding to CA_DsRed2 is slow in this case, in contrast with our previous observation of fast equilibrium in *E. coli*. The *in vitro* on-rate of zinc binding to CA is 10^5 $M^{-1}s^{-1}$, which means that at μM zinc it will reach equilibrium within seconds[257]. Since we did not see a significant increase in FRET fluorescence when high zinc was added together with ionophores, it is possible that the sensor was already saturated. On the other hand, the *in vitro* rate constant for dissociation of zinc bound to CA is very slow at 0.0003 h^{-1}, which means that it will take days for zinc to come off the zinc binding site[257]. Slow zinc dissociation could potentially explain the lack of decrease in the FRET signal when TPEN was added to the cell. Addition of the zinc exchange catalyst dipicolinic acid with TPEN also did not lead to an alteration in the FRET efficiency, though how much dipicolinic acid got into the cell remains unknown. If poor equilibrium was the reason for the lack of response of the CA sensor, the fast-

equilibrating mutant E117A may potentially help in this situation. E117A has an on-rate 100 times faster than WT, and an off-rate 5,000 faster than WT as measured *in vitro*[257]. It can potentially shorten the equilibrium time and respond to changes in zinc concentrations in real time. One potential complication of using the E117A mutant is that it does not express as well as other CA variants, and it failed to generate a FRET signal in *E. coli* (data not shown) in our trials. Anyway, a CA sensor containing the E117A mutation should be tested in HEK293T cells and it might potentially solve the *in situ* calibration issue.

Overall, unique challenges emerge as we develop methods for applying the CA_RFP sensors in eukaryotic cells. We were able to address some of them at this stage of the research, however, much work still needs to be done before we can use the CA_RFP sensors to measure free zinc concentrations in eukaryotic cells.

5.2 STUDY OF *E. COLI* ZINC HOMEOSTASIS

5.2.1 Summary of Key Findings in Zinc Homeostasis Studies

Combining free zinc monitoring using the genetically encoded ratiometric zinc sensors with other methods, we investigated the function and regulation of several transporters in *E. coli*. Specifically, we studied the transporters' roles in the cells' response to sudden exposure to high environmental zinc, i.e. "zinc shock" conditions by comparing the growth effects, intracellular free and total zinc changes, and transcription responses. These experiments provided insight into the different functions of the transporters ZitB and ZntA in zinc regulation, and the *in vivo* regulation of the

transcription of *zntA*. In addition, we investigated the roles of several genes regulated by the two-component system BaeS/R in zinc detoxification and homeostasis.

Multiple transporters are involved in zinc detoxification, and ZntA wa known as the most important player from the growth effects of gene deletions[104]. The function of other transporters, such as ZitB, was less clear. Our experiments revealed that ZntA and ZitB play temporally complementary roles in zinc detoxification. ZitB is the constitutively expressed, first-line defense against high zinc stress, as the Δ*zitB* strain exhibited a dramatic transient increase in intracellular free zinc concentration upon zinc shock. ZntA is up-regulated during zinc shock to effectively export zinc and sustains a non-toxic zinc intracellular free zinc concentration over the long haul.

The transient increase in intracellular free zinc concentration can reach the nanomolar range, more than a thousand-fold higher than the resting picomolar level. Based on my work, this transient zinc peak is very important for inducing the ZntR-mediated *zntA* transcription. This intracellular free zinc fluctuation activates the ZntR-mediated *zntA* transcription, which has a nanomolar *in vivo* apparent K_m for zinc-induced transcription initiation. This result does not agree with the previous *in vitro* measurements of ZntR's apparent zinc K_D in the femtomolar range[41]. Instead of a tightly controlled system with little change in zinc concentration, our data suggest that the cell can temporarily tolerate a fairly wide range of intracellular free zinc concentrations, and the fluctuation of free zinc is a critical signal for turning on the detoxification machinery.

In addition to ZntA and ZitB, many other transporters may also be involved in zinc homeostasis. Transcriptional studies revealed that several transporters and a periplasmic protein regulated by the stress responsive two-component system BaeS/R

were up-regulated during zinc stress[115, 221]. I conducted further studies on these genes to understand their roles in the regulation of zinc homeostasis. I found that two previously known multidrug resistance transporters and a periplamsic molecular chaperone on the BaeS/R regulon, MdtABC, MdtD, and Spy, are involved in zinc regulation. Δ*mdtC*, Δ*mdtD* and Δ*spy* strains exhibited late stage growth defects, increases in intracellular free zinc concentration and increases in total zinc/copper contents under high zinc stress. MdtABC and MdtD may be part of an extensive secondary zinc export network that is functionally complementary to the primary ATP-driven zinc exporters, and Spy may be involved in protecting the membrane transport system from zinc stress.

5.2.2 Future Directions in Zinc Homeostasis Study

E. coli has an extensive regulatory network to combat environmental stresses. We have only explored part of the sophisticated molecular machinery that controls the zinc homeostasis in the cell. Among the many unanswered questions, some topics could be explored further using the research methods that we have developed. Some areas of interest are discussed below.

The response of ZntR-mediated transcription of *zntA* could be further investigated, especially under zinc deplete conditions. Our results demonstrated that this reaction has an *in vivo* K_m for zinc in the nanomolar range when the cells are exposed to high external zinc. However, previous publications have demonstrated that down-regulation of the *zntA* mRNA level also occurs when the cells face zinc deprivation induced by addition of TPEN or EDTA[258]. If the intracellular free zinc concentration decreases under zinc deprivation conditions to below the normal level of ~ 20 pM with addition of zinc

chelators, as it likely will, and the *zntA* mRNA level is primarily regulated by ZntR, then ZntR also appears to respond to changes in picomolar free zinc concentrations. In this case, it appears that ZntR-mediated *zntA* transcription has a much wider dynamic range than previously thought. This wide dynamic range possibly reflects more than one level of transcriptional control. Zinc may regulate multiple events in this process. In addition to DNA binding and transcription initiation, the stability of the ZntR-DNA complex is enhanced upon zinc binding and degradation catalyzed by Lon proteases is significantly reduced[108]. It would be interesting to measure the transcription response of *zntA* to intracellular free zinc concentration under zinc depletion conditions to gauge the apparent dynamic range of ZntR *in vivo*. Also, experiments measuring the rate of ZntR degradation by protease under various free zinc concentration can provide additional information in dissecting the zinc-regulated transcription process.

The other half of story about the transporter network in zinc regulation concerns the importers, especially the high affinity zinc importer ZnuABC. ZnuABC is up-regulated by the transcription factor Zur under zinc deplete conditions[95]. Like ZntR, Zur also exhibited femtomolar sensitivity to zinc measured *in vitro*[41]. If this is true, then Zur should be completely suppressed under normal conditions with 20 pM zinc. However, expression of ZnuABC was detected under normal conditions, indicating that the transcription is partially active. In addition, the *znuABC* transcription was down-regulated upon addition of external zinc as revealed in a previous study[232], indicating that the zinc-mediated suppression of *znuABC* expression also responds to zinc levels higher than picomolar. These data implied that, similar to ZntR, Zur may also have a wide dynamic range, giving *E. coli* the flexibility to survive various challenges to metal

homeostasis. Study of Zur-mediated *znuA/B/C* transcription under various free zinc concentrations *in vivo* will provide insight into this question.

Although we demonstrated the involvement of BaeS/R regulon in metal homeostasis, much remains to be understood about the specific function of each component. First, in addition to the knock-out experiments, the growth effects of over-expression of each component under high zinc concentration should be performed to confirm that they confer metal resistance. Second, biochemical studies of metal transport by MdtABC and MdtD should be conducted to further understand the mechanism. *In vitro* transport assays using everted envelope or lipid vesicles with inserted transporters could be performed to determine whether the substrates are metal ions or ligand complexes, as well as the transport kinetics. Third, studies under a genetic background with other zinc transporter knockouts will be helpful, since the loss of function of a single gene is often compensated by up-regulation of other genes. In this case, the detrimental effects of the BaeS/R component gene knockout could be masked by up-regulation of *zntA* or other genes involved in zinc regulation. Furthermore, multiple knockout strains within the BaeS/R regulon, for example, Δ*mdtABC*Δ*mdtD*, could be studied to better gauge the importance in zinc regulation.

Our results showed that BaeS/R regulon is involved in copper homeostasis as well. It is interesting that zinc shock can induce an increase in the intracellular copper content in Δ*mdtC,* Δ*mdtD* and Δ*spy*. Previous studies have demonstrated that the BaeS/R regulon is up-regulated upon addition of copper, and cells with *mdtABC/acrD* and *baeS/R* deletion grow poorly in the presence of high copper[115]. It is possible that these transporters may export metal ligand complexes using ligands that coordinate both zinc

and copper ions. Further investigation into the growth effects and copper content changes of BaeS/R regulon deletion strains will help better understand its function in copper homeostasis.

5.3 CLOSING REMARKS

In this work, we developed genetically encoded carbonic anhydrase-based ratiometric zinc sensors and applied them to measure the intracellular free zinc concentration in the prokaryotic model organism *E. coli*. These CA_RFP sensors are highly selective, sensitive and quantitative. The intracellular free zinc concentration in *E. coli* BL21(DE3) grown in minimal medium was determined at ~ 20 pM, and variations among the cell population were observed. Using these sensors, we monitored the intracellular free zinc fluctuation upon zinc shock and revealed the importance of these fluctuations in the regulation of zinc detoxification systems. Based on the relationship between the transcript level and intracellular free zinc concentrations, we proposed a kinetic model of ZntR-mediated transcriptional regulation of *zntA*. This model is dramatically different from the previously held view of extremely tight control of intracellular free zinc concentration. We also explored the functions of the BaeRS regulon in metal homeostasis, and concluded that MdtABC, MdtD and Spy are involved in combating zinc stress under energy constraint conditions complementary to the ATP-driven primary exporters. These results expanded our knowledge of the extensive regulatory network for metal homeostasis in *E. coli*.

APPENDIX I

METHOD DEVELOPMENT OF APPLYING CA-BASED SENSORS IN EUKARYOTIC CELLS

The preliminary experiments (methods and results) for sensor development in eukaryotic cells are described in this appendix. See Chapter V Section I for discussions.

A1. 1 METHOD DEVELOPMENT IN YEAST

A1.1.1 CA_TagRFP Sensor Expression in Yeast

The sensor expression plasmid was constructed by inserting the DNA sequence of wild type CA_TagRFP into the high copy yeast expression vector p426_GAL1 (Promega) between the EcoRI and the XhoI restriction digestion sites after the Gal promoter. The plasmid contains a URA3 selection marker (ATCC). The plasmid sensor construct and the control plasmid were transformed into yeast using the standard LiOAc method[259]. The transformed yeast was grown on SRC-U selection agar plates for 3 days at 30°C. A colony was picked from the plate and cultured in 5 ml SRC-U minimal medium overnight. The culture was then diluted into 5 ml of fresh SRC-U minimal medium at OD_{600} ~ 0.02 and grown at 30°C to an OD_{600} of ~ 0.4 before induction with 4% galactose. The cells were then grown for another 12 hours before sampling for imaging.

A1.1.2 Fluorescence Imaging in Yeast

12 hours after induction, 2 µl of yeast culture was placed on a poly-L-lysine coated glass-bottom plate, 100 µl SRC-U medium, with or without 2 µM DPS, was added to parallel sample wells. Fluorescence images were acquired using the same channels as displayed in Table 2.1. The results were shown in Fig. A1.1. The percentage of cells that expressed the CA_TagRFP sensors was relatively low (20 - 30%). The level of expression was low and highly variable, with the average FP channel fluorescence intensity (Fig. A1.1(b)) in one cell being 100 – 1,000 out of a maximum value of 16,000. The background auto-fluorescence from the FRET channel (Fig. A1.1(c)) was high with an average value of 100. In the sample with the control vector and 2 µM DPS, significant background fluorescence from the membrane-bound DPS was observed in the FRET channel (Fig. A1.1(f)), averaging at ~ 500. Overall, the sensor expression level was too low and the DPS background was too high to extract useful information from the fluorescence images.

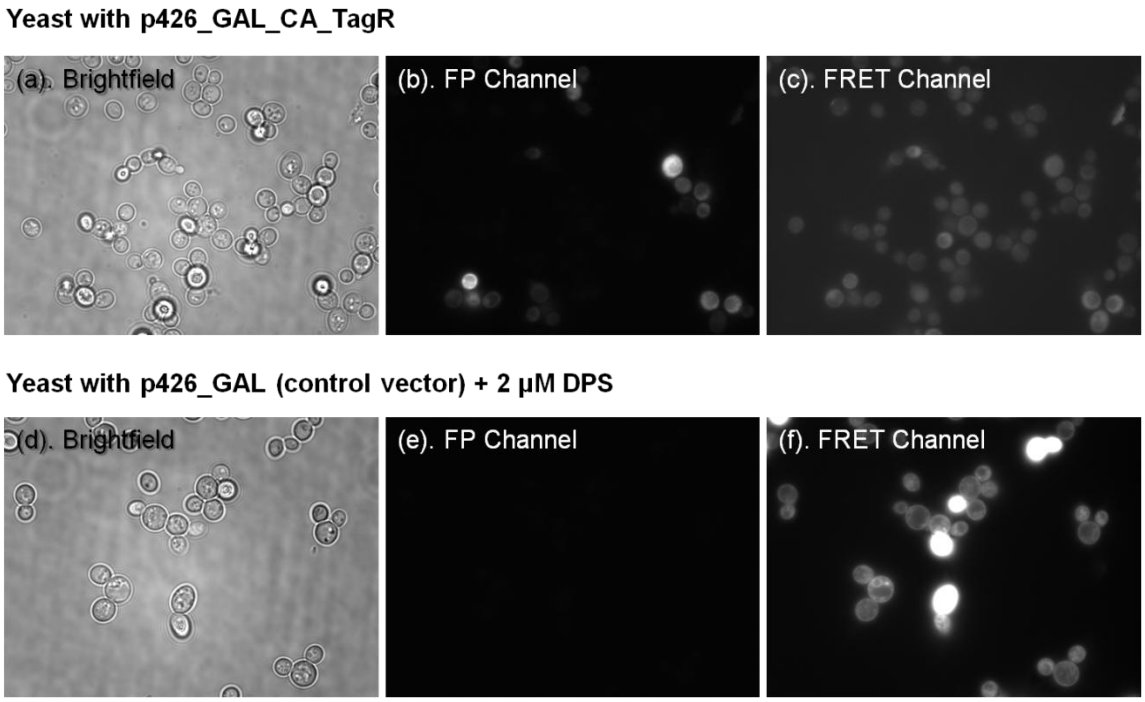

Figure A1.1. Fluorescence images of yeast expressing CA_TagRFP. Top panel shows images of yeast expressing CA_TagRFP without addition of DPS. Bottom panel shows yeast with control vector plus 2 µM DPS. (a). and (d). Brightfield images. (b). the low fluorescence (100 – 1,000) in the FP channel indicates that the CA_RFP sensor expression level is low. (c). Autofluorescence in the FRET channel is significant (~ 100). (e). no fluorescence in the FP channel in cells with control vector. (f). Background from membrane-bound DPS is high (200 – 2,000).

A1.2 METHOD DEVELOPMENT IN MAMMALIAN CELLS

A1.2.1 CA_RFP Sensor Expression in HEK293 Cells

Three red fluorescent proteins (RFPs) were tested as the FRET receptor for imaging in mammalian cells, TagRFP, DsRed2, and RFP611. TagRFP and RFP611 were cloned into the mammalian expression vector pACT (Promega) between the restriction digestion sites of NheI and NotI. pCA_DsRed2 was constructed by cloning the CA gene into the vector pDsRed2-Mito (Clontech) between the NheI and BamHI restriction sites

(constructed by Rebecca Bozym at Thompson lab at the University of Maryland). The HEK293T cells (ATCC# CRL-11268) were grown in DMEM medium (Invitrogen) without phenol red plus 10% fetal bovine serum and 100 U/ml penicillin/streptomycin on a 3.5 ml glass-bottom Petri dish (MatTek). The plasmids were transfected into the HEK293T cells using the Effectene Transfection Kit (Qiagen), and the cells were imaged 48 hrs after transfection.

Of the three CA_RFP sensors, CA_DsRed2 gave the best transfection efficiency (~ 70%) and the brightest signal in the FP channel (3,000 – 6,000) (data not shown). The fluorescence intensity of CA_TagRFP is about 1,500 – 2,500 and no fluorescence was observed with CA_RFP611. Since higher brightness is desired in mammalian cells due to the high bleedthrough from membrane-bound DPS (discussed below), we decided to use CA_DsRed2 in the following experiments.

A1.2.2 Fluorescence Imaging in HEK293T Cells

To correct for the background fluorescence in the FRET channel from membrane-bound DPS, a third, DPS channel was set up in addition to the FP and FRET channels. The fluorescence bleedthrough (BT) from membrane-bound DPS (Fig. A1.2(a)) needs to be calculated and subtracted from the fluorescence collected in the FRET channel. The DPS channel collects the fluorescence only from the membrane-bound DPS, and the ratio of the FRET channel bleedthrough over the DPS channel fluorescence ($R_{BT/DPS}$) was experimentally determined in HEK293T cells incubated with DPS (Fig. A1.2(b)). The ratio was relatively constant at 0.8 ± 0.1 over the DPS intensity range of 500 – 2000,

which is the range that the majority of the DPS intensity values fall into. Therefore, we are able to calculate the background adjusted $I_{FRET,adj.}$ using the following equation:

$$I_{FRET,adj} = I_{FRET} - I_{DPS} \times R_{BT/DPS} \quad \text{Eq. A1.1}$$

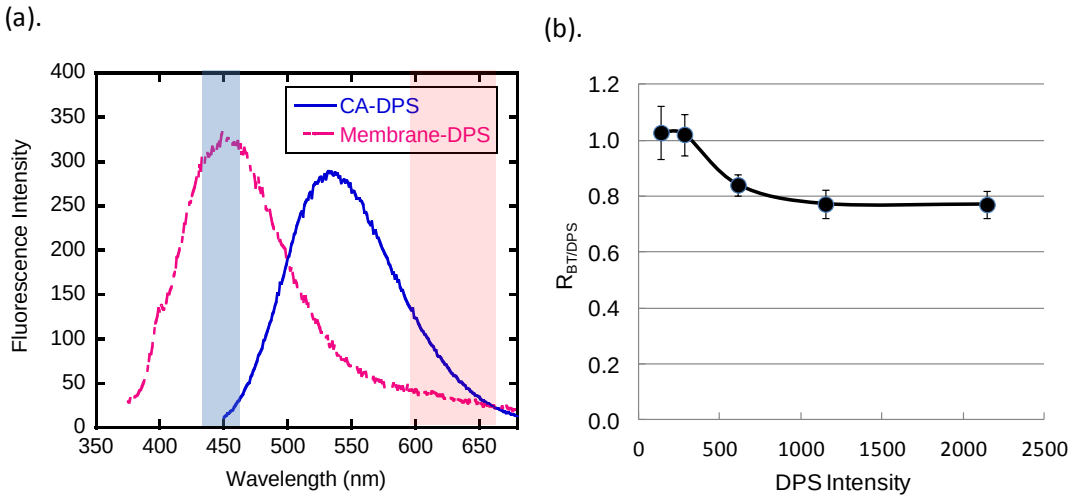

Figure A1.2. Membrane-bound DPS fluorescence bleedthrough and correction. (a). The emission spectra of CA-bound DPS and membrane-bound DPS were scanned using a fluorometer. The blue and pink shaded areas represent the windows of the DPS and FRET channel emission filters, respectively. (b). The ratio of bleedthrough (FRET channel) to DPS intensity (DPS channel) was calculated in HEK293T cells incubated with 0.2 µM DPS for 20 min.

Channel	Ex (nm)	Filter	Em (nm)	Filter
FP	570	HQ570/20x	630	ET630/75m
FRET	350	D350/50x	630	ET630/75m
DPS	350	D350/50x	445	ET445/30m

Table A1.1. Fluorescence channel setup for mammalian cell imaging.

Next, HEK293T cells expressing the sensor CA_DsRed2 were imaged to obtain the $I_{FRET,adj}/I_{FP}$ ratio for zinc measurements. 48 hours after transfection, the cells were washed once with 1 ml pre-warmed Krebs-HEPES-bicarbonate buffer[45] and incubated with DPS in the buffer for 10 - 20 min in the incubator before imaging. One set of representative fluorescence images is shown in Fig. A1.3. The optimal DPS concentration and incubation time were experimentally determined. The concentration of DPS was determined by titrating the cells with 0.1 µM, 0.2 µM, 0.4 µM and 0.8 µM DPS. 0.2 µM DPS was chosen as the average ratio did not increase with additional DPS. A 10-min incubation appeared sufficient for equilibration, as longer incubation times did not change the average ratio among the population of cells (Fig. A1.5).

The average ratio of $I_{FRET,adj}/I_{FP}$ within one single cell is relatively constant (Fig. A1.4). However, the ratio varies from cell to cell with the majority falling into the range of 0.3 – 0.5 (Fig. A1.5). This is within the range of the fluorescence ratios observed for CA_DsRed2, as the low (apo form) and high (holo form) ratios are 0.05 and 0.6 as determined *in vitro*. The scattering in the fluorescence ratios does not appear to be an artifact caused by the variation in the FP intensity as no correlation was observed (Fig. A1.5).

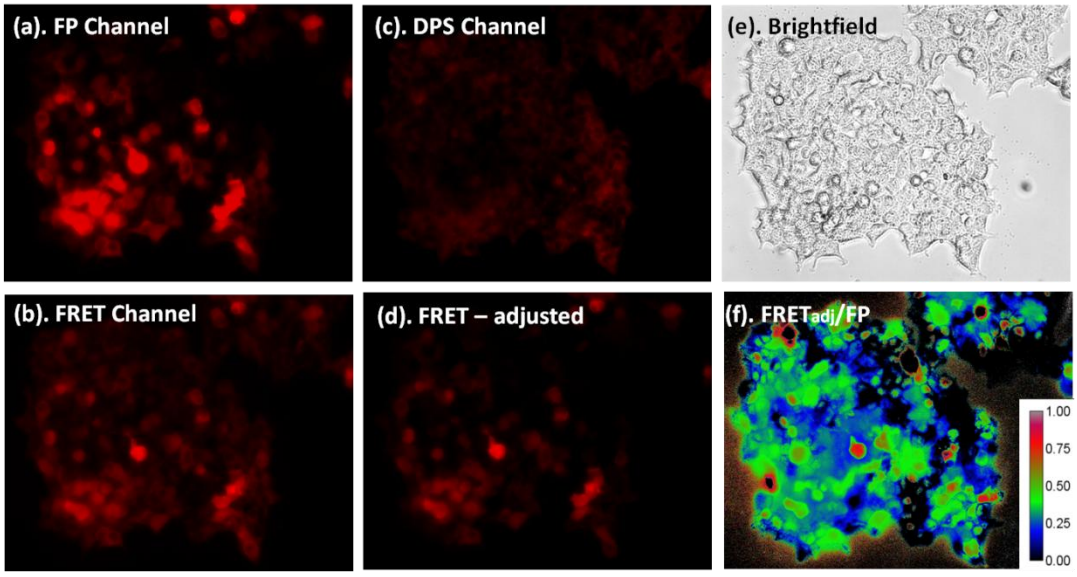

Figure A1.3. Fluorescence imaging in HEK cells with CA_DsRed2. HEK 293T cells expressing CA_DsRed2 were imaged in the presence of 0.2 μM DPS. (a).(b).(c). Raw images. (d). DPS background was subtracted from the raw FRET image. (f). Ratio images of FRET,adj/FP.

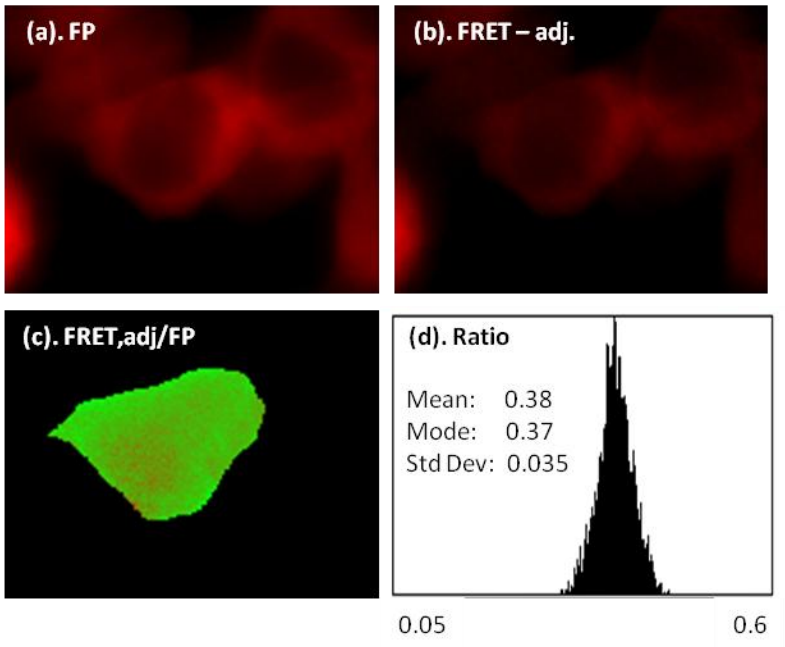

Figure A1.4. Ratio image analysis of a single HEK293 cell with CA_DsRed2.

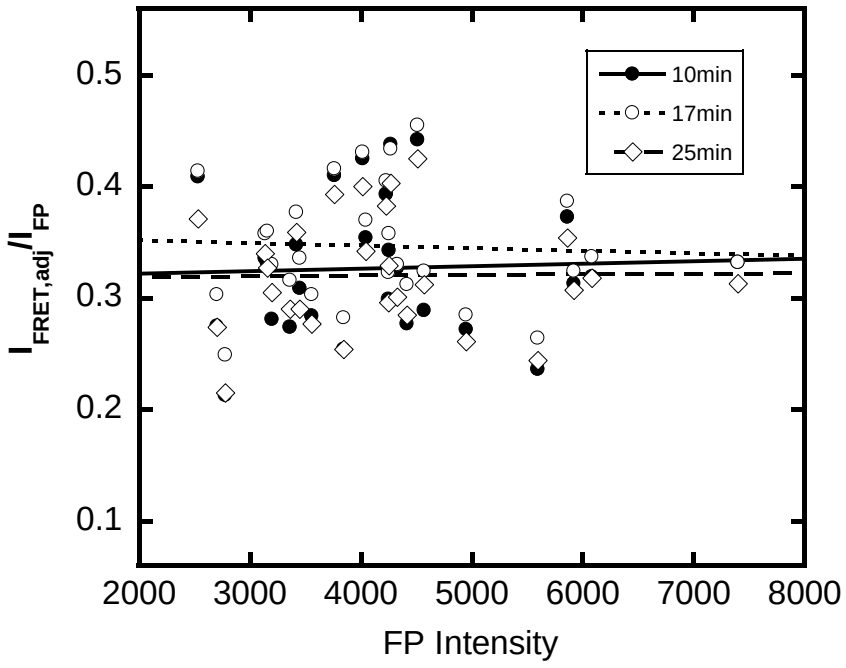

Figure A1.5. Correlation of $I_{FRET,adj}/I_{FP}$ ratio with FP Intensity and incubation time. Fluorescence images were acquired at different time points, and the median $I_{FRET,adj}/I_{FP}$ ratio within a single cell plotted against the median intensity of the FP channel.

A1.2.3 Imaging with CA_DsRed2 Variants in HEK293 Cells

In order to narrow down the range of the intracellular free zinc concentration in HEK293T cells, several CA_DsRed2 sensor variants with mutations at the active site of CA were introduced. The median $I_{FRET.adj}/I_{FP}$ ratio of each sensor variant was plotted in Fig. A1.6. Sensors with low picomolar affinities (WT, T199A and Q92A) exhibited a ratio of ~ 0.4, while sensors with nanomolar to micromolar zinc affinities (H94N and H94A) had minimal fluorescence in the FRET channel. Though not quantitative and conclusive, this set of data confirmed that the intracellular free zinc concentration is in the picomolar range.

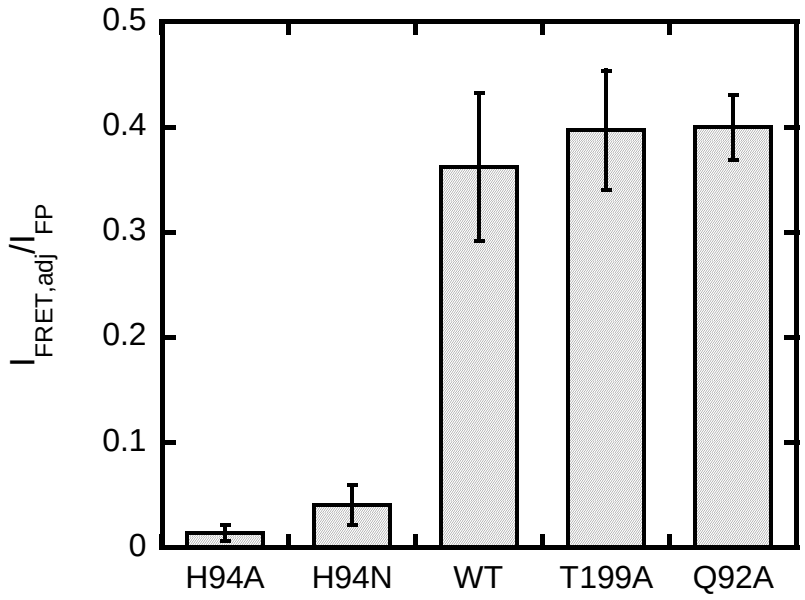

Figure A1.6. $I_{FRET,adj}/I_{FP}$ ratio of CA_DsRed2 mutants in HEK293T cells**.**

A1.3 SUMMARY OF METHODS DEVELOPMENT IN EUKARYOTIC CELLS

We conducted preliminary trials on developing methods for applying the CA_RFP sensors to eukaryotic cells. In yeast, the application was complicated by the poor sensor expression and high DPS background. The sensor expression issue could be potentially addressed by optimizing the cell growth and protein expression conditions, especially with careful control of the pH in the medium (discussed in Chapter V). In the mammalian cell line HEK293T, we optimized the sensor expression of CA_DsRed2, and corrected the fluorescence background from membrane-bound DPS by adding a third channel. We were able to obtain quantifiable ratio images of the adjusted FRET channel and FP channel. The preliminary analysis revealed a fairly even ratio distribution within single cells, but significant variations from cell to cell. Through the differential ratio

responses of CA_DsRed2 variants with different zinc affinities, we confirmed that the intracellular free zinc concentration is within the picomolar range. To accurately quantify the intracellular free zinc in mammalian cells, we will need to conduct *in situ* calibration with these CA_DsRed2 sensors and determine their apparent zinc affinities in the cells. The details of these future experiments are discussed in Chapter V.

REFERENCES

1. *Vallee, B.L. & Auld, D.S. Active zinc binding sites of zinc metalloenzymes. Matrix Suppl **1**, 5-19 (1992).*
2. *Vallee, B.L. & Falchuk, K.H. The biochemical basis of zinc physiology. Physiol Rev **73**, 79-118 (1993).*
3. *Berg, J.M. & Shi, Y. The galvanization of biology: a growing appreciation for the roles of zinc. Science **271**, 1081-1085 (1996).*
4. *Andreini, C., Banci, L., Bertini, I. & Rosato, A. Counting the zinc-proteins encoded in the human genome. J Proteome Res **5**, 196-201 (2006).*
5. *Eide, D.J. Multiple regulatory mechanisms maintain zinc homeostasis in Saccharomyces cerevisiae. J Nutr **133**, 1532S-1535S (2003).*
6. *Eide, D.J. Zinc transporters and the cellular trafficking of zinc. Biochim Biophys Acta **1763**, 711-722 (2006).*
7. *Hantke, K. Bacterial zinc transporters and regulators. Biometals **14**, 239-249 (2001).*
8. *Colvin, R.A., Holmes, W.R., Fontaine, C.P. & Maret, W. Cytosolic zinc buffering and muffling: their role in intracellular zinc homeostasis. Metallomics **2**, 306-317 (2010).*
9. *Dineley, K.E., Votyakova, T.V. & Reynolds, I.J. Zinc inhibition of cellular energy production: implications for mitochondria and neurodegeneration. J Neurochem **85**, 563-570 (2003).*
10. *Yamashita, S. et al. Zinc transporter LIVI controls epithelial-mesenchymal transition in zebrafish gastrula organizer. Nature **429**, 298-302 (2004).*
11. *Devirgiliis, C., Zalewski, P.D., Perozzi, G. & Murgia, C. Zinc fluxes and zinc transporter genes in chronic diseases. Mutat Res **622**, 84-93 (2007).*
12. *Plum, L.M., Rink, L. & Haase, H. The essential toxin: impact of zinc on human health. Int J Environ Res Public Health **7**, 1342-1365 (2010).*
13. *Fukada, T., Yamasaki, S., Nishida, K., Murakami, M. & Hirano, T. Zinc homeostasis and signaling in health and diseases: Zinc signaling. J Biol Inorg Chem **16**, 1123-1134 (2011).*
14. *Cotton, F.A. & Wilkinson, G. Advanced Inorganic Chemistry. A Comprehensive Text Edn. 5th. (Wiley-Inter-science, New York; 1988).*
15. *Christianson, D.W. Structural biology of zinc. Adv Protein Chem **42**, 281-355 (1991).*
16. *Woolley, P. Models for metal ion function in carbonic anhydrase. Nature **258**, 677-682 (1975).*
17. *Christianson, D.W., Mangani, S., Shoham, G. & Lipscomb, W.N. Binding of D-phenylalanine and D-tyrosine to carboxypeptidase A. J Biol Chem **264**, 12849-12853 (1989).*
18. *Coleman, J.E. Structure and mechanism of alkaline phosphatase. Annu Rev Biophys Biomol Struct **21**, 441-483 (1992).*
19. *Brown, D.D. The role of stable complexes that repress and activate eucaryotic genes. Cell **37**, 359-365 (1984).*

20. *Karlin, S. & Zhu, Z.Y. Classification of mononuclear zinc metal sites in protein structures. Proc Natl Acad Sci U S A **94**, 14231-14236 (1997).*
21. *Leon, O. & Roth, M. Zinc fingers: DNA binding and protein-protein interactions. Biol Res **33**, 21-30 (2000).*
22. *Krishna, S.S., Majumdar, I. & Grishin, N.V. Structural classification of zinc fingers: survey and summary. Nucleic Acids Res **31**, 532-550 (2003).*
23. *Grishin, N.V. Treble clef finger--a functionally diverse zinc-binding structural motif. Nucleic Acids Res **29**, 1703-1714 (2001).*
24. *Klug, A. The discovery of zinc fingers and their applications in gene regulation and genome manipulation. Annu Rev Biochem **79**, 213-231 (2010).*
25. *Frederickson, C.J., Koh, J.Y. & Bush, A.I. The neurobiology of zinc in health and disease. Nat Rev Neurosci **6**, 449-462 (2005).*
26. *Kitamura, H. et al. Toll-like receptor-mediated regulation of zinc homeostasis influences dendritic cell function. Nat Immunol **7**, 971-977 (2006).*
27. *Li, Y., Kimura, T., Laity, J.H. & Andrews, G.K. The zinc-sensing mechanism of mouse MTF-1 involves linker peptides between the zinc fingers. Mol Cell Biol **26**, 5580-5587 (2006).*
28. *Bernhardt, M.L., Kong, B.Y., Kim, A.M., O'Halloran, T.V. & Woodruff, T.K. A Zinc-Dependent Mechanism Regulates Meiotic Progression in Mammalian Oocytes. Biol Reprod.*
29. *Tuncay, E. et al. Intracellular free zinc during cardiac excitation-contraction cycle: calcium and redox dependencies. Cardiovasc Res **89**, 634-642 (2011).*
30. *Hambidge, M. Human zinc deficiency. J Nutr **130**, 1344S-1349S (2000).*
31. *Lang, C. et al. Anti-inflammatory effects of zinc and alterations in zinc transporter mRNA in mouse models of allergic inflammation. Am J Physiol Lung Cell Mol Physiol **292**, L577-584 (2007).*
32. *Carter, J.E. et al. Involvement of redox events in caspase activation in zinc-depleted airway epithelial cells. Biochem Biophys Res Commun **297**, 1062-1070 (2002).*
33. *Terres-Martos, C. et al. Serum zinc and copper concentrations and Cu/Zn ratios in patients with hepatopathies or diabetes. J Trace Elem Med Biol **12**, 44-49 (1998).*
34. *Ho, E., Quan, N., Tsai, Y.H., Lai, W. & Bray, T.M. Dietary zinc supplementation inhibits NFkappaB activation and protects against chemically induced diabetes in CD1 mice. Exp Biol Med (Maywood) **226**, 103-111 (2001).*
35. *Taylor, C.G. Zinc, the pancreas, and diabetes: insights from rodent studies and future directions. Biometals **18**, 305-312 (2005).*
36. *Franklin, I., Gromada, J., Gjinovci, A., Theander, S. & Wollheim, C.B. Beta-cell secretory products activate alpha-cell ATP-dependent potassium channels to inhibit glucagon release. Diabetes **54**, 1808-1815 (2005).*
37. *Haase, H. & Maret, W. Protein tyrosine phosphatases as targets of the combined insulinomimetic effects of zinc and oxidants. Biometals **18**, 333-338 (2005).*
38. *Roberts, B.R., Ryan, T.M., Bush, A.I., Masters, C.L. & Duce, J.A. The role of metallobiology and amyloid-beta peptides in Alzheimer's disease. J Neurochem **120 Suppl 1**, 149-166 (2012).*

39. *Bush, A.I. et al. Rapid induction of Alzheimer A beta amyloid formation by zinc. Science **265**, 1464-1467 (1994).*
40. *Adlard, P.A. et al. Rapid restoration of cognition in Alzheimer's transgenic mice with 8-hydroxy quinoline analogs is associated with decreased interstitial Abeta. Neuron **59**, 43-55 (2008).*
41. *Outten, C.E. & O'Halloran, T.V. Femtomolar sensitivity of metalloregulatory proteins controlling zinc homeostasis. Science **292**, 2488-2492 (2001).*
42. *Simons, T.J. Intracellular free zinc and zinc buffering in human red blood cells. J Membr Biol **123**, 63-71 (1991).*
43. *Krezel, A. & Maret, W. Zinc-buffering capacity of a eukaryotic cell at physiological pZn. J Biol Inorg Chem **11**, 1049-1062 (2006).*
44. *Bozym, R.A., Thompson, R.B., Stoddard, A.K. & Fierke, C.A. Measuring picomolar intracellular exchangeable zinc in PC-12 cells using a ratiometric fluorescence biosensor. Acs Chemical Biology **1**, 103-111 (2006).*
45. *Vinkenborg, J.L. et al. Genetically encoded FRET sensors to monitor intracellular Zn2+ homeostasis. Nat Methods **6**, 737-740 (2009).*
46. *Dittmer, P.J., Miranda, J.G., Gorski, J.A. & Palmer, A.E. Genetically encoded sensors to elucidate spatial distribution of cellular zinc. J Biol Chem **284**, 16289-16297 (2009).*
47. *Haase, H. & Beyersmann, D. Intracellular zinc distribution and transport in C6 rat glioma cells. Biochem Biophys Res Commun **296**, 923-928 (2002).*
48. *Heuchel, R. et al. The transcription factor MTF-1 is essential for basal and heavy metal-induced metallothionein gene expression. Embo J **13**, 2870-2875 (1994).*
49. *Lyons, T.J. et al. Genome-wide characterization of the Zap1p zinc-responsive regulon in yeast. Proc Natl Acad Sci U S A **97**, 7957-7962 (2000).*
50. *Liuzzi, J.P. & Cousins, R.J. Mammalian zinc transporters. Annu Rev Nutr **24**, 151-172 (2004).*
51. *Gaither, L.A. & Eide, D.J. Functional expression of the human hZIP2 zinc transporter. J Biol Chem **275**, 5560-5564 (2000).*
52. *Zhao, H. & Eide, D. The yeast ZRT1 gene encodes the zinc transporter protein of a high-affinity uptake system induced by zinc limitation. Proc Natl Acad Sci U S A **93**, 2454-2458 (1996).*
53. *Zhao, H. & Eide, D. The ZRT2 gene encodes the low affinity zinc transporter in Saccharomyces cerevisiae. J Biol Chem **271**, 23203-23210 (1996).*
54. *Bird, A.J., Blankman, E., Stillman, D.J., Eide, D.J. & Winge, D.R. The Zap1 transcriptional activator also acts as a repressor by binding downstream of the TATA box in ZRT2. Embo J **23**, 1123-1132 (2004).*
55. *MacDiarmid, C.W., Gaither, L.A. & Eide, D. Zinc transporters that regulate vacuolar zinc storage in Saccharomyces cerevisiae. Embo J **19**, 2845-2855 (2000).*
56. *Lichten, L.A. & Cousins, R.J. Mammalian zinc transporters: nutritional and physiologic regulation. Annu Rev Nutr **29**, 153-176 (2009).*
57. *Desouki, M.M., Geradts, J., Milon, B., Franklin, R.B. & Costello, L.C. hZip2 and hZip3 zinc transporters are down regulated in human prostate adenocarcinomatous glands. Mol Cancer **6**, 37 (2007).*

58. *Wang, K., Zhou, B., Kuo, Y.M., Zemansky, J. & Gitschier, J. A novel member of a zinc transporter family is defective in acrodermatitis enteropathica. Am J Hum Genet **71**, 66-73 (2002).*
59. *Tozlu, S. et al. Identification of novel genes that co-cluster with estrogen receptor alpha in breast tumor biopsy specimens, using a large-scale real-time reverse transcription-PCR approach. Endocr Relat Cancer **13**, 1109-1120 (2006).*
60. *Dalton, T.P. et al. Identification of mouse SLC39A8 as the transporter responsible for cadmium-induced toxicity in the testis. Proc Natl Acad Sci U S A **102**, 3401-3406 (2005).*
61. *Wimmer, U., Wang, Y., Georgiev, O. & Schaffner, W. Two major branches of anti-cadmium defense in the mouse: MTF-1/metallothioneins and glutathione. Nucleic Acids Res **33**, 5715-5727 (2005).*
62. *Giunta, C., Randolph, A. & Steinmann, B. Mutation analysis of the PLOD1 gene: an efficient multistep approach to the molecular diagnosis of the kyphoscoliotic type of Ehlers-Danlos syndrome (EDS VIA). Mol Genet Metab **86**, 269-276 (2005).*
63. *Palmiter, R.D. & Huang, L. Efflux and compartmentalization of zinc by members of the SLC30 family of solute carriers. Pflugers Arch **447**, 744-751 (2004).*
64. *Ellis, C.D., Macdiarmid, C.W. & Eide, D.J. Heteromeric protein complexes mediate zinc transport into the secretory pathway of eukaryotic cells. J Biol Chem **280**, 28811-28818 (2005).*
65. *Suzuki, T. et al. Two different zinc transport complexes of cation diffusion facilitator proteins localized in the secretory pathway operate to activate alkaline phosphatases in vertebrate cells. J Biol Chem **280**, 30956-30962 (2005).*
66. *Guffanti, A.A., Wei, Y., Rood, S.V. & Krulwich, T.A. An antiport mechanism for a member of the cation diffusion facilitator family: divalent cations efflux in exchange for K+ and H+. Mol Microbiol **45**, 145-153 (2002).*
67. *MacDiarmid, C.W., Milanick, M.A. & Eide, D.J. Biochemical properties of vacuolar zinc transport systems of Saccharomyces cerevisiae. J Biol Chem **277**, 39187-39194 (2002).*
68. *Ellis, C.D. et al. Zinc and the Msc2 zinc transporter protein are required for endoplasmic reticulum function. J Cell Biol **166**, 325-335 (2004).*
69. *Andrews, G.K., Wang, H., Dey, S.K. & Palmiter, R.D. Mouse zinc transporter 1 gene provides an essential function during early embryonic development. Genesis **40**, 74-81 (2004).*
70. *Liuzzi, J.P., Blanchard, R.K. & Cousins, R.J. Differential regulation of zinc transporter 1, 2, and 4 mRNA expression by dietary zinc in rats. J Nutr **131**, 46-52 (2001).*
71. *Piletz, J.E. & Ganschow, R.E. Zinc deficiency in murine milk underlies expression of the lethal milk (lm) mutation. Science **199**, 181-183 (1978).*
72. *Cole, T.B., Wenzel, H.J., Kafer, K.E., Schwartzkroin, P.A. & Palmiter, R.D. Elimination of zinc from synaptic vesicles in the intact mouse brain by disruption of the ZnT3 gene. Proc Natl Acad Sci U S A **96**, 1716-1721 (1999).*
73. *Chimienti, F., Devergnas, S., Favier, A. & Seve, M. Identification and cloning of a beta-cell-specific zinc transporter, ZnT-8, localized into insulin secretory granules. Diabetes **53**, 2330-2337 (2004).*

74. *Vallee, B.L. Introduction to metallothionein. Methods Enzymol **205**, 3-7 (1991).*
75. *Sutherland, D.E. & Stillman, M.J. The "magic numbers" of metallothionein. Metallomics **3**, 444-463 (2011).*
76. *Durnam, D.M. & Palmiter, R.D. Induction of metallothionein-I mRNA in cultured cells by heavy metals and iodoacetate: evidence for gratuitous inducers. Mol Cell Biol **4**, 484-491 (1984).*
77. *Seguin, C., Felber, B.K., Carter, A.D. & Hamer, D.H. Competition for cellular factors that activate metallothionein gene transcription. Nature **312**, 781-785 (1984).*
78. *Robbins, A.H. & Stout, C.D. X-ray structure of metallothionein. Methods Enzymol **205**, 485-502 (1991).*
79. *Eide, D.J. Homeostatic and adaptive responses to zinc deficiency in Saccharomyces cerevisiae. J Biol Chem **284**, 18565-18569 (2009).*
80. *Bird, A.J. et al. A dual role for zinc fingers in both DNA binding and zinc sensing by the Zap1 transcriptional activator. Embo J **19**, 3704-3713 (2000).*
81. *Qiao, W., Mooney, M., Bird, A.J., Winge, D.R. & Eide, D.J. Zinc binding to a regulatory zinc-sensing domain monitored in vivo by using FRET. Proc Natl Acad Sci U S A **103**, 8674-8679 (2006).*
82. *Guerrerio, A.L. & Berg, J.M. Metal ion affinities of the zinc finger domains of the metal responsive element-binding transcription factor-1 (MTF1). Biochemistry **43**, 5437-5444 (2004).*
83. *Bittel, D., Dalton, T., Samson, S.L., Gedamu, L. & Andrews, G.K. The DNA binding activity of metal response element-binding transcription factor-1 is activated in vivo and in vitro by zinc, but not by other transition metals. J Biol Chem **273**, 7127-7133 (1998).*
84. *Saydam, N., Georgiev, O., Nakano, M.Y., Greber, U.F. & Schaffner, W. Nucleo-cytoplasmic trafficking of metal-regulatory transcription factor 1 is regulated by diverse stress signals. J Biol Chem **276**, 25487-25495 (2001).*
85. *Laity, J.H. & Andrews, G.K. Understanding the mechanisms of zinc-sensing by metal-response element binding transcription factor-1 (MTF-1). Arch Biochem Biophys **463**, 201-210 (2007).*
86. *Blindauer, C.A. Bacterial metallothioneins: past, present, and questions for the future. J Biol Inorg Chem **16**, 1011-1024 (2011).*
87. *Noll, M., Petrukhin, K. & Lutsenko, S. Identification of a novel transcription regulator from Proteus mirabilis, PMTR, revealed a possible role of YJAI protein in balancing zinc in Escherichia coli. J Biol Chem **273**, 21393-21401 (1998).*
88. *Appia-Ayme, C. et al. ZraP is a periplasmic molecular chaperone and a repressor of the zinc-responsive two-component regulator ZraSR. Biochem J **442**, 85-93 (2012).*
89. *Yamamoto, K., Ogasawara, H. & Ishihama, A. Involvement of multiple transcription factors for metal-induced spy gene expression in Escherichia coli. J Biotechnol **133**, 196-200 (2008).*
90. *Patzer, S.I. & Hantke, K. The ZnuABC high-affinity zinc uptake system and its regulator Zur in Escherichia coli. Mol Microbiol **28**, 1199-1210 (1998).*

91. *Panina, E.M., Mironov, A.A. & Gelfand, M.S. Comparative genomics of bacterial zinc regulons: enhanced ion transport, pathogenesis, and rearrangement of ribosomal proteins. Proc Natl Acad Sci U S A **100**, 9912-9917 (2003).*
92. *Petrarca, P., Ammendola, S., Pasquali, P. & Battistoni, A. The Zur-regulated ZinT protein is an auxiliary component of the high-affinity ZnuABC zinc transporter that facilitates metal recruitment during severe zinc shortage. J Bacteriol **192**, 1553-1564 (2010).*
93. *Gabbianelli, R. et al. Role of ZnuABC and ZinT in Escherichia coli O157:H7 zinc acquisition and interaction with epithelial cells. BMC Microbiol **11**, 36 (2011).*
94. *Hantke, K. Bacterial zinc uptake and regulators. Curr Opin Microbiol **8**, 196-202 (2005).*
95. *Patzer, S.I. & Hantke, K. The zinc-responsive regulator Zur and its control of the znu gene cluster encoding the ZnuABC zinc uptake system in Escherichia coli. J Biol Chem **275**, 24321-24332 (2000).*
96. *Nanamiya, H. et al. Zinc is a key factor in controlling alternation of two types of L31 protein in the Bacillus subtilis ribosome. Mol Microbiol **52**, 273-283 (2004).*
97. *Grass, G., Wong, M.D., Rosen, B.P., Smith, R.L. & Rensing, C. ZupT is a Zn(II) uptake system in Escherichia coli. J Bacteriol **184**, 864-866 (2002).*
98. *Grass, G. et al. The metal permease ZupT from Escherichia coli is a transporter with a broad substrate spectrum. J Bacteriol **187**, 1604-1611 (2005).*
99. *Beard, S.J. et al. Evidence for the transport of zinc(II) ions via the pit inorganic phosphate transport system in Escherichia coli. FEMS Microbiol Lett **184**, 231-235 (2000).*
100. *Arguello, J.M., Eren, E. & Gonzalez-Guerrero, M. The structure and function of heavy metal transport P1B-ATPases. Biometals **20**, 233-248 (2007).*
101. *Arguello, J.M., Gonzalez-Guerrero, M. & Raimunda, D. Bacterial transition metal P(1B)-ATPases: transport mechanism and roles in virulence. Biochemistry **50**, 9940-9949 (2011).*
102. *Kim, E.H., Nies, D.H., McEvoy, M.M. & Rensing, C. Switch or funnel: how RND-type transport systems control periplasmic metal homeostasis. J Bacteriol **193**, 2381-2387 (2011).*
103. *Silver, S. Bacterial resistances to toxic metal ions--a review. Gene **179**, 9-19 (1996).*
104. *Rensing, C., Mitra, B. & Rosen, B.P. The zntA gene of Escherichia coli encodes a Zn(II)-translocating P-type ATPase. Proc Natl Acad Sci U S A **94**, 14326-14331 (1997).*
105. *Beard, S.J., Hashim, R., Membrillo-Hernandez, J., Hughes, M.N. & Poole, R.K. Zinc(II) tolerance in Escherichia coli K-12: evidence that the zntA gene (o732) encodes a cation transport ATPase. Mol Microbiol **25**, 883-891 (1997).*
106. *Sharma, R., Rensing, C., Rosen, B.P. & Mitra, B. The ATP hydrolytic activity of purified ZntA, a Pb(II)/Cd(II)/Zn(II)-translocating ATPase from Escherichia coli. J Biol Chem **275**, 3873-3878 (2000).*
107. *Outten, C.E., Outten, F.W. & O'Halloran, T.V. DNA distortion mechanism for transcriptional activation by ZntR, a Zn(II)-responsive MerR homologue in Escherichia coli. J Biol Chem **274**, 37517-37524 (1999).*

*108. Pruteanu, M., Neher, S.B. & Baker, T.A. Ligand-controlled proteolysis of the Escherichia coli transcriptional regulator ZntR. J Bacteriol **189**, 3017-3025 (2007).*

*109. Hitomi, Y., Outten, C.E. & O'Halloran, T.V. Extreme zinc-binding thermodynamics of the metal sensor/regulator protein, ZntR. J Am Chem Soc **123**, 8614-8615 (2001).*

*110. Grass, G. et al. ZitB (YbgR), a member of the cation diffusion facilitator family, is an additional zinc transporter in Escherichia coli. J Bacteriol **183**, 4664-4667 (2001).*

*111. Chao, Y. & Fu, D. Kinetic study of the antiport mechanism of an Escherichia coli zinc transporter, ZitB. J Biol Chem **279**, 12043-12050 (2004).*

*112. Munkelt, D., Grass, G. & Nies, D.H. The chromosomally encoded cation diffusion facilitator proteins DmeF and FieF from Wautersia metallidurans CH34 are transporters of broad metal specificity. J Bacteriol **186**, 8036-8043 (2004).*

*113. Wei, Y. & Fu, D. Selective metal binding to a membrane-embedded aspartate in the Escherichia coli metal transporter YiiP (FieF). J Biol Chem **280**, 33716-33724 (2005).*

*114. Grass, G. et al. FieF (YiiP) from Escherichia coli mediates decreased cellular accumulation of iron and relieves iron stress. Arch Microbiol **183**, 9-18 (2005).*

*115. Nishino, K., Nikaido, E. & Yamaguchi, A. Regulation of multidrug efflux systems involved in multidrug and metal resistance of Salmonella enterica serovar Typhimurium. J Bacteriol **189**, 9066-9075 (2007).*

*116. Nagakubo, S., Nishino, K., Hirata, T. & Yamaguchi, A. The putative response regulator BaeR stimulates multidrug resistance of Escherichia coli via a novel multidrug exporter system, MdtABC. J Bacteriol **184**, 4161-4167 (2002).*

*117. Baranova, N. & Nikaido, H. The baeSR two-component regulatory system activates transcription of the yegMNOB (mdtABCD) transporter gene cluster in Escherichia coli and increases its resistance to novobiocin and deoxycholate. J Bacteriol **184**, 4168-4176 (2002).*

*118. Helbig, K., Bleuel, C., Krauss, G.J. & Nies, D.H. Glutathione and transition-metal homeostasis in Escherichia coli. J Bacteriol **190**, 5431-5438 (2008).*

*119. Leonhartsberger, S., Huber, A., Lottspeich, F. & Bock, A. The hydH/G Genes from Escherichia coli code for a zinc and lead responsive two-component regulatory system. J Mol Biol **307**, 93-105 (2001).*

*120. Nishino, K., Honda, T. & Yamaguchi, A. Genome-wide analyses of Escherichia coli gene expression responsive to the BaeSR two-component regulatory system. J Bacteriol **187**, 1763-1772 (2005).*

*121. Ralle, M. & Lutsenko, S. Quantitative imaging of metals in tissues. Biometals **22**, 197-205 (2009).*

*122. Sanz-Medel, A., Montes-Bayon, M. & Luisa Fernandez Sanchez, M. Trace element speciation by ICP-MS in large biomolecules and its potential for proteomics. Anal Bioanal Chem **377**, 236-247 (2003).*

*123. Szpunar, J. Bio-inorganic speciation analysis by hyphenated techniques. Analyst **125**, 963-988 (2000).*

124. *Paunesku, T., Vogt, S., Maser, J., Lai, B. & Woloschak, G. X-ray fluorescence microprobe imaging in biology and medicine. J Cell Biochem **99**, 1489-1502 (2006).*
125. *Fahrni, C.J. Biological applications of X-ray fluorescence microscopy: exploring the subcellular topography and speciation of transition metals. Curr Opin Chem Biol **11**, 121-127 (2007).*
126. *Missiaen, L. et al. Abnormal intracellular Ca2+ homeostasis and disease. Cell Calcium **28**, 1-21 (2000).*
127. *Nicholls, D.G. Mitochondria and calcium signaling. Cell Calcium **38**, 311-317 (2005).*
128. *Taylor, J.T. et al. Calcium signaling and T-type calcium channels in cancer cell cycling. World Journal of Gastroenterology **14**, 4984-4991 (2008).*
129. *Morelle, B., Salmon, J.M., Vigo, J. & Viallet, P. Measurement of intracellular magnesium concentration in 3T3 fibroblasts with the fluorescent indicator Mag-indo-1. Anal Biochem **218**, 170-176 (1994).*
130. *Kress, G.J., Dineley, K.E. & Reynolds, I.J. The relationship between intracellular free iron and cell injury in cultured neurons, astrocytes, and oligodendrocytes. J Neurosci **22**, 5848-5855 (2002).*
131. *Petrat, F., Rauen, U. & de Groot, H. Determination of the chelatable iron pool of isolated rat hepatocytes by digital fluorescence microscopy using the fluorescent probe, phen green SK. Hepatology **29**, 1171-1179 (1999).*
132. *Woodmansee, A.N. & Imlay, J.A. Quantitation of intracellular free iron by electron paramagnetic resonance spectroscopy. Methods Enzymol **349**, 3-9 (2002).*
133. *Kroncke, K.D. Cellular stress and intracellular zinc dyshomeostasis. Arch Biochem Biophys **463**, 183-187 (2007).*
134. *Casey, J.R., Grinstein, S. & Orlowski, J. Sensors and regulators of intracellular pH. Nat Rev Mol Cell Biol **11**, 50-61 (2010).*
135. *Tomat, E. & Lippard, S.J. Imaging mobile zinc in biology. Curr Opin Chem Biol **14**, 225-230 (2010).*
136. *de Silva, A.P. et al. Signaling recognition events with fluorescent sensors and switches. Chemical Reviews **97**, 1515-1566 (1997).*
137. *Frederickson, C.J., Kasarskis, E.J., Ringo, D. & Frederickson, R.E. A Quinoline Fluorescence Method for Visualizing and Assaying the Histochemically Reactive Zinc (Bouton Zinc) in the Brain. Journal of Neuroscience Methods **20**, 91-103 (1987).*
138. *Fahrni, C.J. & O'Halloran, T.V. Aqueous coordination chemistry of quinoline-based fluorescence probes for the biological chemistry of zinc. Journal of the American Chemical Society **121**, 11448-11458 (1999).*
139. *Tonder, N., Johansen, F.F., Frederickson, C.J., Zimmer, J. & Diemer, N.H. Possible Role of Zinc in the Selective Degeneration of Dentate Hilar Neurons after Cerebral-Ischemia in the Adult-Rat. Neuroscience Letters **109**, 247-252 (1990).*
140. *Hendrickson, K.M., Geue, J.P., Wyness, O., Lincoln, S.F. & Ward, A.D. Coordination and fluorescence of the intracellular Zn2+ probe [2-methyl-8-(4-*

*toluenesulfonamido)-6-quinolyloxy]acetic acid (Zinquin a) in ternary Zn2+ complexes. Journal of the American Chemical Society **125**, 3889-3895 (2003).*

141. *Zhang, Y., Guo, X.F., Si, W.X., Jia, L.H. & Qian, X.H. Ratiometric and water-soluble fluorescent zinc sensor of carboxamidoquinoline with an alkoxyethylamino chain as receptor. Organic Letters **10**, 473-476 (2008).*
142. *Liu, Y., Zhang, N., Chen, Y. & Wang, L.H. Fluorescence sensing and binding behavior of aminobenzenesulfonamidoquinolino-beta-cyclodextrin to Zn2+. Organic Letters **9**, 315-318 (2007).*
143. *Burdette, S.C., Walkup, G.K., Spingler, B., Tsien, R.Y. & Lippard, S.J. Fluorescent sensors for Zn2+ based on a fluorescein platform: Synthesis, properties and intracellular distribution. Journal of the American Chemical Society **123**, 7831-7841 (2001).*
144. *Burdette, S. & Lippard, S. Zinpyr and rhodafluor sensors: Fluorescence-based probes for Zn2+. Abstracts of Papers of the American Chemical Society **224**, U640-U641 (2002).*
145. *Nolan, E.M. & Lippard, S.J. The zinspy family of fluorescent zinc sensors: Syntheses and spectroscopic investigations. Inorganic Chemistry **43**, 8310-8317 (2004).*
146. *Chang, C.J. et al. Bright fluorescent chemosensor platforms for imaging endogenous pools of neuronal zinc. Chemistry & Biology **11**, 203-210 (2004).*
147. *Chang, C.J. et al. ZP8, a neuronal zinc sensor with improved dynamic range; Imaging zinc in hippocampal slices with two-photon microscopy. Inorganic Chemistry **43**, 6774-6779 (2004).*
148. *Woodroofe, C.C., Masalha, R., Barnes, K.R., Frederickson, C.J. & Lippard, S.J. Membrane-permeable and -impermeable sensors of the Zinpyr family and their application to imaging of hippocampal zinc in vivo. Chemistry & Biology **11**, 1659-1666 (2004).*
149. *Tomat, E., Nolan, E.M., Jaworski, J. & Lippard, S.J. Organelle-Specific Zinc Detection Using Zinpyr-Labeled Fusion Proteins in Live Cells. Journal of the American Chemical Society **130**, 15776-+ (2008).*
150. *Chang, C.J., Jaworski, J., Nolan, E.M., Sheng, M. & Lippard, S.J. A tautomeric zinc sensor for ratiometric fluorescence imaging: Application to nitric oxide-induced release of intracellular zinc. Proceedings of the National Academy of Sciences of the United States of America **101**, 1129-1134 (2004).*
151. *Hirano, T., Kikuchi, K., Urano, Y. & Nagano, T. Improvement and biological applications of fluorescent probes for zinc, ZnAFs. Journal of the American Chemical Society **124**, 6555-6562 (2002).*
152. *Maruyama, S., Kikuchi, K., Hirano, T., Urano, Y. & Nagano, T. A novel, cell-permeable, fluorescent probe for ratiometric imaging of zinc ion. Journal of the American Chemical Society **124**, 10650-10651 (2002).*
153. *Xu, Z., Yoon, J. & Spring, D.R. Fluorescent chemosensors for Zn(2+). Chem Soc Rev **39**, 1996-2006 (2010).*
154. *Xu, Z.C. et al. Zn(2+)-Triggered Amide Tautomerization Produces a Highly Zn(2+)-Selective, Cell-Permeable, and Ratiometric Fluorescent Sensor. Journal of the American Chemical Society **132**, 601-610 (2010).*

155. *Taki, M., Wolford, J.L. & O'Halloran, T.V. Emission ratiometric imaging of intracellular zinc: Design of a benzoxazole fluorescent sensor and its application in two-photon microscopy. Journal of the American Chemical Society **126**, 712-713 (2004).*
156. *Gee, K.R., Zhou, Z.L., Ton-That, D., Sensi, S.L. & Weiss, J.H. Measuring zinc in living cells. A new generation of sensitive and selective fluorescent probes. Cell Calcium **31**, 245-251 (2002).*
157. *Atar, D., Backx, P.H., Appel, M.M., Gao, W.D. & Marban, E. Excitation-Transcription Coupling Mediated by Zinc Influx through Voltage-Dependent Calcium Channels. Journal of Biological Chemistry **270**, 2473-2477 (1995).*
158. *Simons, T.J.B. Use of Mag-Fura-2 as a Fluorescent Zn-2+ Indicator. Journal of Physiology-London **459**, P304-P304 (1993).*
159. *Easley, C.J., Rocheleau, J.V., Head, W.S. & Piston, D.W. Quantitative measurement of zinc secretion from pancreatic islets with high temporal resolution using droplet-based microfluidics. Anal Chem **81**, 9086-9095 (2009).*
160. *Li, Y.M. et al. Tracing of intracellular zinc(II) fluorescence flux to monitor cell apoptosis by using FluoZin-3AM. Cell Biochem Funct **27**, 417-423 (2009).*
161. *Naik, H.B., Beshire, M., Walsh, B.M., Liu, J. & Soybel, D.I. Secretory state regulates Zn2+ transport in gastric parietal cell of the rabbit. Am J Physiol Cell Physiol **297**, C979-989 (2009).*
162. *Li, Y. & Maret, W. Transient fluctuations of intracellular zinc ions in cell proliferation. Exp Cell Res **315**, 2463-2470 (2009).*
163. *Zhao, J., Bertoglio, B.A., Devinney, M.J., Jr., Dineley, K.E. & Kay, A.R. The interaction of biological and noxious transition metals with the zinc probes FluoZin-3 and Newport Green. Anal Biochem **384**, 34-41 (2009).*
164. *Muylle, F.A., Adriaensen, D., De Coen, W., Timmermans, J.P. & Blust, R. Tracing of labile zinc in live fish hepatocytes using FluoZin-3. Biometals **19**, 437-450 (2006).*
165. *Devinney, M.J., 2nd, Reynolds, I.J. & Dineley, K.E. Simultaneous detection of intracellular free calcium and zinc using fura-2FF and FluoZin-3. Cell Calcium **37**, 225-232 (2005).*
166. *Dineley, K.E., Malaiyandi, L.M. & Reynolds, I.J. A reevaluation of neuronal zinc measurements: artifacts associated with high intracellular dye concentration. Mol Pharmacol **62**, 618-627 (2002).*
167. *Qian, F. et al. Visible Light Excitable Zn(2+) Fluorescent Sensor Derived from an Intramolecular Charge Transfer Fluorophore and Its in Vitro and in Vivo Application. Journal of the American Chemical Society **131**, 1460-1468 (2009).*
168. *Komatsu, K., Urano, Y., Kojima, H. & Nagano, T. Development of an iminocoumarin-based zinc sensor suitable for ratiometric fluorescence imaging of neuronal zinc. Journal of the American Chemical Society **129**, 13447-13454 (2007).*
169. *Godwin, H.A. & Berg, J.M. A fluorescent zinc probe based on metal-induced peptide folding. Journal of the American Chemical Society **118**, 6514-6515 (1996).*
170. *Walkup, G.K. & Imperiali, B. Design and evaluation of a peptidyl fluorescent chemosensor for divalent zinc. Journal of the American Chemical Society **118**, 3053-3054 (1996).*

171. *Shults, M.D., Pearce, D.A. & Imperiali, B. Modular and tunable chemosensor scaffold for divalent zinc. J Am Chem Soc **125**, 10591-10597 (2003).*
172. *Qin, Y., Dittmer, P.J., Park, J.G., Jansen, K.B. & Palmer, A.E. Measuring steady-state and dynamic endoplasmic reticulum and Golgi Zn2+ with genetically encoded sensors. Proc Natl Acad Sci U S A **108**, 7351-7356 (2011).*
173. *Evers, T.H., Appelhof, M.A., de Graaf-Heuvelmans, P.T., Meijer, E.W. & Merkx, M. Ratiometric detection of Zn(II) using chelating fluorescent protein chimeras. J Mol Biol **374**, 411-425 (2007).*
174. *van Dongen, E.M. et al. Ratiometric fluorescent sensor proteins with subnanomolar affinity for Zn(II) based on copper chaperone domains. J Am Chem Soc **128**, 10754-10762 (2006).*
175. *van Dongen, E.M. et al. Variation of linker length in ratiometric fluorescent sensor proteins allows rational tuning of Zn(II) affinity in the picomolar to femtomolar range. J Am Chem Soc **129**, 3494-3495 (2007).*
176. *Meldrum, N.U. & Roughton, F.J. Carbonic anhydrase. Its preparation and properties. J Physiol **80**, 113-142 (1933).*
177. *Hakansson, K., Carlsson, M., Svensson, L.A. & Liljas, A. Structure of native and apo carbonic anhydrase II and structure of some of its anion-ligand complexes. J Mol Biol **227**, 1192-1204 (1992).*
178. *McCall, K.A., Huang, C. & Fierke, C.A. Function and mechanism of zinc metalloenzymes. J Nutr **130**, 1437S-1446S (2000).*
179. *Kiefer, L.L., Ippolito, J.A., Fierke, C.A. & Christianson, D.W. Redesigning the Zinc-Binding Site of Human Carbonic Anhydrase-Ii - Structure of a His2Asp-Zn2+ Metal Coordination Polyhedron. Journal of the American Chemical Society **115**, 12581-12582 (1993).*
180. *Kiefer, L.L. & Fierke, C.A. Functional characterization of human carbonic anhydrase II variants with altered zinc binding sites. Biochemistry **33**, 15233-15240 (1994).*
181. *Alexander, R.S., Kiefer, L.L., Fierke, C.A. & Christianson, D.W. Engineering the Zinc-Binding Site of Human Carbonic Anhydrase-Ii - Structure of the His-94-]Cys Apoenzyme in a New Crystalline Form. Biochemistry **32**, 1510-1518 (1993).*
182. *Lesburg, C.A., Huang, C., Christianson, D.W. & Fierke, C.A. Histidine --> carboxamide ligand substitutions in the zinc binding site of carbonic anhydrase II alter metal coordination geometry but retain catalytic activity. Biochemistry **36**, 15780-15791 (1997).*
183. *Kiefer, L.L., Paterno, S.A. & Fierke, C.A. Hydrogen-Bond Network in the Metal-Binding Site of Carbonic-Anhydrase Enhances Zinc Affinity and Catalytic Efficiency. Journal of the American Chemical Society **117**, 6831-6837 (1995).*
184. *Huang, C.C., Lesburg, C.A., Kiefer, L.L., Fierke, C.A. & Christianson, D.W. Reversal of the hydrogen bond to zinc ligand histidine-119 dramatically diminishes catalysis and enhances metal equilibration kinetics in carbonic anhydrase II. Biochemistry **35**, 3439-3446 (1996).*
185. *Hunt, J.B., Rhee, M.J. & Storm, C.B. A rapid and convenient preparation of apocarbonic anhydrase. Anal Biochem **79**, 614-617 (1977).*

186. *Pocker, Y. & Fong, C.T. Inactivation of bovine carbonic anhydrase by dipicolinate: kinetic studies and mechanistic implications. Biochemistry **22**, 813-818 (1983).*
187. *Lindskog, S. & Malmstrom, B.G. Metal binding and catalytic activity in bovine carbonic anhydrase. J Biol Chem **237**, 1129-1137 (1962).*
188. *McCall, K.A. & Fierke, C.A. Probing determinants of the metal ion selectivity in carbonic anhydrase using mutagenesis. Biochemistry **43**, 3979-3986 (2004).*
189. *McCall, K.A. & Fierke, C.A. Colorimetric and fluorimetric assays to quantitate micromolar concentrations of transition metals. Anal Biochem **284**, 307-315 (2000).*
190. *Hunt, J.A., Ahmed, M. & Fierke, C.A. Metal binding specificity in carbonic anhydrase is influenced by conserved hydrophobic core residues. Biochemistry **38**, 9054-9062 (1999).*
191. *Finney, L.A. & O'Halloran, T.V. Transition metal speciation in the cell: insights from the chemistry of metal ion receptors. Science **300**, 931-936 (2003).*
192. *Chen, R.F. & Kernohan, J.C. Combination of bovine carbonic anhydrase with a fluorescent sulfonamide. J Biol Chem **242**, 5813-5823 (1967).*
193. *Thompson, R.B. & Jones, E.R. Enzyme-Based Fiber Optic Zinc Biosensor. Analytical Chemistry **65**, 730-734 (1993).*
194. *Thompson, R.B. & Patchan, M.W. Lifetime-Based Fluorescence Energy-Transfer Biosensing of Zinc. Analytical Biochemistry **227**, 123-128 (1995).*
195. *Thompson, R.B., Maliwal, B.P., Feliccia, V.L., Fierke, C.A. & McCall, K. Determination of picomolar concentrations of metal lens using fluorescence anisotropy: Biosensing with a "reagentless" enzyme transducer. Analytical Chemistry **70**, 4717-4723 (1998).*
196. *Thompson, R.B., Maliwal, B.P. & Fierke, C.A. Selectivity and sensitivity of fluorescence lifetime-based metal ion biosensing using a carbonic anhydrase transducer. Analytical Biochemistry **267**, 185-195 (1999).*
197. *Thompson, R.B., Whetsell, W.O., Maliwal, B.P., Fierke, C.A. & Frederickson, C.J. Fluorescence microscopy of stimulated Zn(II) release from organotypic cultures of mammalian hippocampus using a carbonic anhydrase-based biosensor system. Journal of Neuroscience Methods **96**, 35-45 (2000).*
198. *Frederickson, C.J. et al. Synaptic release of zinc from brain slices: factors governing release, imaging, and accurate calculation of concentration. J Neurosci Methods **154**, 19-29 (2006).*
199. *Thompson, R.B., Lin, H.J., Ge, Z., Johnson, K. & Fierke, C.A. Fluorescence lifetime-based determination of cyanide using a carbonic anhydrase-based biosensor. Biophysical Journal **72**, Tham6-Tham6 (1997).*
200. *Thompson, R.B., Maliwal, B.P. & Fierke, C.A. Expanded dynamic range of free zinc ion determination by fluorescence anisotropy. Analytical Chemistry **70**, 1749-1754 (1998).*
201. *Thompson, R.B., Maliwal, B.P. & Fierke, C.A. New carbonic anhydrase-based transducers for metal ion determination by fluorescence anisotropy. Biophysical Journal **76**, A260-a260 (1999).*

202. *Thompson, R.B., Cramer, M.L., Bozym, R. & Fierke, C.A. Excitation ratiometric fluorescent biosensor for zinc ion at picomolar levels. Journal of Biomedical Optics **7**, 555-560 (2002).*
203. *Thompson, R.B., Maliwal, B.P. & Zeng, H.H. Zinc biosensing with multiphoton excitation using carbonic anhydrase and improved fluorophores. Journal of Biomedical Optics **5**, 17-22 (2000).*
204. *Lee, Y.E. & Kopelman, R. Nanoparticle PEBBLE sensors in live cells. Methods Enzymol **504**, 419-470 (2012).*
205. *Maret, W., Jacob, C., Vallee, B.L. & Fischer, E.H. Inhibitory sites in enzymes: zinc removal and reactivation by thionein. Proc Natl Acad Sci U S A **96**, 1936-1940 (1999).*
206. *Fosmire, G.J. Zinc toxicity. Am J Clin Nutr **51**, 225-227 (1990).*
207. *Nair, S.K., Calderone, T.L., Christianson, D.W. & Fierke, C.A. Altering the mouth of a hydrophobic pocket. Structure and kinetics of human carbonic anhydrase II mutants at residue Val-121. J Biol Chem **266**, 17320-17325 (1991).*
208. *Bozym, R. et al. Determination of Zinc Using Carbonic Anhydrase-Based Fluorescence Biosensors. Fluorescence Spectroscopy **450**, 287-309 (2008).*
209. *Neidhardt, F.C., Bloch, P.L. & Smith, D.F. Culture medium for enterobacteria. J Bacteriol **119**, 736-747 (1974).*
210. *Campbell, R.E. et al. A monomeric red fluorescent protein. Proc Natl Acad Sci U S A **99**, 7877-7882 (2002).*
211. *Shaner, N.C. et al. Improved monomeric red, orange and yellow fluorescent proteins derived from Discosoma sp. red fluorescent protein. Nat Biotechnol **22**, 1567-1572 (2004).*
212. *Merzlyak, E.M. et al. Bright monomeric red fluorescent protein with an extended fluorescence lifetime. Nat Methods **4**, 555-557 (2007).*
213. *Bevis, B.J. & Glick, B.S. Rapidly maturing variants of the Discosoma red fluorescent protein (DsRed). Nat Biotechnol **20**, 83-87 (2002).*
214. *Hunt, J.A. & Fierke, C.A. Selection of carbonic anhydrase variants displayed on phage. Aromatic residues in zinc binding site enhance metal affinity and equilibration kinetics. J Biol Chem **272**, 20364-20372 (1997).*
215. *Plank, L.D. & Harvey, J.D. Generation time statistics of Escherichia coli B measured by synchronous culture techniques. J Gen Microbiol **115**, 69-77 (1979).*
216. *Maren, T.H. Direct measurements of the rate constants of sulfonamides with carbonic anhydrase. Mol Pharmacol **41**, 419-426 (1992).*
217. *Alakomi, H.L., Paananen, A., Suihko, M.L., Helander, I.M. & Saarela, M. Weakening effect of cell permeabilizers on gram-negative bacteria causing biodeterioration. Appl Environ Microbiol **72**, 4695-4703 (2006).*
218. *Slonczewski, J.L., Rosen, B.P., Alger, J.R. & Macnab, R.M. pH homeostasis in Escherichia coli: measurement by 31P nuclear magnetic resonance of methylphosphonate and phosphate. Proc Natl Acad Sci U S A **78**, 6271-6275 (1981).*
219. *Krebs, J.F., Ippolito, J.A., Christianson, D.W. & Fierke, C.A. Structural and functional importance of a conserved hydrogen bond network in human carbonic anhydrase II. J Biol Chem **268**, 27458-27466 (1993).*

220. *Huang, M., Shaw, I.C. & Petering, D.H. Interprotein metal exchange between transcription factor IIIa and apo-metallothionein. J Inorg Biochem **98**, 639-648 (2004).*
221. *Lee, L.J., Barrett, J.A. & Poole, R.K. Genome-wide transcriptional response of chemostat-cultured Escherichia coli to zinc. J Bacteriol **187**, 1124-1134 (2005).*
222. *Gattis, S.G., Hernick, M. & Fierke, C.A. Active site metal ion in UDP-3-O-((R)-3-hydroxymyristoyl)-N-acetylglucosamine deacetylase (LpxC) switches between Fe(II) and Zn(II) depending on cellular conditions. J Biol Chem **285**, 33788-33796 (2010).*
223. *Blencowe, D.K. & Morby, A.P. Zn(II) metabolism in prokaryotes. FEMS Microbiol Rev **27**, 291-311 (2003).*
224. *Lee, S.M. et al. Functional analysis of the Escherichia coli zinc transporter ZitB. FEMS Microbiol Lett **215**, 273-278 (2002).*
225. *Anton, A. et al. Characteristics of zinc transport by two bacterial cation diffusion facilitators from Ralstonia metallidurans CH34 and Escherichia coli. J Bacteriol **186**, 7499-7507 (2004).*
226. *Wang, D., Hurst, T.K., Thompson, R.B. & Fierke, C.A. Genetically encoded ratiometric biosensors to measure intracellular exchangeable zinc in Escherichia coli. J Biomed Opt **16**, 087011 (2011).*
227. *Blindauer, C.A. et al. Multiple bacteria encode metallothioneins and SmtA-like zinc fingers. Mol Microbiol **45**, 1421-1432 (2002).*
228. *Rae, T.D., Schmidt, P.J., Pufahl, R.A., Culotta, V.C. & O'Halloran, T.V. Undetectable intracellular free copper: the requirement of a copper chaperone for superoxide dismutase. Science **284**, 805-808 (1999).*
229. *Baba, T. et al. Construction of Escherichia coli K-12 in-frame, single-gene knockout mutants: the Keio collection. Mol Syst Biol **2**, 2006 0008 (2006).*
230. *Brocklehurst, K.R. & Morby, A.P. Metal-ion tolerance in Escherichia coli: analysis of transcriptional profiles by gene-array technology. Microbiology **146 (Pt 9)**, 2277-2282 (2000).*
231. *MacDiarmid, C.W., Milanick, M.A. & Eide, D.J. Induction of the ZRC1 metal tolerance gene in zinc-limited yeast confers resistance to zinc shock. J Biol Chem **278**, 15065-15072 (2003).*
232. *Yamamoto, K. & Ishihama, A. Transcriptional response of Escherichia coli to external zinc. J Bacteriol **187**, 6333-6340 (2005).*
233. *Akanuma, G., Nanamiya, H., Natori, Y., Nomura, N. & Kawamura, F. Liberation of zinc-containing L31 (RpmE) from ribosomes by its paralogous gene product, YtiA, in Bacillus subtilis. J Bacteriol **188**, 2715-2720 (2006).*
234. *Hensley, M.P., Tierney, D.L. & Crowder, M.W. Zn(II) binding to E. coli 70S ribosomes. Biochemistry (2011).*
235. *Buchsbaum, J.C. & Berg, J.M. Kinetics of metal binding by a zinc finger peptide. Inorg. Chim. Acta **297**, 217-219 (2000).*
236. *Leblanc, S.K.D., Oates, C.W. & Raivio, T.L. Characterization of the induction and cellular role of the BaeSR two-component envelope stress response of Escherichia coli. Journal of bacteriology **193**, 3367-3375 (2011).*
237. *Raffa, R.G. & Raivio, T.L. A third envelope stress signal transduction pathway in Escherichia coli. Mol Microbiol **45**, 1599-1611 (2002).*

238. *Nagasawa, S., Ishige, K. & Mizuno, T. Novel members of the two-component signal transduction genes in Escherichia coli. J Biochem **114**, 350-357 (1993).*
239. *Hirakawa, H., Inazumi, Y., Masaki, T., Hirata, T. & Yamaguchi, A. Indole induces the expression of multidrug exporter genes in Escherichia coli. Mol Microbiol **55**, 1113-1126 (2005).*
240. *Nishino, K. & Yamaguchi, A. Analysis of a complete library of putative drug transporter genes in Escherichia coli. J Bacteriol **183**, 5803-5812 (2001).*
241. *Pao, S.S., Paulsen, I.T. & Saier, M.H., Jr. Major facilitator superfamily. Microbiol Mol Biol Rev **62**, 1-34 (1998).*
242. *Radchenko, M.V. et al. Potassium/proton antiport system of Escherichia coli. J Biol Chem **281**, 19822-19829 (2006).*
243. *Rosenberg, E.Y., Ma, D. & Nikaido, H. AcrD of Escherichia coli is an aminoglycoside efflux pump. J Bacteriol **182**, 1754-1756 (2000).*
244. *Elkins, C.A. & Nikaido, H. Substrate specificity of the RND-type multidrug efflux pumps AcrB and AcrD of Escherichia coli is determined predominantly by two large periplasmic loops. J Bacteriol **184**, 6490-6498 (2002).*
245. *Yamasaki, S., Nagasawa, S., Hayashi-Nishino, M., Yamaguchi, A. & Nishino, K. AcrA dependency of the AcrD efflux pump in Salmonella enterica serovar Typhimurium. J Antibiot (Tokyo) **64**, 433-437 (2011).*
246. *Hagenmaier, S., Stierhof, Y.D. & Henning, U. A new periplasmic protein of Escherichia coli which is synthesized in spheroplasts but not in intact cells. J Bacteriol **179**, 2073-2076 (1997).*
247. *Quan, S. et al. Genetic selection designed to stabilize proteins uncovers a chaperone called Spy. Nat Struct Mol Biol **18**, 262-269 (2011).*
248. *Akerlund, T., Nordstrom, K. & Bernander, R. Analysis of cell size and DNA content in exponentially growing and stationary-phase batch cultures of Escherichia coli. J Bacteriol **177**, 6791-6797 (1995).*
249. *Ali Azam, T., Iwata, A., Nishimura, A., Ueda, S. & Ishihama, A. Growth phase-dependent variation in protein composition of the Escherichia coli nucleoid. J Bacteriol **181**, 6361-6370 (1999).*
250. *Murakami, S., Nakashima, R., Yamashita, E., Matsumoto, T. & Yamaguchi, A. Crystal structures of a multidrug transporter reveal a functionally rotating mechanism. Nature **443**, 173-179 (2006).*
251. *Nikaido, H. & Takatsuka, Y. Mechanisms of RND multidrug efflux pumps. Biochim Biophys Acta **1794**, 769-781 (2009).*
252. *Yamada, S. et al. Effect of drug transporter genes on cysteine export and overproduction in Escherichia coli. Appl Environ Microbiol **72**, 4735-4742 (2006).*
253. *Slavik, J. Intracellular pH of yeast cells measured with fluorescent probes. FEBS Lett **140**, 22-26 (1982).*
254. *The Molecular Probes Handbook. (Life Technologies, 2010).*
255. *Saleemuddin, M. & Husain, Q. Concanavalin A: a useful ligand for glycoenzyme immobilization--a review. Enzyme Microb Technol **13**, 290-295 (1991).*
256. *Erdahl, W.L., Chapman, C.J., Wang, E., Taylor, R.W. & Pfeiffer, D.R. Ionophore 4-BrA23187 transports Zn2+ and Mn2+ with high selectivity over Ca2+. Biochemistry **35**, 13817-13825 (1996).*

*257. Fierke, C.A. & Thompson, R.B. Fluorescence-based biosensing of zinc using carbonic anhydrase. Biometals **14**, 205-222 (2001).*
*258. Sigdel, T.K., Easton, J.A. & Crowder, M.W. Transcriptional response of Escherichia coli to TPEN. J Bacteriol **188**, 6709-6713 (2006).*
259. Amberg, D.C., Burke, D.J. & Strathern, J.N. Methods in Yeast Genetics: A Cold Spring Harbor Laboratory Course Manual. (2005).